# Biodegradation of Polycyclic Aromatic Hydrocarbons: Mechanistic Insights and Intensification

**A**
**Thesis**
**Submitted in**
**Partial Fulfillment of the**
**Requirements for the Degree of**

## DOCTOR OF PHILOSOPHY

***by***


## Niharika Kashyap




**CENTRE FOR THE ENVIRONMENT**
**Indian Institute of Technology Guwahati**
Guwahati – 781 039, Assam, India

December 2020

Dedicated

to

My Parents

(Papa and Ma)

**INDIAN INSTITUTE OF TECHNOLOGY GUWAHATI**

**CENTER FOR THE ENVIRONMENT**

# STATEMENT

I do hereby declare that the content embodied in this thesis entitled **"Biodegradation of Polycyclic Aromatic Hydrocarbons: Mechanistic Insights and Intensification"** is the result of investigations carried out by me in Centre for the Environment, Indian Institute of Technology Guwahati, Guwahati, India, under the guidance of Prof. Vijayanand S. Moholkar.

In keeping with the general practice of reporting scientific observations, due acknowledgements have been made wherever the work described is based on the findings of other investigators.

Date: Niharika Kashyap

(Roll No.: 14615201

**INDIAN INSTITUTE OF TECHNOLOGY GUWAHATI**

**CENTER FOR THE ENVIRONMENT**

# CERTIFICATE

It is certified that the work contained in the thesis entitled **"Biodegradation of Polycyclic Aromatic Hydrocarbons: Mechanistic Insights and Intensification"**, by **Niharika Kashyap** (Roll No: 146152011), has been carried out under my supervision and that this work has not been submitted elsewhere for a degree.

Date:

**Prof. Vijayanand S. Moholkar**
Professor
Department of Chemical Engineering
Indian Institute of Technology, Guwahati
Guwahati – 781 039
Assam, India

# ACKNOWLEDGEMENTS

I take utmost pleasure to express my deepest gratitude to all those who stood by me constantly and made this thesis possible. I am thankful to God for giving me the confidence and strength for successful completion of the entire Ph.D. First and foremost, appreciation goes to my thesis supervisor ***Prof. Vijayanand S. Moholkar*** for his valuable suggestions, encouragement and constant support throughout my research work. He has been a true source of inspiration and has given his precious time for discussion from which I have gained immense skill and knowledge in terms of research. I could not have imagined a better advisor and mentor for my Ph.D.

I would like to acknowledge my sincere gratitude to my doctoral committee members, ***Prof. Ranjan Tamuli***, ***Dr. Sachin Kumar*** and ***Dr. Manish Kumar*** for their insightful advices and suggestions throughout the research work.

I am grateful to the faculty and staff members of **Centre for the Environment**, **Centre for Energy** and **Department of Chemical Engineering** for their constant help and support. I am thankful to Centre for the Environment, Centre for Energy, Department of Chemical Engineering and **Central Instruments Facilities (CIF)** for providing facilities to carry out my research work. I am also thankful to the **Indian Institute of Technology Guwahati** for providing me with the state of the art infrastructure for advance level of research.

I am immensely thankful to my seniors *Dr. Shuchi Singh*, *Dr. Pritam Dikshit*, *Dr. Shyamali Sarma*, *Dr. Arup J. Bora*, *Dr. Ritesh S. Malani* and *Dr. Amit H. Batghare*

for their valuable guidance. I also extend my thanks to my research group members, *Neha*, *Kuldeep*, *Philip*, *Bhaskar*, *Udangshree*, *Kajal*, *Karan*, *Pushpita*, *Aradhana*, *Saptarishi*, *Kaustubh*, *Rishiraj*, for their constant help and enthusiastic company.

My Ph.D. endeavor would not have been successful without the endless support and trust of my brother *Mr. Nayan J. Kashyap* and sister *Miss. Priyanka Kashyap*. Finally, I would like to express my heartfelt thanks to my affectionate and ever-loving friend and husband *Mr. Sachankar Buragohain* who has stood by me like an anchor and supported me in every step of my Ph.D. journey. Last but not the least, I am highly indebted to my parents, *Mr. Satyen Haloi* and *Mrs. Arati Haloi* for all their sacrifices they made for my better future and giving me the freedom to take my own decision. My Ph.D. endeavor would not have been completed without their endless love and blessing.

# ABSTRACT

Different pollutants arising from natural and anthropogenic sources have contaminated our nature and have grave impact on human health. Polycyclic aromatic hydrocarbons (PAHs) are ubiquitous pollutant which cause great damage to terrestrial and aquatic ecosystems. Efficient and safe removal of these pollutants from environment has been an intensely active research area. Bioremediation is a well–established technique employed for the clean–up of PAHs. In this thesis, we have studied the process of PAHs removal through yeast, *Candida tropicalis*. This type of non–ligninolytic fungi have an edge over other fungi owing to their higher tolerance towards pollutants. To begin with, we have addressed the primary facet of a typical bioprocess, i.e. optimization of physical parameters and kinetic analysis of microbial growth. The model system was phenanthrene and pyrene as pollutants and native yeast strain of *Candida tropicalis* MTCC 184. The physical parameters related to phenanthrene and pyrene biodegradation were optimized using statistical design of experiments. The tolerance test revealed marked decrease in yeast cell growth after 100 and 75 mg $L^{-1}$ of phenanthrene and pyrene, respectively. The values of the optimised parameters were similar for both the PAHs. Under optimum conditions, ~ 66% of phenanthrene and ~ 53% of pyrene was degraded in 14 days. Kinetics of the process was studied using different substrate inhibition models. The profiles were best described with Haldane substrate inhibition model. Next intensification of biodegradation of PAHs with ultrasound was studied from a mechanistic viewpoint. After optimization of sonication duty cycle, ultrasound was applied in the log phase of yeast growth cycle. A marked rise of ~ 25% in phenanthrene removal and ~ 30% in pyrene removal was seen with sonication. Kinetic analysis revealed that the biomass yield coefficient increased while the decay coefficient of the cells reduced in presence of sonication. No significant alteration in the cellular morphology and topography was seen with ultrasound treatment. Further, we have studied the biomechanism of degradation of phenanthrene and pyrene by *Candida tropicalis*. It was found that same route of degradation (*meta*– pathway) was followed in both test and control experiments, thereby signifying that ultrasound did not alter the route of degradation. SDS–PAGE analysis revealed higher protein expression in the test samples as compared to control samples. GC–MS analysis of intermediate metabolites revealed

two parallel pathways of degradation, first triggered by intracellular cytochrome P450 monooxygenase enzyme, and second initiated by dioxygenase enzymes. Finally, the co–bioremediation of both the PAHs have been studied. Experimental results have been analyzed using a kinetic model for cell growth that takes into account self– and cross–inhibition of both substrates. In dual substrate system, specific degradation rate of phenanthrene was significantly higher than pyrene, which indicated relatively lower tolerance of *C. tropicalis* cells towards pyrene. The values of interaction parameters of inhibition revealed strong competitive cross–inhibition between two substrates, due to which biomass yield with dual substrates was reduced significantly. Inhibition induced by pyrene on cell growth was higher than phenanthrene. On a whole the thesis presents a complete lab scale process design and intensification of bioremediation of PAHs through non–ligninolytic fungi. Moreover, the methodology presented in the thesis forms a general framework that can be extended to other bioremediation systems.

# CONTENTS

# LIST OF TABLES

# LIST OF FIGURES

## Chapter 4



## Chapter 5

## Appendix I

# ABBREVIATIONS

| | |
|---|---|
| ANOVA | Analysis of variance |
| BH | Bushnell–Haas |
| BM | Basal medium |
| C1,2–D | Catechol 1,2– dioxygenase |
| C2,3–D | Catechol 2,3– dioxygenase |
| CCD | Central composite design |
| COD | Chemical oxygen demand |
| FE–SEM | Field emission scanning electron microscope |
| FSC | Forward scatter |
| GC–MS | Gas chromatography–Mass spectrometry |
| HMW | High molecular weight |
| HMSA | Hydroxymuconic semialdehyde |
| HPLC | High performance liquid chromatography |
| kDa | Kilo dalton |
| LMW | Low molecular weight |
| MSM | Mineral salt medium |
| MTCC | Microbial type culture collection |
| NIST | National Institute Standard and Technology |
| NSW | Natural sea water |
| OD | Optical density |
| PAH | Polycyclic aromatic hydrocarbon |
| PBS | Phosphate buffer saline |

| | |
|---|---|
| PI | Propidium iodide |
| RMSE | Root Mean Square Error |
| SDS–PAGE | Sodium dodecyl sulfate polyacrylamide gel electrophoresis |
| SSC | Side scatter |
| TCA | Tricarboxylic acid |
| TPH | Total petroleum hydrocarbon |
| US EPA | United States Environmental Protection Agency |
| UV | Ultraviolet |
| YEPD | Yeast extract peptone dextrose |

# CHAPTER 1

# INTRODUCTION AND LITERATURE REVIEW

CHAPTER 1

# Introduction and Literature Review

## 1.1 INTRODUCTION

The 20th century was an era of rigorous industrialization, modernization, population growth and scientific development. Progress in science and technology from the phase of industrial revolution resulted in increasing excavation of conventional fuels sources and the introduction of pharmaceuticals and agricultural chemicals have assisted in upgrading the living standard of people. Industrial processes, agricultural practices and the usage of chemicals in different areas has led to intentional or accidental discharge of chemicals into the environment (Harms et al., 2011). These released chemicals may have adversative health effects on living beings and environment (Valentin et al., 2013). The chemicals of concern are petroleum

hydrocarbons (aliphatic, aromatic, polycyclic aromatic hydrocarbons), BTEX (benzene, toluene, ethylbenzene, and xylenes), chlorinated hydrocarbons, nitroaromatic compounds, organophosphorus compounds, halogenated solvents, agricultural chemicals, heavy metals and metalloids (Megharaj et al., 2011). Chemicals like organochlorides and nitroaromatic compounds are intentionally manufactured, while the production and incineration of some other products, such as polyvinyl chloride (PVC) plastic lead to creation of unwanted lethal by–products. After these chemicals serve their purpose, they are generally released into the environment (soil, water and atmosphere). These persistent chemicals often end up in soil, or if passed through a water treatment plant, accumulate and sediment at the bottom of water bodies, thereby creating pollution in the environment (Valentin et al., 2013). Among the various toxic pollutants of global concern, polycyclic aromatic hydrocarbons (PAHs) occupy a special position due to their widespread occurrence in the ecosystem (Cachada et al., 2016) posing severe effects on terrestrial and aquatic ecosystem and human health (Majumdar et al., 2016).

## 1.2 Polycyclic aromatic hydrocarbons (PAHs)

PAHs belong to subset of a set of compounds identified as polycyclic organic matters (POM). These group of multiple ringed aromatic hydrocarbons are ubiquitous in the natural environment. The term “PAH” mostly signifies compounds comprising of carbon and hydrogen atoms. They are basically hydrocarbons formed by fusion of two or more benzene rings in linear, angular or clustered arrangements (Abdel–Shafy and Mansour, 2016). They are distributed in two classes: low molecular weight (LMW) compounds comprising of less than four rings and high molecular weight (HMW) compounds consisting of four or more rings. PAHs in pure form occur as

colourless, white/pale yellow–green solids, lipophilic in nature with high boiling and melting point and low vapour pressure (Kim et al., 2013). They are extremely recalcitrant compounds due to their hydrophobicity and molecular stability (Ortega–Calvo et al., 2013) and possess toxic, genotoxic, carcinogenic and/or mutagenic properties (Cerniglia, 1993; WHO, 1983). Because of these properties, the presence of PAHs in the eco– and biosphere is quite alarming. The rise in the number of aromatic rings in a PAH structure, indicates increase in the hydrophobicity, carcinogenic property, potential to bio–accumulate and resistance to degradation of the PAH. With an ever–increasing global awareness in the last few decades regarding the hazardous consequences of these contaminants on human health and ecosystem, studies on remediation and renovation of polluted environment have received great attention (Hong et al., 2016.). Based on abundance and toxicity, the United States Environmental Protection Agency (US EPA) has declared 16 PAHs as priority pollutants (Srogi, K., 2007; Agency for Toxic Substances and Disease Registry [ATSDR], 1990) which are enlisted in Fig. 1.1. PAHs that are probable carcinogens: chrysene, benzo(a)anthracene, benzo(a)pyrene (BaP), dibenzo(a,h)anthracene, benzo(b)fluoranthene, benzo(k)fluoranthene, indeno(1,2,3–c,d)pyrene and benzo(g,h,i) perylene. Several physicochemical properties and relevant information of the 16 priority PAHs are provided in Table 1.1.

### 1.2.1 Sources of PAHs

As depicted in Fig. 1.2, PAHs originate either naturally or anthropogenically. They are formed as by–products of natural and anthropogenic carbon combustion. Natural sources can form recalcitrant PAHs possessing toxic properties (Haritash and Kaushik, 2009).

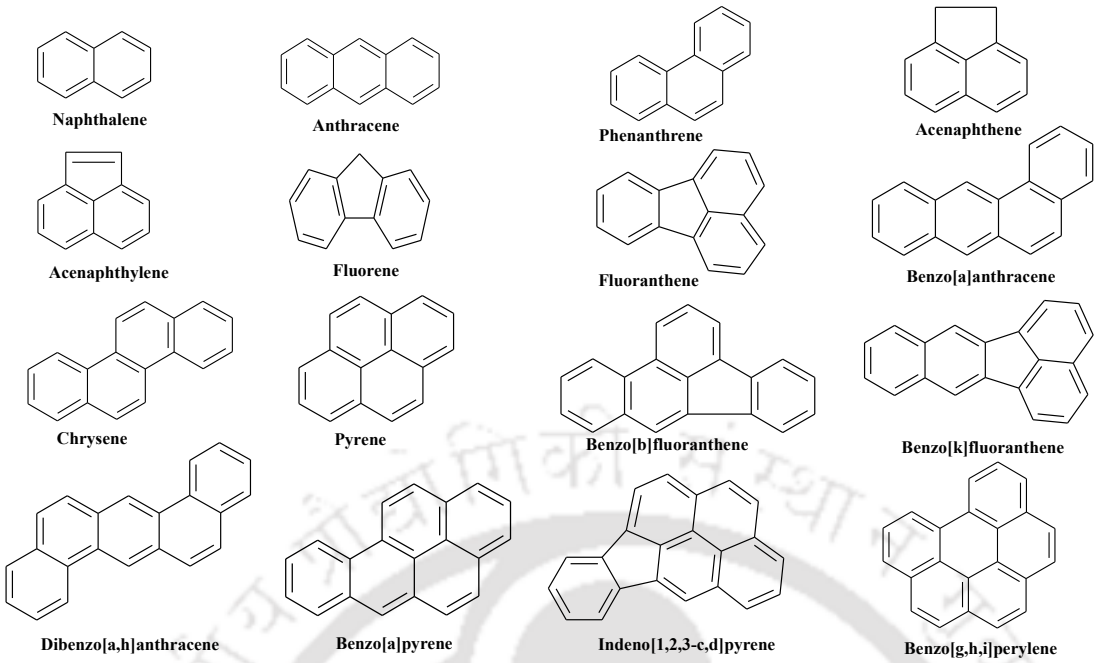


**Figure 1.1.** Structures of 16 PAHs enlisted as priority pollutants by US EPA.

Examples belonging to this category comprise: forest fires, volcanoes, hydrothermal processes, bacterial and plant reactions, petroleum leaks, erosion of sedimentary rocks comprising of petroleum hydrocarbons and vegetative decay. Anthropogenic sources include incomplete combustion like incinerators and industrial processes. PAHs originated from sources such as vehicle emissions, smoke from wood–burning stoves, cigarette and cigar smoke and smoked food also fall in this category. Other anthropogenic sources include sewage sludge, petroleum product spills, and tarry or creosote waste materials. It is rather essential to cite that incomplete combustion in any form has been recognised as the sole major contributor of PAHs in the environment (Lawal, 2017; Abdel–Shafy and Mansour, 2016). Nevertheless, anthropogenic contribution of PAHs in the ecosystem is higher than natural sources.

**Table 1.1.** Properties of 16 PAHs enlisted as priority pollutants by US EPA.

| Order | Name | CAS registry no. | Molecular formula | Molecular weight (g $mol^{-1}$) | Boiling point (°C) | Melting point (°C) | Vapor pressure (mmHg at 25°C) |
|---|---|---|---|---|---|---|---|
| 1 | Naphthalene | 91-20-3 | $C_{10}H_8$ | 128.1 | 218 | 80.2 | $8.5 \times 10^{-2}$ |
| 2 | Acenaphthene | 83-32-9 | $C_{12}H_{10}$ | 154.2 | 279 | 93.4 | $2.5 \times 10^{-3}$ |
| 3 | Acenaphthylene | 208-96-8 | $C_{12}H_8$ | 152.1 | 280 | 92.5 | $6.68 \times 10^{-3}$ |
| 4 | Anthracene | 120-12-7 | $C_{14}H_{10}$ | 178.2 | 342 | 218 | $6.53 \times 10^{-6}$ |
| 5 | Phenanthrene | 85-01-8 | $C_{14}H_{10}$ | 178.2 | 340 | 101 | $1.2 \times 10^{-4}$ |
| 6 | Fluorene | 86-73-7 | $C_{13}H_{10}$ | 166.2 | 295 | 116 | $6.0 \times 10^{-4}$ |
| 7 | Fluoranthene | 206-44-0 | $C_{16}H_{10}$ | 202.2 | 375 | 110.8 | $9.22 \times 10^{-6}$ |
| 8 | Benzo[a]anthracene | 56-55-3 | $C_{18}H_{12}$ | 228.3 | 438 | 158 | $4.11 \times 10^{-3}$ |
| 9 | Chrysene | 218-01-9 | $C_{18}H_{12}$ | 228.3 | 448 | 254 | $6.23 \times 10^{-9}$ |
| 10 | Pyrene | 129-00-00 | $C_{16}H_{10}$ | 202.2 | 404 | 151 | $4.5 \times 10^{-6}$ |
| 11 | Benzo[a]pyrene | 50-32-8 | $C_{20}H_{12}$ | 252.3 | 495 | 179 | $5.49 \times 10^{-9}$ |
| 12 | Benzo[b]fluoranthene | 205-99-2 | $C_{20}H_{12}$ | 252.3 | 481 | 168.3 | $5.0 \times 10^{-7}$ |
| 13 | Benzo[k]fluoranthene | 207-08-9 | $C_{20}H_{12}$ | 252.3 | 480 | 217 | $9.7 \times 10^{-10}$ |
| 14 | Dibenzo[a,h]anthracene | 53-70-3 | $C_{22}H_{14}$ | 278.3 | 524 | 269.5 | $9.55 \times 10^{-10}$ |
| 15 | Benzo[g,h,i]perylene | 191-24-2 | $C_{22}H_{12}$ | 276.3 | 550 | 278 | $1.0 \times 10^{-10}$ |
| 16 | Indenol[1,2,3-cd]pyrene | 193-39-5 | $C_{22}H_{12}$ | 276.3 | 536 | 163.6 | $1.25 \times 10^{-3}$ |

The most common regions of these pollutants are soil and waste proximate to oil refineries, gas plants, air bases, fuel stations and chemical industries (Shahsavari et al., 2019; Juhasz et al., 2005). From all the above–mentioned sources, PAHs are widely dispersed and detected as in air, soil, sediment, surface water and ground water. Natural and anthropogenic sources, combined with the global transport phenomena, leads to the widespread distribution resulting in dispersion of PAHs from the atmosphere to vegetation and in all other places leading to bioaccumulation in various food chains thereby posing serious threat to life and ecosystem (Ghosal et al., 2016; Wagrowski and Hites, 1997).

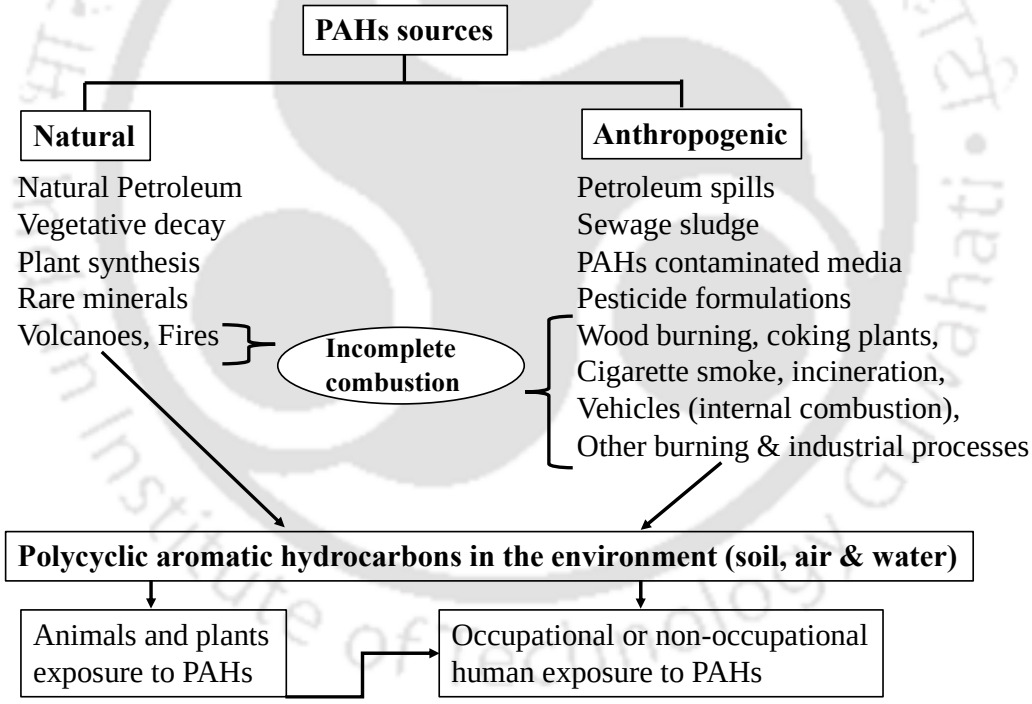


**Figure 1.2.** Sources of PAHs in the environment (Adopted from Abdel–Shafy and Mansour, 2016, Okonkwo et al., 2014).

### 1.2.2 PAHs exposure routes to humans

The main route of PAHs exposure among human population is through inhalation of smoke from cigarette and open fireplace or from consumption of food

having PAHs (ACGIH, 2005). Different types of PAHs released from tobacco smoke are carcinogenic to humans (Lannero et al., 2008). Food also can be polluted with PAHs through environmental sources (natural and mostly anthropogenic), food processing industries and household cooking practices. These pollutants enter into the food chain by deposition and transfer from air, water and soil (Chen and Chen, 2001). Various agricultural crops may produce PAHs or absorb them through soil, water or air (Ciecierska and Obiedzinski, 2013). Spread of PAHs is assisted by water that leaches out PAH content of soil, and enters into water bodies, or also from liquid discharges from industries or accidental spills during oil shipping. Besides, intake of PAHs may happen from polluted soil through ingestion, inhalation, or dermal exposure (Wang et al., 2012). Workforces (mechanics, street sellers, or automobile drivers) suffer from occupational exposure to PAHs by inhaling exhaust fumes and those working in mines, metal, or oil refining industries (See et al., 2006; Armstrong et al., 2004). Therefore, pathway of exposure to PAHs comprises of ingestion, inhalation, and dermal interaction in both occupational and non–occupational settings (Ravindra et al., 2008). Moreover, simultaneous exposures via numerous ways like dermal and inhalation exposures result in increase of the overall dose of absorbed PAHs.

### 1.2.3 Effects of PAHs exposure

Exposure to PAHs at different levels and from different occupations results in short term and long term health effects. These effects also differ according to the intensity, concentration, frequency, duration of contact, toxicity and the pathway of exposure (inhalation, ingestion, dermal) through which the pollutant absorbed (ACGIH, 2005). Exposures to high concentrations of pollutants comprising PAHs results in symptoms such as eye and skin irritation, vomiting, nausea, inflammation

etc. Naphthalene, anthracene and benzo(a)pyrene are direct skin irritants, while anthracene and benzo(a)pyrene are reported to be skin sensitizers in human beings and animals (Unwin et al., 2006). Various health troubles like lung, skin, bladder, and gastrointestinal cancers have been reported (Diggs et al., 2011; Olsson et al., 2010). Long–term exposure to PAHs like pyrene and BaP has been recognized to cause cancer in laboratory animals (Diggs et al., 2012). Exposure to PAHs also results in cataracts, liver and kidney damage. Various authors reported DNA damage due to PAH exposure (Garcia–Suastegui et al., 2010; John et al., 2009; Gunter et al., 2007). PAHs exposure for long time is supposed to elevate the threats of cell damage through gene mutation and cardiopulmonary mortality (Kuo et al., 2003). Fig. 1.3 portrays a simple flow chart linking impact on health due to short and long term exposure of PAHs.

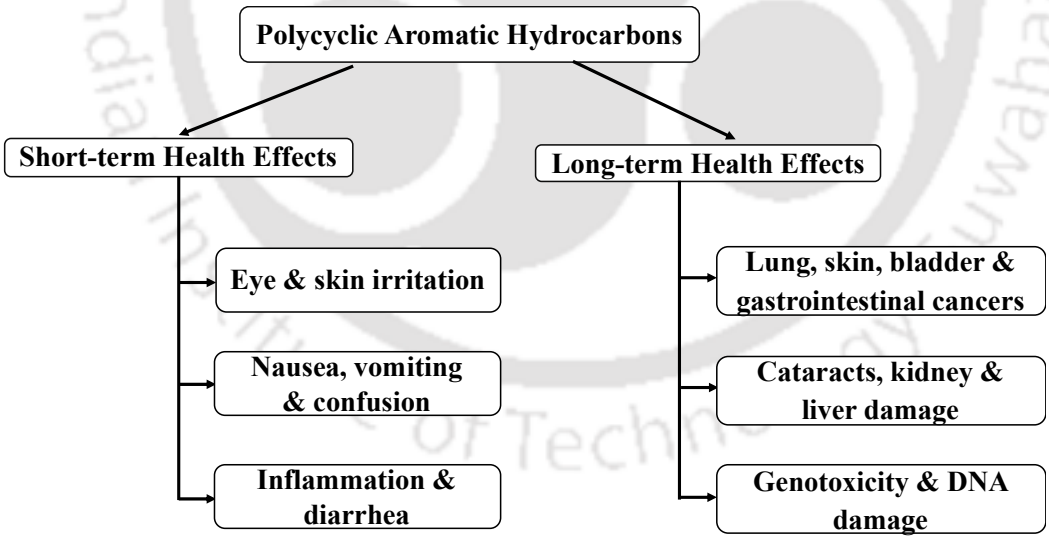


**Figure 1.3.** Short and long term health effects of exposure to PAHs (Adopted from Kim et al., 2013).

### 1.2.4 Removal of PAHs

PAHs are considered to be main pollutant of air, but soil and water are the ultimate depository of these pollutants. The fate of PAHs in the ecosystem involves: volatilization, photo–oxidation, biodegradation, chemical oxidation, adsorption to soil particles and leaching (Haritash and Kaushik, 2009). These pollutants do not degrade easily in natural conditions and their persistence enhances with higher molecular weight. Thus, they have become a matter of huge worry due to their extensive occurrence in the ecosystem. Their resistance to degradation, capacity of bio–accumulation and cancer–causing effects make these pollutants even more unsafe. Contact with these pollutants occurs through inhaling PAHs contaminated air, or from water, or soil of nearby hazardous waste sites, or via consuming polluted water or milk etc. (Albanese et al., 2014; Zhao et al., 2014).

The clean–up of PAHs polluted sites has been considered to be one of the critical issues of preventing/restoration of environmental damage. Several conventional remediation practises have been developed and studied to reduce the ever–increasing environmental pollution issue. Different treatment methods (physical and chemical) like incineration, base–catalyzed dechlorination, UV oxidation, solvent extraction etc. are already in practice (Varjani, 2017; Ghosal et al., 2016; Gan et al., 2009). Each of these treatments affects in different way depending on the PAHs physical, chemical and biological properties. Such traditional techniques possess limited efficiency, and are expensive as they involve excavation and transportation of contaminated materials. Moreover, these conventional practices, in several situations, do not destroy the pollutants entirely, but instead relocate them from one location or phase to another. These serious issues and limitations in decontamination have spurred researchers to devise alternative effective and environmental friendly clean–

up practice to fight pollution. Bioremediation is a green option that utilizes and manipulates the detoxification capabilities of microorganisms and plants to transform/eliminate toxic wastes into harmless products, often water and $CO_2$ (Macaulay and Rees, 2014; Niti et al., 2013; Bamforth and Singleton, 2005). Basically, it is an important tool for conversion of pollutants to less/non–hazardous form with relatively low energy and chemicals consumption. It mostly obviates the constraints and demerits of former physicochemical procedures by degrading/removing organic pollutants at low expense and in ambient conditions. Therefore, it has been widely adopted for removal of wide range of pollutants. It is a procedure that utilises microbes, green plants, fungi, or their enzymes to remove pollutants and make the environment free from contaminants (Mani and Kumar, 2014). Although bioremediation was known for decades, it is only in recent years that serious endeavours have been attempted to harness nature's own potential – with the purpose of environmental applications for inexpensive and effective protection of ecosystems (Abdel–Shafy and Mansour, 2016; Megharaj et al., 2011; Andreoni and Gianfreda, 2007). This progress has requisite of: (1) amalgamation of basic laboratory facilities to classify and characterize biological processes, (2) testing of different bioremediation technologies and pilot–scale development, (3) acceptance by regulators and people, and (4) on–site application to ensure their efficiency and safety.

## 1.3 Bioremediation of PAHs

Bioremediation technique has emerged as an efficient strategy for cleaning–up pollutants and has rightfully addressed the limitations associated with the conventional remediation processes. This process has been widely accepted by

environmentalists worldwide as it transforms the pollutants into less hazardous or non–hazardous forms. Abundant microorganisms: bacteria, fungi, or algae have capability to biodegrade PAHs (Luo et al., 2014). Both free cells and immobilized cells possess capability to degrade PAHs (Partovinia and Naeimpoor 2014). Biodegradation of these pollutants have been explored by various researchers (Rodriguez–Morgado et al., 2015; Biswas et al., 2015; Jiang et al., 2014; Haritash and Kaushik, 2009; Peng et al., 2008; Cerniglia 1993). The mechanism of this process involves breakdown of organic complexes through biotransformation into simpler metabolites, and through mineralization into inorganic minerals, $H_2O$, $CO_2$ (aerobic) or $CH_4$ (anaerobic). It occurs on the basis of: growth and co–metabolism. For growth, the pollutants are the sole carbon and energy source, resulting in a complete biodegradation of pollutants. Co–metabolism refers to the breakdown of pollutants in presence of a growth substrate which acts as the primary source of carbon and energy (Fritsche and Hofrichter, 2008). The PAH biodegradation rate is indirectly proportional to the number of aromatic rings existing in structure of a particular PAH; LMW PAHs are more readily degradable as compared to HMW PAHs. For the successful occurrence of biodegradation, various factors are responsible. The extent and rate of this process is dependent on numerous factors: temperature, pH, oxygen, microbe population, microbial acclimatization, nutrients, bioavailability, physicochemical properties of PAH, cellular transport properties and chemical partitioning in growth medium (Haritash and Kaushik, 2009). Biodegradation pathway is highly selective with specific pathway dependent on the type of microorganism involved.

Some of the hydrocarbon–degrading bacterial genera in environments that are worth mentioning include *Achromobacter, Acinetobacter, Alcaligenes, Arthrobacter,*

*Bacillus*, *Brevibacterium*, *Burkholderia*, *Collimonas*, *Corynebacterium*, *Flavobacterium*, *Gordonia*, *Micrococcus*, *Mycobacterium*, *Nocardia*, *Nocardioides*, *Ochrobactrum*, *Pseudomonas*, *Ralstonia*, *Rhodococcus*, *Sphingomonas* (Darmawan et al., 2015; Okai et al., 2015; Sun et al., 2014a; Hamamura et al., 2013; Mao et al., 2012; Arulazhagan and Vasudevan, 2011; Chikere et al., 2011; Kanaly and Harayama, 2010; Haritash and Kaushik, 2009; Cybulski et al., 2003; Kanaly and Harayama, 2000). Bacterial strains belonging to genera such as *Mycobacterium*, *Pseudomonas* and *Sphingomonas* have been reported to dominate biodegradation of PAHs in soil (Bisht et al., 2015). Some common fungi genera responsible for hydrocarbon degradation are: *Aspergillus*, *Candida*, *Cladosporium*, *Cunninghamella*, *Debaromyces*, *Fusarium*, *Irpex*, *Leucosporidium*, *Lodderomyces*, *Mucor*, *Phanerochaete*, *Pleurotus*, *Polyporus*, *Penicillium*, *Pichia*, *Rhodosporidium*, *Rhodotorula*, *Saccharomyces*, *Scopulariopsis*, *Sporidiobolus*, *Sporobolomyces*, *Stephanoascus*, *Trametes*, *Trichoderma*, *Trichosporon*, *Yarrowia* (Hashem et al., 2018; Hadibarata et al., 2017; Aranda, 2016; Jove et al., 2016; Okerentugba et al., 2016; Gargouri et al., 2015; Marco-Urrea et al., 2015; Mineki et al., 2015; Simister et al., 2015; Hadibarata and Kristanti, 2014; Harms et al., 2011; Kumari and Abraham., 2011; Passarini et al., 2011; Borras et al., 2010; Csutak et al., 2010; Hadibarata et al., 2009; Wu et al., 2009; Li et al., 2005).

### 1.3.1 Factors Affecting Biodegradation of PAHs

Microorganisms possess the potential to degrade several organic contaminants owing to their metabolic machinery and ability to adjust in hostile environments. This effectiveness has been mostly studied in ideal laboratory environment having neutral pH and ambient mesophilic temperature (Ghosal et al., 2016; Joutey et al., 2013). However, in real situation, bioremediation efficiency is dependent on the existence

and growth of microbial consortia adept in biodegrading organic pollutants and converting them to harmless products, and bioavailability of the pollutant to microbial attack. Different biotic as well as abiotic factors like (medium pH, temperature, oxygen level, moisture, nutritional, PAH concentrations, toxicity, etc.) either accelerate or inhibit the bioremediation process (Abel–Shafy and Mansour, 2016; Joutey et al., 2013; Ukiwe et al., 2013; Luo et al., 2012). Bioavailability of pollutants followed by contaminant mass transfer and subsequent metabolism are the major elements that regulate the entire bioremediation effectiveness, especially in cases of hydrophobic pollutants such as PAHs (Amodu et al., 2013; Mohan et al., 2006). Fig. 1.4 illustrates various factors influencing PAHs degradation.

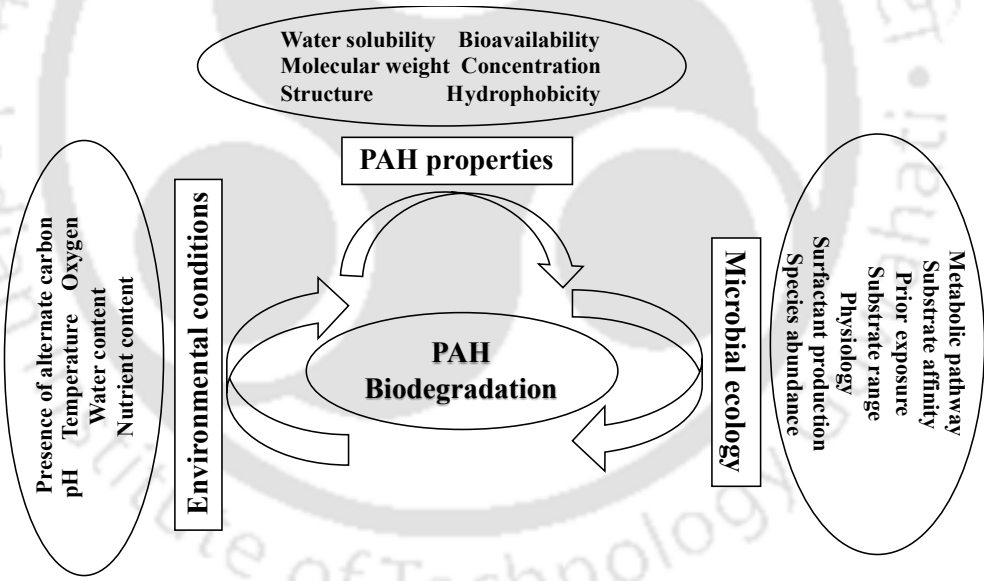


**Figure 1.4.** Biotic and abiotic factors influencing degradation of PAHs in environment (Adopted from Ghosal et al., 2016).

These factors affecting PAHs biodegradation can be classified in three major domains (Vidali, 2001)

A. PAH properties: physico–chemical properties (molecular weight, chemical structure, hydrophobicity), PAH concentration, associated bioavailability of the

pollutant for the microbial population, and hydrophobicity and toxic or inhibitory effects of the pollutant and their metabolites.

B. Environmental conditions: type of medium, organic and nutritional contents, salinity, temperature, pH, water content, presence of oxygen or other electron acceptor and presence of alternate carbon sources.

C. Microbial ecology: A particular microbial population having potential of degrading pollutants depends on type of species, population, distribution and prior exposure. Microbial species that exist in previously polluted sites possess the capability to metabolize PAHs at higher rates than microbes present in unpolluted sites. An acclimatisation phase is essential for microorganisms after contamination prior to the commencement of degradation process. During this particular phase, suitable microbial communities develop through growth and enzyme induction. The bioremediation efficiency is also largely governed by the metabolic pathway of degradation, potential of surfactant production, substrate affinity and substrate range.

### 1.3.2 Bacterial Degradation of PAHs

Bacteria belong to the class of microorganisms which have evolved billions of years ago and have developed strategies to obtain energy from everywhere by quick adaptability. Therefore, they are considered as nature's greatest scavengers. Bacteria have been largely used to remediate or degrade toxic environmental pollutants. Different bacterial species have been vigorously involved in biodegradation of organic contaminants such as PAHs. The metabolic pathways for bacterial degradation of PAHs, as represented in Fig. 1.5, have been very well documented and presented in numerous review articles (Shahsavari et al., 2019; Mallick et al., 2011; Seo et al., 2009; Cerniglia, 1993).

Predominantly, bacterial species favour aerobic conditions for degradation where the initial attack on hydrocarbons involves molecular oxygen as co–substrate. The enzymes in the metabolic pathways of alkanes are monooxygenases, whereas aromatic hydrocarbons are attacked by either monooxygenases or dioxygenases. The initial step in aerobic bacterial metabolism of PAHs is oxidation of the aromatic ring by dioxygenase enzymes to form *cis*–dihydrodiols. This initial enzymatic process is generally the rate limiting step in PAHs degradation process. Then re–aromatization of the aromatic nucleus occurs by the action of *cis*–dihydriol dehydrogenase to form dihydroxylated intermediates, which undergo further oxidation leading to catechol formation. The subsequent step is confirmation–dependent aromatic ring fission. When the hydroxyl groups of the dihydroxylated intermediates are in *ortho*–position, then cleavage is catalysed by intradiol (*ortho*) dioxygenase forming *cis*, *cis*–muconic acid. If the hydroxyl groups are in *meta*–position, cleavage occurs adjacent to hydroxyl groups by extradiol (*meta*) cleaving dioxygenase, thereby forming 2–hydroxymuconic semialdehyde (Mallick et al., 2011; Elliot et al., 2010). Ring cleavage results in the formation of succinic, fumaric, pyruvic, acetic acids and aldehydes, which are consumed by microbes for the synthesis of cellular constituents and energy. The by–products of this reaction are carbon dioxide and water. Bacteria can also degrade PAHs through cytochrome P450 enzyme system resulting in the production of *trans*–dihydrodiols and phenols (Moody et al., 2004).

### 1.3.3 Anaerobic PAHs Degradation

Though several PAHs are known to be degraded in aerobic conditions, anaerobic biodegradation of different pollutants including PAHs have been reported in previous works (Li et al., 2015; Aburto et al., 2009; Phelps et al., 2002) and reviewed (Aburto–Medina and Ball, 2015; Yang et al., 2013; Karthikeyan and

Bhandari, 2001). This can be considered a favourable substitute in soil bioremediation specially in subsurface and deep sediments and in situations of low soil porosity and air permeability (i.e., oil spills), where oxygen transfer in the system is problematic (Li et al., 2010a). PAH degradation in this condition is a time–consuming process in comparison to aerobic conditions and its mechanism has not yet been elucidated clearly (Sun et al., 2014b; Haritash and Kaushik, 2009). In this process, biodegradation occurs under sulfidogenic conditions which is followed by methanogenic and nitrate–reducing conditions (Fig. 1.5) (Chang et al., 2002). Li et al. (2015) reported that the PAHs degradation rates under anaerobic conditions are considerably boosted when inoculated with PAH–enriched microbial consortium. This lead to better microbial activity, resulting in faster and complete degradation with the half–lives of the target PAHs reduced considerably.

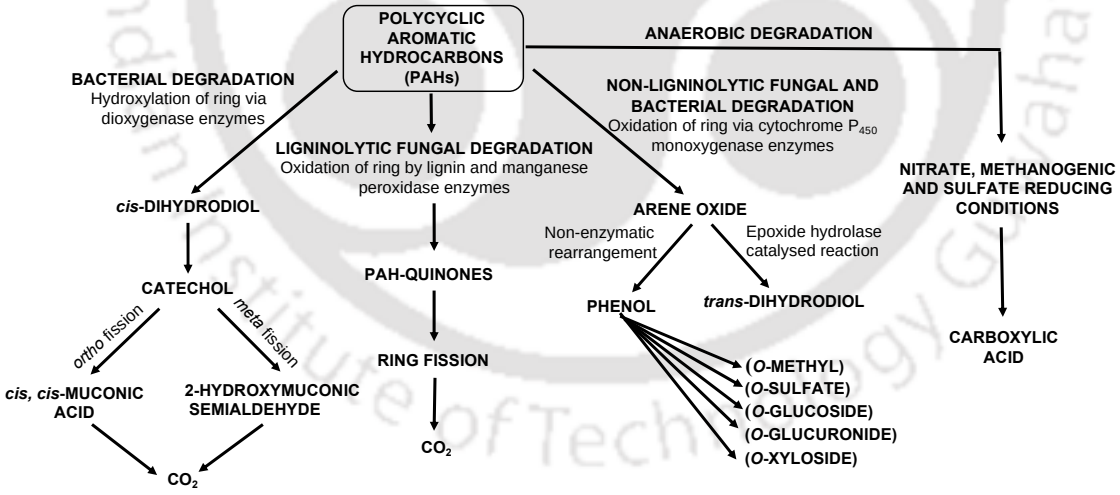


**Figure 1.5.** Major pathways for PAHs degradation by fungi and bacteria (Adopted from Shahsavari et al., 2019; Cerniglia & Sutherland, 2001).

### 1.3.4 Fungal Degradation of PAHs

Numerous studies have reported the potential of diverse fungal species for PAH biodegradation and mineralization (Cerniglia and Sutherland, 2010). Fungi

possess both biochemical and ecological potential to degrade organic pollutants making them a promising species for bioremediation. In conditions of bacterial malfunction such as over–polluted and too acidic habitats, pollutants are physically inaccessible to unicellular organisms or complex xenobiotic structures, and in such cases, fungal remediation can be a promising alternative. PAHs transformation by fungi comprises of numerous enzymatic routes and is mainly dependent on the type of species and environment for growth. Fungi which are responsible for PAHs degradation falls in two categories: (1) non–ligninolytic and (2) ligninolytic fungi or white–rot fungi. Non–ligninolytic fungi produces cytochrome P450 monoxygenase enzyme for degradation, while ligninolytic fungi produces extracellular enzymes for catabolism. These enzymes are nonspecific and oxidize a broad range of organic complexes (Li et al., 2010b; Peng et al., 2008; Tortella et al., 2005). Although ligninolytic fungi possess remarkable biochemical qualities, they cannot compete in the natural environment because of their requirement of ligninolytic conditions to secrete their enzymes and lignocellulosic substrates. Therefore, the application of wood–inhabiting fungi in remediation of polluted soil environments turns out to be challenging and resulted in poor success (Harms et al., 2011; Baldrian, 2008).

#### 1.3.4.1 PAHs catabolism by ligninolytic fungi

Ligninolytic fungi, also recognised as white–rot fungi have been investigated for their PAH–degradation potential (Verma et al., 2007). These fungi have widespread application in the field of bioremediation because of their ability to entirely mineralize PAHs to water and carbon dioxide (Cerniglia and Sutherland, 2010). They secrete extracellular enzymes with considerably low substrate specificity, making them apt for degradation of lignin and other organic complexes (Haritash and Kaushik, 2009). Moreover, they can also degrade individual PAHs and their complex

mixtures (Pozdnyakova, 2012). Ligninolytic enzymes are basically of two types: laccases and peroxidases. Depending on the type of substrate, peroxidase enzymes are further classified into: lignin peroxidase and manganese peroxidase. These enzymes oxidise the PAHs by producing hydroxyl free radicals, resulting in formation of PAH–quinones as shown in Fig. 1.5. These quinones further undergo ring fission leading to complete mineralization of PAHs. Thus, these fungi and their extracellular enzymes degrade PAHs with their low substrate specificity and ability to diffuse into sediment or soil matrix. They have the ability of degrading highly recalcitrant compounds (Bamforth and Singleton, 2005).

**1.3.4.2 PAHs catabolism by non–ligninolytic fungi**

The metabolic pathway of PAHs degradation followed by non–ligninolytic fungi is analogous to that of mammals. Cytochrome P450 belongs to protein superfamily– hemoprotein, capable of catalysing hydroxylation, monooxygenation and epoxidation reactions. In fungi, these enzymes have a pivotal function in metabolite biosynthesis during degradation and detoxification of xenobiotic compounds (Aranda, 2016). In the case of non–ligninolytic fungi, initial oxidation of PAHs takes place through cytochrome P450 monooxygenase enzymes which catalyses a ring epoxidation, thereby forming unstable arene oxides, which are initial products of PAH metabolism (Cerniglia and Sutherland, 2010). The resultant arene oxide intermediate is carcinogenic which undergoes further hydrolysis by epoxide hydrolase to form their corresponding *trans*–dihydrodiols or undergo non–enzymatic reactions resulting in phenols which can subsequently form many conjugates of sulfate, glucose, xylose or glucuronic acid (Fig. 1.5). In living creatures that utilise cytochrome P450 system for biodegradation, *trans*–dihydrodiol cannot be consumed further as a source of energy (Pozdnyakova, 2012). However, it is more soluble and

potentially accessible for bacterial biodegradation (Al–Turki, 2009). Thus, along with bacteria, both yeasts and fungi can also be explored as valuable endeavour for bioremediation in places polluted with PAHs. The ability of yeasts to utilise n–alkanes as carbon source is facilitated by the presence of multiple microsomal cytochrome P450 family CYP52. These enzymes are reported to be present in several yeasts such as *Candida maltosa*, *Candida tropicalis*, *Candida apicola* and *Yarrowia lipolytica* (Hanano et al., 2014). Two categories of CYP450 are responsible in this catabolic pathway: (1) CYP450–ALKs: involved in aliphatic hydrocarbons (n–alkanes) catabolism leading to terminal oxidation of n–alkanes to fatty alcohols, and (2) Non–characterized epoxide/ hydroxy–forming CYP450s, which catalyse the oxygenation of PAHs. Moreover, yeasts with dimorphic behaviour possess an additional benefit for application in hydrocarbon remediation (Priya et al., 2016). Therefore, yeasts can be considered as a potent candidate for the study of PAHs bioremediation.

## 1.4 Literature review on pollutant biodegradation by different *Candida* sp.

As mentioned earlier, non–ligninolyitc fungi might possess certain advantages over other microbes with respect to biodegradation owing to their tolerance towards pollutants, ability of penetration in soil through mycelia and fast colonization in solid substrates (Harms et al., 2011). These types of fungi undoubtedly possess great potential in the field of bioremediation of organic pollutants. Although various studies have been conducted to study the degradation potential, pathway and metabolites formed during bioremediation of pollutants by non–ligninolytic fungi, there is not enough literature in support of the theories about the PAH biodegradation ability of these type of fungi. Numerous filamentous fungi have been identified to degrade

organic pollutants owing to their rapid growth and resistance to adverse environmental conditions. *Candida* sp. is one of the prominent fungi recognised for its xenobiotic degradation potential. Various researchers have reported its capability to degrade petroleum hydrocarbons, phenols, PAHs etc. The ability of this fungi to degrade pollutants mainly depends on their capacity to secrete specific enzymes (Hadibarata et al., 2007; Wang et al., 2007). Table 1.2 presents a literature review on biodegradation studies of different pollutants by various *Candida* sp. strains. It was observed that *Candida* strains degraded a wide range of pollutants at different initial concentrations using a variety of degradation media. Researchers have studied the capability of *Candida tropicalis* strain to degrade phenolic pollutants such as phenol, m–cresol and 4–chlorophenol at different initial concentration of pollutant and have achieved almost 100% degradation within a duration of 2–3 days (de Silva et al., 2019; Basak et al., 2014; Wang et al., 2011; Jiang et al., 2007; Yan et al., 2006 and Yan et al., 2005). From the above–mentioned works, it can be concluded that phenols being comparatively simple structured pollutants are easily degraded and consumed by microbes as sole carbon source in shorter duration in mineral salt medium. Rigo and his co–workers investigated the degradation of catechol by yeast, *Candida parapsilopsis* in standard medium and found that longer lag period was caused due to high catechol concentration. The yeast could totally biodegrade a concentration of 910 mg $L^{-1}$ in a duration of 48 h (Rigo et al., 2010). Total petroleum hydrocarbon (TPH) degradation was also studied using strains *Candida digboiensis* and *Candida tropicalis*. Sood et al. (2010) employed *Candida digboiensis* TERI ASN6 in corn cob powder medium with peptone and yeast extract to degrade TPH, and achieved ~ 95% degradation in 175 days. Fan et al. (2014) could degrade 83% TPH by *Candida tropicalis* SK21 in Bushnell–Haas (BH) medium in 180 days. Degradation of crude

petroleum oil and n–hexadecane was also successfully performed using different *Candida* sp. strains within 3–4 days (Priya et al., 2016; Farag and Soliman, 2011; Zeng et al., 2011). *Candida viswanathii* KA–2011 strain was found to effectively biodegrade lubricating and diesel oils (58.6 and 93.9%, respectively) in mineral salt medium at 6% salt concentration within 4 days (Ramadan et al., 2012). Biodegradation of PAHs is not an easy process owing to their complex ring structures and hydrophobic nature. Increasing number of aromatic rings in PAH structure leads to rise in hydrophobicity, carcinogenic properties, and potential to bio–accumulate and resistance to degradation. Hesham et al. (2009) have studied the biodegradation of phenanthrene using *Candida viswanathii* and found that the yeast had the capability to degrade both LMW and HMW PAHs (naphthalene: 89.76%, phenanthrene: 77.21%, pyrene: 60.77% and benzo(a)pyrene: 55.53%) at the end of 10 days. *Candida digboiensis* TERI ASN6 was used to perform pyrene biodegradation in mineral salt medium (MSM) with yeast extract and a low output of 15% was achieved in 10 days (Sood et al., 2010), whereas *Candida tropicals* degraded 67% pyrene in 4 days in glucose–potato medium (Wang et al., 2007). This mainly occurred due to the presence of additional carbon source in the medium in the later study. Both Priya et al. (2016) and Farag and Soliman (2011) studied PAHs degradation (naphthalene, phenanthrene and pyrene) by using *Candida* sp. strains in sea water as the medium and achieved a considerable amount of degradation, signifying that the strain is a potent candidate for PAHs degradation. 75% pyrene degradation was achieved by using *Candida* sp. S1 with 24 g $L^{-1}$ of NaCl. The extent of degradation decreased with increasing salinity (Hadibarata et al., 2017).

**Table 1.2.** Literature review on different pollutant degradation by various *Candida* sp. strains.

| Strain | Pollutant | Degradation medium | Initial conc. | Time of degradation | Degradation | Reference |
|---|---|---|---|---|---|---|
| *Candida tropicalis* | Phenol | Mineral salt medium (MSM) | 2000 mg $L^{-1}$ | 66 h | 100% | Yan et al., 2005 |
| *Candida tropicalis* | Phenol<br>*m*-cresol | Mineral salt medium (MSM) | 2000 mg $L^{-1}$<br>280 mg $L^{-1}$ | 66 h<br>52 h | 100% | Yan et al., 2006 |
| *Candida tropicalis* | Phenol<br>4-chlorophenol | Mineral salt medium (MSM) | 2000 mg $L^{-1}$<br>350 mg $L^{-1}$ | 66 h<br>55 h | 100% | Jiang et al., 2007 |
| *Candida tropicals* Y 219 + Y 220 | Pyrene | 2% glucose + 0.3% leavening + 20% potato | 100 mg $kg^{-1}$ | 4 days | 67% | Wang et al., 2007 |
| *Candida viswanathii* | Naphthalene<br>Phenanthrene<br>Pyrene<br>Benzo(a)pyrene | Basal medium (BM) + 0.5 g yeast extract | 1.79 mg $kg^{-1}$<br>1.89 mg $kg^{-1}$<br>1.96 mg $kg^{-1}$<br>1.98 mg $kg^{-1}$ | 10 days | 89.76%<br>77.21%<br>60.77%<br>55.53% | Hesham et al., 2009 |
| *Candida parapsilopsis* | Catechol | Standard medium | 910 mg $L^{-1}$ | 48 h | 100% | Rigo et al., 2010 |
| *Candida digboiensis* TERI ASN6 | Pyrene | Mineral salt medium (MSM) + yeast extract | 5 mg | 10 days | 0.75 mg | Sood et al., 2010 |
| | Total petroleum hydrocarbons (TPH) | Corn cob powder + yeast extract + peptone | 184.06 g $kg^{-1}$ | 175 days | 176.10 g $kg^{-1}$ | |

**Table 1.2.** (*continued…*)

| Strain | Pollutant | Degradation medium | Initial conc. | Time of degradation | Degradation | Reference |
|---|---|---|---|---|---|---|
| *Candida tropicalis* | Petroleum crude oil | Natural sea water (NSW) + 0.5% yeast extract | 0.5 % | 72 h | 7.7% | Farag and Soliman, 2011 |
| | Phenol<br>Naphthalene<br>Phenanthrene | Natural sea water (NSW) | 500 mg $L^{-1}$ | 3 days | 53.6%<br>97.85 %<br>22% | |
| *Candida tropicalis* JH8 | Phenol | Mineral salt medium (MSM) | 1800 mg $L^{-1}$ | 62 h | 100% | Wang et al., 2011 |
| *Candida tropicalis* | n-hexadecane | Mineral salt medium (MSM) + monoRL | 500 mg $L^{-1}$ | 96 h | 93.1% | Zeng et al., 2011 |
| *Candida viswanathii* KA-2011 | Diesel oil<br>Lubricating oil | Mineral salt medium (MSM) + 6% NaCl | 5 mL<br>2 mL | 4 days | 93.9%<br>58.6% | Ramadan et al., 2012 |
| *Candida tropicalis* PHB5 | Phenol | Mineral salt medium (MSM) | 2400 mg $L^{-1}$ | 48 h | 99.4% | Basak et al., 2014 |
| *Candida tropicalis* SK21 | Total petroleum hydrocarbons (TPH) | Bushnell-Haas (BH) medium | 16300 mg $kg^{-1}$ | 180 days | 83% | Fan et al., 2014 |
| *Candida vishwanathii* TERI MS1 | Petroleum crude oil<br>Pyrene<br>Naphthalene | Sea water | 1 % (w/v)<br>0.1% (w/v)<br>0.1% (w/v) | 72 h | 49%<br>83%<br>69% | Priya et al., 2016 |
| *Candida* sp. S1 | Pyrene | Mineral extract broth (MEB) + NaCl | 20 mg $L^{-1}$ | 15 days | 75% | Hadibarata et al., 2017 |
| *Candida tropicalis* NN4 | Indeno(1,2,3-cd) pyrene | Minimal salt medium + NaCl + Fe nanoparticles | 1 mg $L^{-1}$ | 15 days | 90.68% | Ojha et al., 2019 |
| *Candida tropicalis* ATCC 750 | Phenol | Inorganic medium | 1100 mg $L^{-1}$ | 72 h | 99.97% | Silva et al., 2019 |

Ojha and her colleagues attempted degradation of 1 mg $L^{-1}$ indeno(1,2,3–c,d) pyrene (InP) in minimal salt medium by using *Candida tropicalis* NN4 and achieved ~90% degradation in 15 days (Ojha et al., 2019). These results demonstrated possible application of the yeast for bioremediation of InP–polluted locations. From this literature, it is evident that further research and in–depth study is required in the field of bioremediation by using *Candida* sp. strains, especially in biodegradation of ubiquitous PAHs. Such studies could shed light on the degradation potential of fungi in pollutant biotransformation, thereby facilitating an effective application of non–ligninolyitc fungi in bioremediation.

## 1.5 Literature review on phenanthrene degradation using different microbial strains

Phenanthrene, a LMW PAH comprising of three benzene rings in an angular manner, is a widespread and typical representative of this genre of pollutants. Its molecular structure comprises of bay– and K– regions, which allows the formation of epoxides, indicating it to be a carcinogen (Huang et al., 2016). Thus, phenanthrene is studied as a model compound to investigate the catabolism of carcinogenic PAHs. As mentioned earlier, the compound is also on the priority pollutants list given by US EPA and is known for its harmful effects on human health and environment (Hadibarata and Tachibana, 2010). Various studies have been conducted to study the phenanthrene degradation pattern and pathway by using different microbial species. Any biodegradation process is regulated by numerous factors like pH, temperature, agitation, initial concentration of pollutant, degradation medium and carbon source (Csutak et al., 2010). Table 1.3 represents literature review on phenanthrene degradation using different microbial strains. Hesham and his co–workers (Hesham et

al., 2009) have studied the biodegradation of phenanthrene using *Candida viswanathii* and obtained a degradation of 77% in 10 days. They used phenanthrene and glucose as carbon source, along with Tween 80 to increase the bioavailability of pollutant to the yeast. In another work (Farag and Soliman, 2011), the biodegradation potential of *Candida tropicalis* strain was analysed using phenanthrene as sole carbon source and a biodegradation of 22% was attained within 3 days at neutral pH. Another non–ligninolytic fungi, *Fusarium solani* has been reported in the work of Hesham et al., 2017 to degrade phenanthrene upto 40% in 10 days. The medium contained phenanthrene as carbon source along with Tween 80 to facilitate degradation. Ligninolytic fungi such as *Trametes hirsute* and *Polyporus* sp. are also known to degrade phenanthrene from the works of Hidayat and Yanto, 2018 and Hadibarata and Tachibana, 2010. Phenanthrene was efficiently degraded with Tween 80 in the degradation medium in a time period of 15–30 days. This indicated that it is somewhat difficult to biodegrade phenanthrene when it is present as sole carbon source in the medium. Pan and his colleagues (Pan et al., 2004) reported phenanthrene biodegradation of upto 60% by *Pichia anomala*. Halotolerant yeast like *Hortaea* sp. has also been reported to degrade 100% phenanthrene in 6 days (Kristanti et al., 2018). Both these works degraded phenanthrene with aid of surfactant. Some additional nutrient or booster is needed to facilitate the degradation of phenanthrene. Acevedo and his collagenous investigated the PAHs degradation potential of ligninolytic fungus, *Anthracophyllum discolour*. The white–rot fungus was able to biodegrade phenanthrene in Kirk medium with the highest removal of ~ 23% within 28 days at nearly neutral pH. The phenanthrene removal efficiency enhanced upto 62% when inoculated in autoclaved soil (Acevedo et al., 2011). The fungus, *Acremonium* sp. P0997 displayed good potential of phenanthrene degradation in the

work portrayed by Ma et al., 2014. Removal capacity for phenanthrene was ~ 90% and the strain also displayed reasonable resistance towards heavy metals indicating fungal bioremediation of organic contaminants in metal–organic mixed polluted sites. Another study aimed to investigate the phenanthrene metabolic mechanism and bioremediation capability by *Phomopsis liquidambari*. The fungal strain was able to grow on the pollutant, and ~ 77% of initial 50 mg $L^{-1}$ phenanthrene was removed after 10 days (Fu et al., 2018). Bacterial strains belonging to *Pseudomonas* genus are recognized as pollutant degraders and have been extensively used to degrade PAHs. Previous authors have reported that this particular bacterial strain possesses the potential to degrade 80–98% phenanthrene at neutral pH at different initial concentrations (Ma et al., 2018; Chebbi et al., 2017; Singh and Tiwary, 2017; Lin et al., 2014; Zhao et al., 2009). To improve the biodegradation efficiency, microbial consortia were also constructed and studied. Mnif and co–workers have studied phenanthrene degradation by halotolerant bacterial consortium comprising of two major species belonging to genera *Pseudomonas* and *Staphylococcus* (Mnif et al., 2017). They have achieved complete degradation of 200 mg $L^{-1}$ phenanthrene within 10 days in presence salinity and at neutral pH. Other bacterial species of varied community such as *Klebsiella* sp., *Achromobacter* sp., *Massilia* sp., *Rhizobium* sp., *Achromobacter* sp., *Stenotrophomonas* sp. have also been described to efficiently degrade phenanthrene as sole carbon source or with additional supplements (Hou et al., 2018; Arulazhagan et al., 2017; Li et al., 2017; Huang et al., 2016; Wang et al., 2016; Hassan et al., 2015).

**Table 1.3.** Literature review on phenanthrene degradation using different microbial strains.

| Microbial strain | Carbon source | Degradation medium | Initial conc. | Process parameters | Degradation | Reference |
|---|---|---|---|---|---|---|
| *Pichia anomala* | Phenanthrene + Tween 80 | Basal medium | 5.20 mg $L^{-1}$ | Temperature = 27°C<br>Agitation = 150 rpm<br>Time = 96 h | 3.10 mg $L^{-1}$ | Pan et al., 2004 |
| *Candida viswanathii* | Phenanthrene + 50 g Tween 80 + 10 g glucose | Basal medium (BM) + 0.5g yeast extract | 1.89 mg $kg^{-1}$ | pH = 5.0-6.0<br>Temperature = 27°C<br>Agitation = 150 rpm<br>Time = 10 days | 77.21% | Hesham et al., 2009 |
| *Pseudomonas stutzeri* ZP2 | Phenanthrene | Mineral salt medium (MSM) | 250 mg $L^{-1}$ | pH = 8.0<br>Temperature = 37°C<br>Agitation = 180 rpm<br>Time = 6 days | 96% | Zhao et al., 2009 |
| *Polyporus* sp. S133 | Phenanthrene + Tween 80 | Mineral salt broth (MSB) | 1 mmol $L^{-1}$ | Temperature = 25°C<br>Agitation = 120 rpm<br>Time = 30 days | 92% | Hadibarata and Tachibana, 2010 |
| *Anthracophyllum discolor* | Phenanthrene + Tween 80 (0.05% v/v) | Kirk medium | 50 mg $L^{-1}$ | pH = 6.6<br>Temperature = 30°C<br>Time = 28 days | 22.6% | Acevedo et al., 2011 |
| *Candida tropicalis* | Phenanthrene | Natural sea water (NSW) medium | 500 mg $L^{-1}$ | pH = 7.0<br>Temperature = 30°C<br>Agitation = 200 rpm<br>Time = 3 days | 22% | Farag and Soliman, 2011 |
| *Pseudomonas* sp. BZ-3 | Phenanthrene | Mineral salt medium (MSM) + 20 g $L^{-1}$ salinity | 50 mg $L^{-1}$ | pH = 7.0<br>Temperature = 30°C<br>Agitation = 180 rpm<br>Time = 7 days | 75% | Lin et al., 2014 |
| *Acremonium* sp. P0997 | Phenanthrene | Mineral medium | 500 mg $L^{-1}$ | pH = 6.5<br>Temperature = 28°C<br>Agitation = 160 rpm<br>Time = 15 days | 89.9% | Ma et al., 2014 |

**Table 1.3.** (*continued…*)

| Microbial strain | Carbon source | Degradation medium | Initial conc. | Process parameters | Degradation | Reference |
|---|---|---|---|---|---|---|
| *Klebsiella* sp. | Phenanthrene | Bushenll-Haas (BH) medium | 400 mg $L^{-1}$ | pH = 9.0<br>Temperature = 35°C<br>Agitation = 150 rpm<br>Time = 3 days | 84.9% | Hassan et al., 2015 |
| *Rhizobium petrolearium* SL-1 | Phenanthrene | Mineral salt medium (MSM) + 0.02 % salinity | 100 mg $L^{-1}$ | pH = 7.0<br>Temperature = 30°C<br>Agitation = 150 rpm<br>Time = 21 days | 100% | Huang et al., 2016 |
| *Cupriavidus* sp. MTS-7 | Phenanthrene | M9 medium | 150 mg $L^{-1}$ | pH = 7.0<br>Temperature = 25°C<br>Agitation = 175 rpm<br>Time = 4 days | 100% | Kuppusamy et al., 2016 |
| *Massilia* sp. WF1 | Phenanthrene | Mineral salt medium (MSM) | 100 mg $L^{-1}$ | pH = 6.0<br>Temperature = 28°C<br>Agitation = 130 rpm<br>Time = 2 days | 100 mg $L^{-1}$ | Wang et al., 2016 |
| *Stenotrophomonas maltophilia* AJH1 | Phenanthrene | Acidophilic mineral salt medium (AMSM) | 500 mg $L^{-1}$ | pH = 2.0<br>Temperature = 30°C<br>Agitation = 150 rpm<br>Time = 10 days | 82% | Arulazhagan et al., 2017 |
| *Pseudomonas* sp. W10 | Phenanthrene | Basal medium (BM) | 200 mg $L^{-1}$ | pH = 7.0<br>Temperature = 37°C<br>Agitation = 180 rpm<br>Time = 30 days | 80% | Chebbi et al., 2017 |
| *Fusarium solani* | Phenanthrene + Tween 80 (50g) | Mineral basal salt | 6.55 mg $kg^{-1}$ | Temperature = 27°C<br>Agitation = 150 rpm<br>Time = 10 days | 40.09% | Hesham et al., 2017 |

**Table. 1.3.** (*continued…*)

| Microbial strain | Carbon source | Degradation medium | Initial conc. | Process parameters | Degradation | Reference |
|---|---|---|---|---|---|---|
| *Achromobacter* sp. LH-1 | Phenanthrene | Mineral salt medium (MSM) | 100 mg $L^{-1}$ | pH = 7.2<br>Temperature = 33.2°C<br>Time = 5 days | 92.3% | Li et al., 2017 |
| *Pseudomonas* sp. & *Staphylococcus* sp. | Phenanthrene | Basal medium + 10 g $L^{-1}$ NaCl | 200 mg $L^{-1}$ | pH = 7.0<br>Temperature = 37°C<br>Agitation = 150 rpm<br>Time = 10 days | 100% | Mnif et al, 2017 |
| *Pseudomonas stutzeri* P2 | Phenanthrene | Carbon-free mineral medium (CFMM) | 1000 mg $L^{-1}$ | pH = 7.0<br>Temperature = 30°C<br>Agitation = 150 rpm<br>Time = 7 days | 98% | Singh and Tiwary, 2017 |
| *Achromobacter* sp. LH1 | Phenanthrene | Mineral salt medium (MSM) | 100 mg $L^{-1}$ | Temperature = 30°C<br>Agitation = 150 g | 94% | Hou et al., 2018 |
| *Trametes hirsuta* D7 | Phenanthrene + 1% Tween 80 | Mineral salt broth (MSB) | 0.056 mM | Temperature = 25°C<br>Time = 15 days | 71.73% | Hidayat and Yanto, 2018 |
| *Phomopsis liquidambari* | Phenanthrene | Mineral salt medium (MSM) | 50 mg $L^{-1}$ | Temperature = 28°C<br>Agitation = 180 rpm<br>Time = 10 days | 77.38% | Fu et al., 2018 |
| *Hortaea* sp. B15 | Phenanthrene + Tween 80 | Mineral liquid medium | 100 mg $L^{-1}$ | pH = 8.0<br>Temperature = 37°C<br>Agitation = 120 rpm<br>Time = 6 days | 100% | Kristanti et al., 2018 |
| *Pseudomonas* sp. Ph6 | Phenanthrene + Rhamnolipid (100 mg $L^{-1}$) | Mineral salt medium with yeast extracts (MSMY) | 50 mg $L^{-1}$ | Temperature = 30°C<br>Agitation = 150 rpm<br>Time = 14 days | 99.5% | Ma et al., 2018 |
| *Burkholderia fungorum* FM-2 | Phenanthrene | Minimal medium (MM) + 0.5 % (w/v) salinity | 300 mg $L^{-1}$ | pH = 7.0<br>Temperature = 25°C<br>Agitation = 200 rpm<br>Time = 3 days | 85.71% | Liu et al., 2019 |

Some of the bacterial species such as *Cupriavidus* sp., *Pseudomonas* sp. and *Burkholderia* sp. also showed heavy metal tolerance apart from efficient degradation of phenanthrene at pH 7 within 3–4 days (Liu et al., 2019; Singh et al., 2017; Kuppuswamy et al., 2016). This literature clearly demonstrates the potential of non-ligninolytic fungi for bioremediation, and thus also justify further study and research in the areas such as metabolism mechanism.

## 1.6 Literature review on pyrene degradation using different microbial strains

HMW PAHs exhibit greater resistance to biodegradation owing to their complex structure, low bioavailability and hydrophobic nature. The pollutant pyrene belongs to the class of peri–condensed 4–ring HMW PAH and is a priority pollutant as listed by US EPA. It is highly toxic with evidence of harmful effects on humans and ecosystem (Hadibarata et al., 2017). Moreover, the pollutant is also a signature compound for the degradation study of carcinogenic HMW PAHs (benzo(a)pyrene) because of its structural similarity (Kamyabi et al., 2018). Therefore, due to its toxic properties and xenobiotic characteristic, it is very essential to remove this PAH from environment. Various researchers have explored pyrene biodegradation using different microbial strains at different operating conditions. Table 1.4 presents literature review on pyrene degradation by different microbial strains. Among the various microbes mentioned in the Table, yeasts belonging to *Candida* sp. such as *C. tropicalis*, *C. vishwanathii* and *C. digboiensis* have been reported to biodegrade pyrene effectively by several authors (Hadibarata et al., 2017; Priya et al., 2016; Sood et al., 2010; Hesham et al., 2009; Wang et al., 2007). The results of both Wang et al. (2007) and Hesham et al. (2009) indicate that *Candida* sp. can degrade 60–65% pyrene when supplemented with additional carbon source. The strain TERI ASN6

was not capable of consuming pyrene as sole carbon source and degraded only 15% pyrene in MSM with yeast extract in acidic pH (Sood et al., 2010). Both Priya et al. (2016) and Hadibarata et al. (2017) worked on finding microbial strains that were sufficiently robust to withstand the rough nature of sea environment. They reported that this genre of species has been reported to be halotolerant in nature and as a result it adapts to conditions of higher salinity, and can grow in marine environment (Hadibarata et al., 2017; Priya et al., 2016). This trait of the yeast is advantageous since PAHs also exist in saline waste water or sea water. Moreover, most of the work on pyrene biodegradation by *Candida* sp. has been done with the aid of surfactants or additional nutritional supplements. Yeasts like *Basidioascus persicus* and *Hortaea* sp. possessing halotolerant nature have also been reported to degrade ~80–90% pyrene in ~20–25 days when supplemented with surfactant and salinity (Farraj et al., 2019; Kamyabi et al., 2018). Ligninolytic fungi, *Trichoderma* sp. has also been able to degrade 78% pyrene in 15 days when the culture conditions were fixed at 100 mg $L^{-1}$ initial pyrene concentration, pH 5 at 27°C with Tween 80 in the medium (Al Farraj et al., 2020). Oleaginous yeasts like *Cryptococcus psychrotolerans* have been reported to entirely degrade pyrene within 6 days with the aid of glucose as additional carbon source. Both substrates, viz. glucose and pyrene, were consumed simultaneously by the yeast (Deeba et al., 2018). Another ligninolytic fungus, *Anthracophyllum discolour*, was investigated for pyrene degradation capability both in liquid medium and in soil. It was found that the strain could transform only 8.5% pyrene in Kirk medium in neutral pH and 60% pyrene in autoclaved soil, indicating its capacity to grow rigorously in autoclaved soil. In non–autoclaved soil, the inoculation with the fungus did not lead to efficient removal of pyrene due to the existence of indigenous soil microorganisms (Acevedo et al., 2011).

Apart from fungi and yeasts, a wide range of bacterial species have also been investigated to study and explore their degradation capabilities. *Pseudomonas* sp. have been studied by various researchers and revealed different results. Chebbi and his associates found that only ~ 20% pyrene was degraded from a concentration of 200 mg $L^{-1}$, when incubated as the sole carbon source within 30 days at pH 7 (Chebbi et al., 2017). While Ping and colleagues reported ~ 57% degradation of 20 mg $L^{-1}$ pyrene degradation by *Pseudomonas monteilii* PL5 within 10 days (Ping et al., 2017). Also, Singh and Tiwary (2017) have reported a high pyrene degradation potential of ~ 93% by *Pseudomonas stutzeri* P2 in 10 days. These variations in the biodegradation capacity by the same bacterial group might due to different operating conditions, pollutant concentrations and species of the microbe. Yuan and co–workers investigated the removal capacity of pyrene by *Acinetobacter* strain USTB–X and reported ~ 63 % degradation for the initial concentration of 100 mg $L^{-1}$ at neutral pH in 16 days (Yuan et al., 2014). *Rhodococcus* sp. has also been investigated for pyrene degradation. On the basis of the experimental results, the optimum degradation conditions for the strain were pH 7, 5 mg $L^{-1}$ yeast extract, 0.5% NaCl and 90 mg $L^{-1}$ rhamnolipid, which resulted in pyrene biodegradation rate of 48.77% in 5 days (Jia et al., 2019). Salam et al. (2017) revealed the catabolic versatility of *Microbacterium* sp. and its bioremediation capability in environments co–contaminated with pyrene and heavy metals. The biodegradation potential of acidophilic *Stenotrophomonas maltophilia* AJH1 has also been studied, and this strain was an efficient pyrene degrader in contaminated wastewater at acidic pH (Arulazhagan et al., 2017).

**Table 1.4.** Literature review on pyrene degradation using different microbial strains.

| Microbial strain | Carbon source | Degradation medium | Initial conc. | Process parameters | Degradation | Reference |
|---|---|---|---|---|---|---|
| *Candida tropicals* Y 219 + Y 220 | Pyrene | 2% glucose + 0.3% leavening + 20% potato | 100 mg $kg^{-1}$ | pH = 7.0<br>Temperature = 28°C<br>Agitation = 160 rpm<br>Time = 4 days | 67% | Wang et al., 2007 |
| *Candida viswanathii* | Pyrene + 50 g Tween 80 + 10 g glucose | Basal medium (BM) + 0.5g yeast extract | 1.96 mg $kg^{-1}$ | pH = 5.0-6.0<br>Temperature = 27°C<br>Agitation = 150 rpm<br>Time = 10 days | 60.77% | Hesham et al., 2009 |
| *Candida digboiensis* TERI ASN6 | Pyrene | Mineral salt medium (MSM) + 25 mg yeast extract | 5 mg | pH = 3.0<br>Temperature = 30°C<br>Agitation = 180 rpm<br>Time = 10 days | 0.75 mg | Sood et al., 2010 |
| *Anthracophyllum discolor* | Pyrene + Tween 80 (0.05% v/v) | Kirk medium | 50 mg $L^{-1}$ | pH = 6.6<br>Temperature = 30°C<br>Time = 28 days | 8.5% | Acevedo et al., 2011 |
| *Klebsiella pneumonia* PL1 | Pyrene | Minimal medium (MM) | 20 mg $L^{-1}$ | pH = 7.0<br>Temperature = 40°C<br>Agitation = 180 rpm<br>Time = 10 days | 63.4% | Ping et al., 2014 |
| *Acinetobacter* sp. USTB-X | Pyrene | Mineral salt medium (MSM) | 100 mg $L^{-1}$ | pH = 7.0<br>Temperature = 30°C<br>Agitation = 150 rpm<br>Time = 16days | 63% | Yuan et al., 2014 |
| *Cupriavidus* sp. MTS-7 | Pyrene | M9 medium | 150 mg $L^{-1}$ | pH = 7.0<br>Temperature = 25°C<br>Agitation = 175 rpm<br>Time = 20 days | 100% | Kuppusamy et al., 2016 |

**Table 1.4.** (*continued…*)

| Microbial strain | Carbon source | Degradation medium | Initial conc. | Process parameters | Degradation | Reference |
|---|---|---|---|---|---|---|
| *Thalassospira* sp. TSL5-1 | Pyrene | Mineral salt medium (MSM) + 5% salinity | 20 mg $L^{-1}$ | pH = 7.4<br>Temperature = 30°C<br>Time = 25days | 42.5% | Zhou et al., 2016 |
| *Candida vishwanathii* TERI MS1 | Pyrene | Sea water | 0.1% (w/v) | Temperature = 30°C<br>Agitation = 180 rpm<br>Time = 72 h | 83% | Priya et al., 2016 |
| *Microbacterium esteraromaticum* | Pyrene | Mineral salt medium (MSM) | 50 mg $L^{-1}$ | pH = 7.0<br>Temperature = 30°C<br>Agitation = 180 rpm<br>Time = 21days | 89.28% | Salam et al.,2017 |
| *Pseudomonas stutzeri* P2 | Pyrene | Carbon-free mineral medium (CFMM) | 500 mg $L^{-1}$ | pH = 7.0<br>Temperature = 30°C<br>Agitation = 150 rpm<br>Time = 10 days | 92.6% | Singh and Tiwary, 2017 |
| *Pseudomonas* sp. W10 | Pyrene | Basal medium | 200 mg $L^{-1}$ | pH = 7.0<br>Temperature = 37°C<br>Agitation = 180 rpm<br>Time = 30 days | 20% | Chebbi et al., 2017 |
| *Candida* sp. S1 | Pyrene | Mineral extract broth (MEB) + 24 mg $L^{-1}$ NaCl | 20 mg $L^{-1}$ | pH = 5.0<br>Temperature = 28°C<br>Agitation = 80 rpm<br>Time = 15 days | 75% | Hadibarata et al., 2017 |
| *Pseudomonas monteilii* PL5 | Pyrene | Degradation medium | 20 mg $L^{-1}$ | pH = 6.0<br>Temperature = 35°C<br>Agitation = 180 rpm<br>Time = 10 days | 56.5% | Ping et al., 2017 |

**Table 1.4.** (*continued…*)

| Microbial strain | Carbon source | Degradation medium | Initial conc. | Process parameters | Degradation | Reference |
|---|---|---|---|---|---|---|
| *Stenotrophomonas maltophilia* AJH1 | Pyrene | Acidophilic Mineral Salt Medium (AMSM) | 200 mg $L^{-1}$ | pH = 2.0<br>Temperature = 30°C<br>Agitation = 150 rpm<br>Time = 14 days | 77% | Arulazhagan et al., 2017 |
| *Cryptococcus psychrotolerans* IITRFD | Pyrene + glucose (4%) | Yeast nitrogen base (YNB) | 0.50 g $L^{-1}$ | pH = 7.0<br>Temperature = 25°C<br>Agitation = 200 rpm<br>Time = 144 h | 100% | Deeba et al., 2018 |
| *Basidioascus persicus* EBL-C16 | Pyrene | Bushnell-Haas (BH) medium + 2.5% NaCl | 500 mg $L^{-1}$ | Temperature = 28°C<br>Agitation = 120 rpm<br>Time = 21 days | 79% | Kamyabi et al., 2018 |
| *Hortaea* sp. B15 | Pyrene + Tween 80 | Bushnell-Haas (BH) medium | 100 mg $L^{-1}$ | pH = 7.0<br>Temperature = 25°C<br>Agitation = 150 rpm<br>Time = 25 days | 92% | Farraj et al., 2019 |
| *Mycobacterium gilvum* | Pyrene | Mineral salt medium (MSM) | 50 mg $L^{-1}$ | pH = 8.0-9.0<br>Temperature = 35°C<br>Time = 7 days | 95% | Wu et al., 2019 |
| *Rhodococcus* sp. T1 | Pyrene + rhamnolipid (90 mg $L^{-1}$) | Mineral salt medium (MSM) + yeast extract + NaCl (0.5%) | 200 mg $L^{-1}$ | pH = 7.0<br>Temperature = 35°C<br>Agitation = 200 rpm<br>Time = 5 days | 48.77% | Jia et al., 2019 |
| *Trichoderma* sp. F03 | Pyrene + Tween 80 | Malt extract liquid medium | 100 mg $L^{-1}$ | pH = 5.0<br>Temperature = 27°C<br>Time = 15 days | 78% | Al Farraj et al., 2020 |
| *Achromobacter* sp. AC15 | Pyrene | Mineral salt medium (MSM) | 300 mg $L^{-1}$ | pH = 7.0<br>Temperature = 30°C<br>Agitation = 200 rpm<br>Time = 14 days | 40.6% | Li et al., 2020 |

Other bacterial species like *Klebsiella* sp., *Achromobacter* sp., *Cupriavidus* sp., *Thalassospira* sp., *Mycobacterium* sp. have also been reported to degrade pyrene at different initial concentrations – both as sole carbon source or with extra nutritional supplements (Li et al., 2020; Wu et al., 2019; Kuppusamy et al., 2016; Zhou et al., 2016; Ping et al., 2014). It could be inferred from published literature that the subject of pyrene biodegradation by non–ligninolytic fungus as sole carbon has not been explored in–depth.This subject is more crucial from viewpoint of practical application of bioremediation, as supplementation with additional substrates like glucose or other components like surfactants is not feasible on large scale. Systematic optimization and mechanistic studies are needed to in the area of bioremediation of PAHs as single carbon source, which can form general framework for bioremediation of other carcinogenic PAHs.

## 1.7 Literature review on bioremediation in systems comprising mixed PAHs

PAHs with different solubilities co–exist in contaminated areas, and those PAHs having higher solubility have more probability to come in contact with microbes and get degraded. Degradation kinetics in any PAH–polluted environment is complex due to the probability of substrate interactions. Very little is known about the biodegradation in systems comprising mixtures of PAHs, and when present in combinations, these pollutants affect the extent and rate of degradation of other components present in the mixture. These interactions turn out positive in some cases, resulting in enhancement of degradation of one or more components, whereas in other cases negative effects that retard biodegradation have been observed.

To explain the extent of such interactions, PAHs degradation in single, dual and multi–substrate systems have been investigated (Stringfellow and Aitken, 1995;

Dean–Ross et al., 2002). Substrate interactions can occur due to dual effects of competitive metabolism and biomass growth due to multiple substrates. The first will adversely affect the degradation rate of substrate while the second will boost it. Understanding this interaction mechanisms would also facilitate in the optimization of bioremediation approaches. The probable interactions among different PAHs comprise of co–metabolism (Acevedo et al., 2011; Van Herwijnen et al., 2003), inhibition (Zhong et al., 2010), and non–interaction (Baboshin and Golovleva, 2011). The remediation potential of any individual microbe or consortium depends not only on the pollutant degradation capability of the organism(s), but also on the organism's tolerance towards inhibitors. Therefore, it is essential to investigate and understand the substrate interaction in any multi–substrate PAH system. Studies on single PAHs cannot reflect and portray the actual complications of PAH biodegradation in natural environment where the pollutants exist in multicomponent mixtures. Various authors have studied binary or multi–PAHs bioremediation systems and it has been displayed in Table 1.5. The study conducted by Stringfellow and Aitken (1995) reported multi–substrate biodegradation of PAHs. In this work, a mathematical model based on competitive inhibition was proposed that demonstrated involvement of common enzyme systems of *Pseudomonas* strains for degradation. Naphthalene was found to be a competitive inhibitor for phenanthrene biodegradation and the bacteria was found to utilize both phenanthrene and naphthalene as sole carbon source. Analogous observations were also reported by Ma et al. (2013) that similar enzymes may be involved in biodegradation of multi–substrate system. They employed *Pseudomonas sp. Jpyr*–1 strain to investigate the competitive inhibition by other PAHs in pyrene biodegradation. It was revealed that simultaneous presence of multiple substrates would lead to competition for active site(s) of the enzyme. Another study revealed

that the biodegradation of pyrene by strain *Pseudomonas putida* KBM–1 was inhibited competitively by phenanthrene (McNally et al., 1999). Multi–substrate model has been applied to predict the kinetics of biodegradation of naphthalene, pyrene and phenanthrene by mixed culture using parameters derived from single substrate experiments (Guha et al., 1999). They predicted interactions among substrates in binary and ternary mixtures and concluded that biodegradation kinetics of otherwise easily degradable pollutants is retarded due to competitive inhibition. Moreover, higher degradation of recalcitrant PAHs happens due to simultaneous growth of biomass on multiple substrates. The study by Dean–Ross and co–workers reported the capability of two bacterial strains to consume different PAHs. The study established the phenomenon of simultaneous consumption of PAHs in a multi–substrate system and the kinetic experiments suggested that fluoranthene acted as a competitive inhibitor (Dean–Ross et al., 2002). A study demonstrated that the fungus *Pichia anomala* degraded phenanthrene in a four PAH–mixture at a slower rate than in single experiment due to competitive inhibition between phenanthrene and dibenzothiophene. Chrysene persisted in the mixture and could be degraded only in presence of naphthalene (Pan et al., 2004). Another study conducted using the same fungus revealed possible metabolic competitions between chrysene and benzo(a)pyrene (HMW PAHs) and naphthalene and phenanthrene (LMW PAHs) leading to delayed degradation rates of LMW PAHs (Hesham et al., 2006). Desai and Zhong, along with their respective colleagues studied degradation of PAH mixtures using *Sphingomonas* sp. and revealed that there were competitive interactions among the substrates and the biodegradation rates of individual PAH reduced in presence of other PAHs (Zhong et al., 2010; Desai et al., 2008).

**Table 1.5.** Literature review on different mixed substrate (PAHs) system undergoing microbial degradation.

| Mixed substrate system | Microorganism | Type of substrate inhibition | References |
|---|---|---|---|
| Naphthalene-methylnaphthalenes-fluorene-phenanthrene | Pseudomonads | Competitive | Stringfellow and Aitken, 1995 |
| Naphthalene-phenanthrene-pyrene | Mixed culture | Competitive | Guha et al., 1999 |
| Naphthalene-phenanthrene-pyrene | *Pseudomonas putida* KBM-1 | Competitive | McNally et al., 1999 |
| Anthracene-Pyrene-Fluoranthene-Phenanthrene | *Mycobacterium flavescens* & *Rhodococcus* sp. | Competitive | Dean-Ross., 2002 |
| Naphthalene-dibenzothiophene-phenanthrene-chrysene | *Pichia anomala* | Competitive | Pan et al., 2004 |
| Naphthalene-phenanthrene-chrysene-benzo(a)pyrene | *Pichia anomala* | Competitive | Hesham et al., 2006 |
| Fluorene-naphthalene-1,5-dimethylnaphthalene-1-methylfluorene | *Sphingomonas paucimobilis* EPA505 | Competitive | Desai et al., 2008 |
| Phenanthrene-pyrene-fluoranthene | *Sphingomonas sp.* PheB4 | Competitive | Zhong et al., 2010 |
| Fluorene-phenanthrene-anthracene-fluoranthene-pyrene | *Pseudomonas* sp. Jpyr-1 | Competitive | Ma et al., |
| Phenanthrene-fluoranthene-pyrene | *Pseudomonas aeruginosa* LBP9 | Competitive | Bezza and Chirwa, 2017 |
| Anthracene-naphthalene | *Acinetobacter johnsonii* | Competitive | Jiang et al., 2018a |
| Naphthalene-anthracene-pyrene-phenanthrene | *Acinetobacter johnsonii* | Competitive | Jiang et al., 2018b |
| Naphthalene-pyrene | *Ochrobactrum* sp. | Competitive | Wang et al., 2019 |

Moreover, it was also concluded that despite biosurfactant–enhanced bioavailability of PAHs, the microbial degradation rate was still competitively inhibited in PAH mixtures system (Bezza and Chirwa, 2017). Jiang and his co–workers studied co–biodegradation in multi–PAH system by using *Acinetobacter* sp. HMW PAHs exhibited greater inhibition as compared to LMW PAHs and competitive inhibition between PAHs was also embodied in cell growth behaviors (Jiang et al., 2018a; Jiang et al., 2018b). Wang et al., 2019 reported co–biodegradation of pyrene and naphthalene by *Ochrobactrum* sp. Naphthalene removal was 99% against 41% removal of pyrene. The interaction pattern between the two pollutants was of competitive nature.

## 1.8 Strategy for intensification of biodegradation

Authors have employed various methods to intensify the biodegradation process such as addition of alternate carbon source, immobilization of microbes and by enhancing the bioavailability through the aid of nutritional supplements like surfactants, humic substances, etc. Another way of process intensification is through coupling microbial degradation with ultrasound irradiation or sonication. Suitably controlled ultrasonic waves have revealed favorable effects on the microbial growth and metabolic performance in live systems. Low power ultrasound results in steady cavitation and causes repairable damages to microbes which leads to rise in their proliferation. However, high power ultrasound causes unrepairable damages to microbial cells (Huang et al., 2017a).

Ultrasound essentially refers to mechanic or sound waves that requires an elastic medium for propagation. The frequencies of ultrasound are above human hearing range but lower than microwaves frequencies, i.e. from 20 kHz to 10 MHz

(Chemat and Khan, 2011). Being a longitudinal wave, it can pass via compressible medium like water and air, in series of alternative compression and rarefaction cycles due to oscillatory motion of fluid elements in the direction of propagation of the wave (Shah et al., 1999). These waves are produced with the help of transducer i.e. electric energy is converted to mechanical energy. The key characteristics of this wave are velocity, frequency and pressure amplitude. For propagation of ultrasound wave via any liquid, bubbles in the medium scatter the waves triggering severe attenuation. The gas bubbles present in the liquid also changes the compressibility of the medium, thereby reducing the speed of sound in the medium. The sound wave properties in gas are immensely affected due to static pressure in the medium. For sound wave propagation in liquids, the static pressure does not have any major impact due to insensitivity of liquid properties to static pressure (at least at moderate pressure levels). Cavitation can be described as nucleation, growth, oscillation and transient collapse of gas/vapor bubbles driven by variation in bulk pressure in the medium. This variance in bulk pressure can be result of acoustic wave propagation or change in flow geometry, or in general, energy dissipation in the system. Cavitation has been proved as an effective tool for introducing energy into a system for intensification of numerous physical/chemical/biological processes. Both ultrasound and cavitation have several impacts on a reaction system. The main manifestation of these phenomena is generation of intense micro–convection and micro–mixing in a reaction system.

Different beneficial factors have been reported in literature regarding application of ultrasound in enhancement of microbial productivity. Firstly, ultrasound facilitates in loosening of cell bunches formed in any microbial culture. Nutrient utilization by microbes also boosts following the increase of cell biomass

and higher production of target substances. Avhad and Rathod (2015) investigated the ultrasound–assisted production of a fibrinolytic enzyme from *Bacillus sphaericus*. They reported ~1.5–fold rise in the yield of the enzyme by sonication treatment. Secondly, ultrasound augments the cell membrane permeability resulting in quicker transfer of components and stimulates biomass growth and proliferation. It was reported in a study that low power ultrasound could impressively boost the total $Ca^{2+}$ content accumulation in *Saccharomyces cerevisiae* cells. Moreover, ultrasonic waves also improved the effusion and accumulation of cellular metabolism products was also improved by ultrasound, resulting in greater yield (Bochu et al. 2003). Another study investigated the ultrasound–assisted ethanol production from cassava–based plants. Ultrasound not only decreased the fermentation period by ~ 24 h but also increased the final ethanol titre. The ethanol yield from the sonication-assisted experiments was considerably higher than the conventional experiments, and the overall production costs also decreased (Nitayavardhana et al. 2010). Dai and co–workers studied the impact of low ultrasonic stimulus on riboflavin yielding strain *Ecemothecium ashbyii*. They established that ultrasound of low frequency can stimulate mycelium growth and enhance the riboflavin output. The optimum frequency was ~ 24 kHz and several other significant biochemical parameters associated with cell growth were also measured. Exposure to sonication reduced fermentation period by 36 h, simultaneously boosting riboflavin productivity ~ 5 times, as compared to conventional fermentation (Chuanyun et al., 2003). The rigid cell membrane structure of *E. ashbyii* always acted as hindrance in the enhancement of riboflavin productivity by hampering riboflavin release from cells in the fermentation broth. This issue of riboflavin excretion was effectively solved by application of ultrasound (Chuanyun et al., 2004). Thirdly, ultrasound is used to

provide an ideal ecosystem for biomass growth and proliferation in the medium. The influence of ultrasound on *S. cerevisiae* growth cycle (lag, exponential and stationary phase) was investigated (Lanchun et al. 2003). Low–power ultrasound could augment the cell growth in both lag and exponential phase under different conditions, but had nearly negligible impact on the yeast cells in the stationary phase. The underlying cause is that the pH of the broth was stationary in the lag phase and increased ~ 0.2–0.3 in exponential phase in comparison to control experiments. Another cause is the foam produced due to sonication in the medium, which results in increase of the exchange area between liquid and gas, and the residence time of air bubbles in medium. These exchanges improve oxygen transfer rate, thereby benefitting the growth of the yeast. Fourthly, ultrasonic irradiation has impact on the cellular components and functions of microbes. A study by Zhao et al. (2012) proposed low–intensity pulsed ultrasound stimulation for boosting the production of mycophenolic acid (MPA) by using *Penicillium brevicompactum*. Under the optimum conditions, MPA production increased by 60% along with a rise in the number of cell hyphae tips. Moreover, ultrasound has also been reported to improve the functional characteristics of *S. cerevisiae* in beer production. Enhancement in the microbial fermentation strength and the proteinase activity was also reported, however no genetic variation has been reported to occur by ultrasound exposure (Lanchun et al., 2003). Another study reported the intensification of cellular permeability and biomass of *Candida tropicalis* cells treated with low–intensity sonication in a sweeping frequency mode. (Huang et al., 2017b). Significant increment in yeast biomass was witnessed, the hyphae became considerably longer, the seeped cellular protein and nucleic acid from the yeast increased and the cellular $Ca^{2+}$ content decreased. Therefore, the effects of ultrasound can be elucidated at both cellular and molecular

level. At cellular level, sonication stimulates cell growth by loosening cell bunches, enhances membrane permeability, adjusts the culture medium and affects the cell components, functions and genetics. At molecular level, ultrasound induces conformational changes in secondary structure of enzyme that boosts their activity.

## 1.9 OBJECTIVES, APPROACH AND SCOPE OF THE PRESENT THESIS

From the literature review and analysis presented in the preceding sections, it could be inferred that bioremediation is an effective removal technique for the ubiquitous polycyclic aromatic hydrocarbons (PAHs) pollutants. Bioremediation has many distinct merits over other conventional processes such as eco–friendly operation. Among large number of microorganisms investigated for degradation of variety of PAHs, non–ligninolytic fungi/yeasts possess certain advantages owing to their tolerance towards contaminants, penetration in soil through mycelia and ability to rapidly colonize in substrates. Still, the research in the area of PAH degradation by non–ligninolytic fungi is rather limited, and has originated from microbiology community. Studies with engineering approach addressing issues like kinetics, optimization and bioreactor design are relatively few. Moreover, most authors have used a supplemental carbon or nutritional source during PAH biodegradation studies using fungi.

Considering the potential and promise of non–ligninolytic fungi and yeasts for biodegradation, there is an urgent need to study these processes from engineering perspective. Moreover, bioremediation with PAHs as sole carbon source also needs to be studied in–depth keeping in view the additional cost of co–substrates like glucose and surfactants. Moreover, due to inadequate understanding of the metabolic pathway of PAHs degradation (especially HMW) followed by microbes and thus more studies

are needed in this area. Another lacuna in previous literature is that most studies have focused on degradation of a single substrate (or PAH) at a time. The interactive effects in multi-substrate systems have not been explored much. Again, from practical perspective, these are quite important as PAHs are persistent in environment and can influence each other's degradation. More detailed studies are needed that can give insight into biokinetics of multi–substrate system and the inhibitive effects rendered by one PAH over another.

Engineering research in the area of bioremediation by non–ligninolytic fungi should comprise of two simultaneous components, viz. experiments and simulations. A detailed kinetic study along with attempts to intensify the bioremediation process are required. One of the relatively new techniques developed for intensification of microbial/enzymatic processes is to provide external stimuli in the form of ultrasound irradiation or sonication. Use of such techniques of process intensification are especially advantageous as these techniques do not interfere with the basic mechanism of the process, and only augment the kinetics of the process with reduction in time and rise in yields. Therefore, the working objectives of this thesis research have been formulated to address above issues.

The present thesis has focused on degradation of two ubiquitous PAHs, viz. phenanthrene and pyrene by yeast, *Candida tropicalis* MTCC 184. Process optimization was performed to obtain maximum degradation followed by the identification of pathway of degradation. An attempt has also been made to intensify the process by application of ultrasound. Both of these PAHs are on the priority pollutant list declared by US EPA. The co–biodegradation of PAHs has been studied with a kinetic model and the interactive effects have been identified. This thesis

comprises of total 6 chapters (including the present chapter) and brief content of each chapter is given below:

- Chapter 1 presents a general introduction on environmental pollution and bioremediation process. Degradation of PAHs (mainly phenanthrene and pyrene), by different microbial strains, and biodegradation abilities of *Candida* sp. were reviewed. A brief literature focussing on co–biodegradation of PAHs and ultrasound–assisted bioprocess intensification has also been presented. Finally, the objectives and approach of the thesis has been stated along with the brief description of the chapter contents.
- Chapter 2 presents the statistical optimization of the physical parameters of bioremediation by *Candida tropicalis* strain with phenanthrene and pyrene as model PAHs. Kinetic study was also performed using different substrate inhibition models to analyse the specific growth rate and specific degradation rate of the process. Both physical parameter optimization and kinetic study is essential to have a fundamental knowledge and the smooth functioning of the biodegradation process.
- Chapter 3 presents the attempts in ultrasound–assisted biodegradation of PAHs using the yeast, *C. tropicalis*. Optimization of ultrasound duty cycle using flow cytometry was done prior to biodegradation experiments. Kinetic study was performed to see the impact of ultrasound on parameters of cell growth and substrate utilization. This chapter also involves the results on flow cytometry and FESEM analysis to observe changes in cell morphology due to application of sonication.
- Chapter 4 presents investigations in following areas: (1) identification of pathway followed during degradation, (2) enzymes responsible for triggering

the degradation process, and (3) identification of metabolites/intermediates formed during the degradation process of phenanthrene and pyrene by *C. tropicalis*.

- Chapter 5 presents the mechanistic investigations in the co–biodegradation behavior of phenanthrene and pyrene by coupling experiments with a mathematical model to quantify the growth and degradation parameters of co–biodegradation. The kinetics of degradation has also been studied with varying initial concentrations of the two substrates. The results of this study should provide an in–depth insight into the interactive effects and mechanism involved in co–degradation by *C. tropicalis.*
- Chapter 6 represents the summary of the results obtained for all the four working objectives and overall conclusion of the thesis. The new insights into the process of PAH bioremediation obtained in this thesis research have been identified and listed. Some suggestions have been made for further research in the area of PAH bioremediation based on the results of present study.

## REFERENCES

Abdel–Shafy, H.I. and Mansour, M.S., 2016. A review on polycyclic aromatic hydrocarbons: source, environmental impact, effect on human health and remediation. Egyptian journal of petroleum, 25 (1), 107–123.

Aburto, A., Fahy, A., Coulon, F., Lethbridge, G., Timmis, K.N., Ball, A.S., McGenity, T.J., 2009. Mixed aerobic and anaerobic microbial communities in benzene–contaminated groundwater. Journal of applied microbiology, 106 (1), 317–328.

Aburto–Medina, A. and Ball, A.S., 2015. Microorganisms involved in anaerobic benzene degradation. Annals of microbiology, 65 (3), 1201–1213.

Acevedo, F., Pizzul, L., del Pilar Castillo, M., Cuevas, R., Diez, M.C., 2011. Degradation of polycyclic aromatic hydrocarbons by the Chilean white–rot fungus *Anthracophyllum discolor*. Journal of hazardous materials, 185 (1), 212–219.

ACGIH (American Conference of Governmental Industrial Hygienists). Polycyclic aromatic hydrocarbons (PAHs) biologic exposure indices (BEI) Cincinnati. OH: American Conference of Governmental Industrial Hygienists; 2005.

Agency for Toxic Substances and Disease Registry [ATSDR] 1990. Toxicological profile for polycyclic aromatic hydrocarbons. Acenaphthene, Acenaphthylene, Anthracene, Benzo[a]anthracene, Benzo[a]pyrene, Benzo[b]fluoranthene, Benzo[g,i,h]perylene, Benzo[k]fluoranthene, Chrysene, Dibenzo[a,h]anthracene, Fluoranthene, Fluorene, Indeno[1,2,3–c,d]pyrene, Phenanthrene, Pyrene. Atlanta, GA: Agency for Toxic Substances and Disease Registry.

Al Farraj, D.A., Hadibarata, T., Elshikh, M.S., Al Khulaifi, M.M., Kristanti, R.A., 2020. Biotransformation and Degradation Pathway of Pyrene by Filamentous Soil Fungus *Trichoderma* sp. F03. Water, Air, & Soil Pollution, 231, 1–9.

Albanese, S., Fontaine, B., Chen, W., Lima, A., Cannatelli, C., Piccolo, A., Qi, S., Wang, M., De Vivo, B., 2015. Polycyclic aromatic hydrocarbons in the soils of a densely populated region and associated human health risks: the Campania Plain (Southern Italy) case study. Environmental geochemistry and health, 37 (1), 1–20.

Al Farraj, D.A., Hadibarata, T., Yuniarto, A., Syafiuddin, A., Surtikanti, H.K., Elshikh, M.S., Al Khulaifi, M.M., Al–Kufaidy, R., 2019. Characterization of pyrene and chrysene degradation by halophilic *Hortaea* sp. B15. Bioprocess and biosystems engineering, 42 (6), 963–969.

Al–Turki, A.I., 2009. Microbial polycyclic aromatic hydrocarbons degradation in soil. Research Journal of Environmental Toxicology, 3, 1–8.

Amodu, O.S., Ojumu, T.V., Ntwampe, S.K.O., 2013. Bioavailability of high molecular weight polycyclic aromatic hydrocarbons using renewable resources. Environmental Biotechnology–New Approaches and Prospective Applications, 171.

Andreoni, V. and Gianfreda, L., 2007. Bioremediation and monitoring of aromatic–polluted habitats. Applied Microbiology and Biotechnology, 76 (2), 287–308.

Aranda, E., 2016. Promising approaches towards biotransformation of polycyclic aromatic hydrocarbons with Ascomycota fungi. Current opinion in biotechnology, 38, 1–8.

Armstrong, B., Hutchinson, E., Unwin, J., Fletcher, T., 2004. Lung cancer risk after exposure to polycyclic aromatic hydrocarbons: a review and meta–analysis. Environmental health perspectives, 112 (9), 970–978.

Arulazhagan, P. and Vasudevan, N., 2011. Role of nutrients in the utilization of polycyclic aromatic hydrocarbons by halotolerant bacterial strain. Journal of Environmental Sciences, 23 (2), 282–287.

Arulazhagan, P., Al–Shekri, K., Huda, Q., Godon, J.J., Basahi, J.M., Jeyakumar, D., 2017. Biodegradation of polycyclic aromatic hydrocarbons by an acidophilic *Stenotrophomonas maltophilia* strain AJH1 isolated from a mineral mining site in Saudi Arabia. Extremophiles, 21 (1), 163–174.

Avhad, D.N. and Rathod, V.K., 2015. Ultrasound assisted production of a fibrinolytic enzyme in a bioreactor. Ultrasonics sonochemistry, 22, 257–264.

Baboshin, M. and Golovleva, L., 2011. Multisubstrate kinetics of PAH mixture biodegradation: analysis in the double–logarithmic plot. Biodegradation, 22, 13–23.

Baldrian, P., 2008. Wood–inhabiting ligninolytic basidiomycetes in soils: ecology and constraints for applicability in bioremediation. Fungal Ecology, 1 (1), 4–12.

Bamforth, S.M. and Singleton, I., 2005. Bioremediation of polycyclic aromatic hydrocarbons: current knowledge and future directions. Journal of Chemical Technology & Biotechnology: International Research in Process, Environmental & Clean Technology, 80 (7), 723–736.

Basak, B., Bhunia, B., Dutta, S., Chakraborty, S., Dey, A., 2014. Kinetics of phenol biodegradation at high concentration by a metabolically versatile isolated yeast *Candida tropicalis* PHB5. Environmental Science and Pollution Research, 21 (2), 1444–1454.

Bezza, F.A. and Chirwa, E.M.N., 2017. Biosurfactant–assisted bioremediation of polycyclic aromatic hydrocarbons (PAHs) in liquid culture system and substrate interactions. Polycyclic Aromatic Compounds, 37 (5), 375–394.

Bisht, S., Pandey, P., Bhargava, B., Sharma, S., Kumar, V., Sharma, K.D., 2015. Bioremediation of polyaromatic hydrocarbons (PAHs) using rhizosphere technology. Brazilian Journal of Microbiology, 46 (1), 7–21.

Biswas, B., Sarkar, B., Rusmin, R., Naidu, R., 2015. Bioremediation of PAHs and VOCs: Advances in clay mineral–microbial interaction. Environment International, 85, 168–181.

Bochu, W., Lanchun, S., Jing, Z., Yuanyuan, Y., Yanhong, Y., 2003. The influence of $Ca^{2+}$ on the proliferation of *S. cerevisiae* and low ultrasonic on the concentration of $Ca^{2+}$ in the *S. cerevisiae* cells. Colloids and Surfaces B: Biointerfaces, 32 (1), 35–42.

Borràs, E., Caminal, G., Sarrà, M., Novotný, Č., 2010. Effect of soil bacteria on the ability of polycyclic aromatic hydrocarbons (PAHs) removal by *Trametes versicolor* and *Irpex lacteus* from contaminated soil. Soil Biology and Biochemistry, 42 (12), 2087–2093.

Cachada, A., da Silva, E.F., Duarte, A.C., Pereira, R., 2016. Risk assessment of urban soils contamination: the particular case of polycyclic aromatic hydrocarbons. Science of the Total Environment, 551, 271–284.

Cerniglia, C.E., 1993. Biodegradation of polycyclic aromatic hydrocarbons. Current opinion in biotechnology, 4 (3), 331–338.

Cerniglia, C.E. and Sutherland, J.B., 2001. Bioremediation of polycyclic aromatic hydrocarbons by ligninolytic and non–ligninolytic fungi. In British Mycological Society Symposium Series, 23, 136–187.

Cerniglia, C.E. and Sutherland, J.B., 2010. Degradation of polycyclic aromatic hydrocarbons by fungi. In Handbook of hydrocarbon and lipid microbiology.

Chang, B.V., Shiung, L.C., Yuan, S.Y., 2002. Anaerobic biodegradation of polycyclic aromatic hydrocarbon in soil. Chemosphere, 48 (7), 717–724.

Chebbi, A., Hentati, D., Zaghden, H., Baccar, N., Rezgui, F., Chalbi, M., Sayadi, S., Chamkha, M., 2017. Polycyclic aromatic hydrocarbon degradation and biosurfactant production by a newly isolated *Pseudomonas* sp. strain from used motor oil–contaminated soil. International Biodeterioration & Biodegradation, 122, 128–140.

Chemat, F. and Khan, M.K., 2011. Applications of ultrasound in food technology: processing, preservation and extraction. Ultrasonics sonochemistry, 18 (4), 813–835.

Chen, B.H. and Chen, Y.C., 2001. Formation of polycyclic aromatic hydrocarbons in the smoke from heated model lipids and food lipids. Journal of agricultural and food chemistry, 49 (11), 5238–5243.

Chikere, C.B., Okpokwasili, G.C., Chikere, B.O., 2011. Monitoring of microbial hydrocarbon remediation in the soil. 3 Biotech, 1 (3), 117–138.

Chuanyun, D., Bochu, W., Chuanren, D., Sakanishi, A., 2003. Low ultrasonic stimulates fermentation of riboflavin producing strain *Ecemothecium ashbyii*. Colloids and surfaces B: Biointerfaces, 30 (1–2), 37–41.

Chuanyun, D., Bochu, W., Huan, Z., Conglin, H., Chuanren, D., Wangqian, L., Toyama, Y. Sakanishi, A., 2004. Effect of low frequency ultrasonic stimulation on the secretion of siboflavin produced by *Ecemothecium Ashbyii*. Colloids and Surfaces B: Biointerfaces, 34 (1), 7–11.

Ciecierska, M. and Obiedziński, M.W., 2013. Polycyclic aromatic hydrocarbons in the bakery chain. Food chemistry, 141 (1), 1–9.

Csutak, O., Stoica, I., Ghindea, R., Tanase, A.M., Vassu, T., 2010. Insights on yeast bioremediation processes. Romanian Biotechnological Letters, 15 (2), 5066–5071.

Cybulski, Z., Dziurla, E., Kaczorek, E., Olszanowski, A., 2003. The influence of emulsifiers on hydrocarbon biodegradation by *Pseudomonadacea* and *Bacillacea* strains. Spill Science & Technology Bulletin, 8 (5–6), 503–507.

Darmawan, R., Nakata, H., Ohta, H., Niidome, T., Takikawa, K., Morimura, S., 2015. Isolation and evaluation of PAH degrading bacteria. Journal of Bioremediation & Biodegredation, 6 (3), 1.

Dean–Ross, D., Moody, J., Cerniglia, C.E., 2002. Utilization of mixtures of polycyclic aromatic hydrocarbons by bacteria isolated from contaminated sediment. FEMS microbiology ecology, 41 (1), 1–7.

Deeba, F., Pruthi, V., Negi, Y.S., 2018. Aromatic hydrocarbon biodegradation activates neutral lipid biosynthesis in oleaginous yeast. Bioresource Technology, 255, 273–280.

Desai, A.M., Autenrieth, R.L., Dimitriou–Christidis, P., McDonald, T.J., 2008. Biodegradation kinetics of select polycyclic aromatic hydrocarbon (PAH) mixtures by *Sphingomonas paucimobilis* EPA505. Biodegradation, 19 (2), 223–233.

Diggs, D.L., Huderson, A.C., Harris, K.L., Myers, J.N., Banks, L.D., Rekhadevi, P.V., Niaz, M.S., Ramesh, A., 2011. Polycyclic aromatic hydrocarbons and digestive tract cancers: a perspective. Journal of environmental science and health, part c, 29 (4), 324–357.

Diggs, D.L., Harris, K.L., Rekhadevi, P.V., Ramesh, A., 2012. Tumor microsomal metabolism of the food toxicant, benzo (a) pyrene, in Apc Min mouse model of colon cancer. Tumor Biology, 33 (4), 1255–1260.

Elliot, R., Singhal, N., Swift, S., 2010. Surfactants and bacterial bioremediation of polycyclic aromatic hydrocarbon contaminated soil–unlocking the targets. Critical Reviews in Environmental Science and Technology, 41 (1), 78–124.

e Silva, N.C.G., de Macedo, A.C., Pinheiro, A.D.T., Rocha, M.V.P., 2019. Phenol biodegradation by *Candida tropicalis* ATCC 750 immobilized on cashew apple bagasse. Journal of Environmental Chemical Engineering, 7 (3), 103076.

Fan, M.Y., Xie, R.J., Qin, G., 2014. Bioremediation of petroleum–contaminated soil by a combined system of biostimulation–bioaugmentation with yeast. Environmental technology, 35 (4), 391–399.

Farag, S. and Soliman, N.A., 2011. Biodegradation of crude petroleum oil and environmental pollutants by *Candida tropicalis* strain. Brazilian Archives of biology and Technology, 54 (4), 821–830.

Fritsche, W. and Hofrichter, M., 2008. Aerobic degradation by microorganisms, Biotechnology: Environmental Processes II, Vol. 11. Chapter, 6, 147–155.

Fu, W., Xu, M., Sun, K., Hu, L., Cao, W., Dai, C., Jia, Y., 2018. Biodegradation of phenanthrene by endophytic fungus *Phomopsis liquidambari* in vitro and in vivo. Chemosphere, 203, 160–169.

Gan, S., Lau, E.V., Ng, H.K., 2009. Remediation of soils contaminated with polycyclic aromatic hydrocarbons (PAHs). Journal of Hazardous Materials, 172 (2–3), 532–549.

Garcia–Suastegui, W.A., Huerta–Chagoya, A., Carrasco–Colín, K.L., Pratt, M.M., John, K., Petrosyan, P., Rubio, J., Poirier, M.C., Gonsebatt, M.E., 2010. Seasonal variations in the levels of PAH–DNA adducts in young adults living in Mexico City. Mutagenesis, 26 (3), 385–391.

Gargouri, B., Mhiri, N., Karray, F., Aloui, F., Sayadi, S., 2015. Isolation and characterization of hydrocarbon–degrading yeast strains from petroleum contaminated industrial wastewater. BioMed research international, 2015.

Ghosal, D., Ghosh, S., Dutta, T.K. and Ahn, Y., 2016. Current state of knowledge in microbial degradation of polycyclic aromatic hydrocarbons (PAHs): a review. Frontiers in microbiology, 7, 1369.

Guha, S., Peters, C.A., Jaffé, P.R., 1999. Multisubstrate biodegradation kinetics of naphthalene, phenanthrene, and pyrene mixtures. Biotechnology and bioengineering, 65 (5), 491–499.

Gunter, M.J., Divi, R.L., Kulldorff, M., Vermeulen, R., Haverkos, K.J., Kuo, M.M., Strickland, P., Poirier, M.C., Rothman, N., Sinha, R., 2007. Leukocyte polycyclic aromatic hydrocarbon–DNA adduct formation and colorectal adenoma. Carcinogenesis, 28 (7), 1426–1429.

Hadibarata, T., Tachibana, S., Itoh, K., 2007. Biodegradation of phenanthrene by fungi screened from nature. Pakistan Journal of Biological Sciences, 10 (15), 2535–2543.

Hadibarata, T., Tachibana, S., Itoh, K., 2009. Biodegradation of chrysene, an aromatic hydrocarbon by *Polyporus* sp. S133 in liquid medium. Journal of Hazardous Materials, 164 (2–3), 911–917.

Hadibarata, T. and Tachibana, S., 2010. Characterization of phenanthrene degradation by strain *Polyporus* sp. S133. Journal of Environmental Sciences, 22 (1), 142–149.

Hadibarata, T. and Kristanti, R.A., 2014. Potential of a white–rot fungus *Pleurotus eryngii* F032 for degradation and transformation of fluorene. Fungal biology, 118 (2), 222–227.

Hadibarata, T., Khudhair, A.B., Kristanti, R.A., Kamyab, H., 2017. Biodegradation of pyrene by *Candida* sp. S1 under high salinity conditions. Bioprocess and Biosystems Engineering, 40 (9), 1411–1418.

Hamamura, N., Ward, D.M., Inskeep, W.P., 2013. Effects of petroleum mixture types on soil bacterial population dynamics associated with the biodegradation of hydrocarbons in soil environments. FEMS microbiology ecology, 85 (1), 168–178.

Hanano, A., Al–Arfi, M., Shaban, M., Daher, A., Shamma, M., 2014. Removal of petroleum–crude oil from aqueous solution by *Saccharomyces cerevisiae* SHSY strain necessitates at least an inducible CYP450ALK homolog gene. Journal of Basic Microbiology, 54 (5), 358–368.

Haritash, A.K. and Kaushik, C.P., 2009. Biodegradation aspects of polycyclic aromatic hydrocarbons (PAHs): a review. Journal of hazardous materials, 169 (1–3), 1–15.

Harms, H., Schlosser, D., Wick, L.Y., 2011. Untapped potential: exploiting fungi in bioremediation of hazardous chemicals. Nature Reviews Microbiology, 9 (3), 177–192.

Hashem, M., Alamri, S.A., Al–Zomyh, S.S., Alrumman, S.A., 2018. Biodegradation and detoxification of aliphatic and aromatic hydrocarbons by new yeast strains. Ecotoxicology and Environmental Safety, 151, 28–34.

Hassan, S.E.D., Desouky, S.E., Fouda, A., El–Gamal, M.S., Alemam, A., 2015. Biodegradation of phenanthrene by *Klebsiella* sp isolated from organic contaminated sediment. Journal of Advances in Biology & Biotechnology, 1–12.

Hesham, A.E.L., Wang, Z., Zhang, Y., Zhang, J., Lv, W., Yang, M., 2006. Isolation and identification of a yeast strain capable of degrading four and five ring aromatic hydrocarbons. Annals of microbiology, 56 (2), 109.

Hesham, A.E., Alamri, S.A., Khan, S., Mahmoud, M.E., Mahmoud, H.M., 2009. Isolation and molecular genetic characterization of a yeast strain able to degrade petroleum polycyclic aromatic hydrocarbons. African Journal of Biotechnology, 8 (10).

Hesham, A.E.L., Mohamed, E.A., Mawad, A.M., Elfarash, A., El–Fattah, A., Bahaa, S., El–Rawy, M.A., 2017. Molecular characterization of *Fusarium solani* degrades a mixture of low and high molecular weight polycyclic aromatic hydrocarbons. The Open Biotechnology Journal, 11 (1).

Hidayat, A. and Yanto, D.H.Y., 2018. Biodegradation and metabolic pathway of phenanthrene by a new tropical fungus, *Trametes hirsuta* D7. Journal of Environmental Chemical Engineering, 6 (2), 2454–2460.

Hong, W., Jia, H., Ma, W.L., Sinha, R.K., Moon, H.B., Nakata, H., Minh, N.H., Chi, K.H., Li, W.L., Kannan, K., Sverko, E., 2016. Distribution, fate, inhalation exposure and lung cancer risk of atmospheric polycyclic aromatic

hydrocarbons in some Asian countries. Environmental science & technology, 50 (13), 7163–7174.

Hou, N., Zhang, N., Jia, T., Sun, Y., Dai, Y., Wang, Q., Li, D., Luo, Z., Li, C., 2018. Biodegradation of phenanthrene by biodemulsifier–producing strain *Achromobacter* sp. LH–1 and the study on its metabolisms and fermentation kinetics. Ecotoxicology and Environmental Safety, 163, 205–214.

Huang, X., Shi, J., Cui, C., Yin, H., Zhang, R., Ma, X., Zhang, X., 2016. Biodegradation of phenanthrene by *Rhizobium petrolearium* SL–1. Journal of applied microbiology, 121 (6), 1616–1626.

Huang, G., Chen, S., Dai, C., Sun, L., Sun, W., Tang, Y., Xiong, F., He, R., Ma, H., 2017a. Effects of ultrasound on microbial growth and enzyme activity. Ultrasonics Sonochemistry, 37, 144–149.

Huang, G., Tang, Y., Sun, L., Xing, H., Ma, H., He, R., 2017b. Ultrasonic irradiation of low intensity with a mode of sweeping frequency enhances the membrane permeability and cell growth rate of *Candida tropicalis*. Ultrasonics Sonochemistry, 37, 518–528.

Jia, X., He, Y., Huang, L., Jiang, D., Lu, W., 2019. n–Hexadecane and pyrene biodegradation and metabolization by *Rhodococcus* sp. T1 isolated from oil contaminated soil. Chinese Journal of Chemical Engineering, 27 (2), 411–417.

Jiang, Y., Wen, J., Lan, L., Hu, Z., 2007. Biodegradation of phenol and 4–chlorophenol by the yeast *Candida tropicalis*. Biodegradation, 18 (6), 719–729.

Jiang, Y., Yang, Y., Zhang, X., 2014. Review on the biodegradation and conversion mechanisms of typical polycyclic aromatic hydrocarbons. Shiyou Xuebao,

Shiyou Jiagong/Acta Petrolei Sinica [Petroleum Processing Section], 30, 1137–1150.

Jiang, Y., Qi, H., Zhang, X.M., 2018a. Co–biodegradation of anthracene and naphthalene by the bacterium *Acinetobacter johnsonii*. Journal of Environmental Science and Health, Part A, 53 (5), 448–456.

Jiang, Y., Zhang, Z., Zhang, X., 2018b. Co–biodegradation of pyrene and other PAHs by the bacterium *Acinetobacter johnsonii*. Ecotoxicology and Environmental Safety, 163, 465–470.

Joutey, N.T., Bahafid, W., Sayel, H., El Ghachtouli, N., 2013. Biodegradation: involved microorganisms and genetically engineered microorganisms. Biodegradation–life of science, 289–320.

Jové, P., Olivella, M.À., Camarero, S., Caixach, J., Planas, C., Cano, L., de las Heras, F.X., 2016. Fungal biodegradation of anthracene–polluted cork: A comparative study Part A Toxic/hazardous substances & environmental engineering, 51, 70–77.

Juhasz AL, Waller N, Lease C, Bentham R, Stewart R., 2005. Pilot scale bioremediation of creosote–contaminated soil – efficacy of enhance natural attenuation and bioaugmentation strategies. Bioremediation journal, 9 (3–4), 139–154.

Kamyabi, A., Nouri, H., Moghimi, H., 2018. Characterization of pyrene degradation and metabolite identification by *Basidioascus persicus* and mineralization enhancement with bacterial–yeast co–culture. Ecotoxicology and Environmental Safety, 163, 471–477.

Kanaly, R.A. and Harayama, S., 2000. Biodegradation of high–molecular–weight polycyclic aromatic hydrocarbons by bacteria. Journal of bacteriology,182 (8), 2059–2067.

Kanaly, R.A. and Harayama, S., 2010. Advances in the field of high–molecular–weight polycyclic aromatic hydrocarbon biodegradation by bacteria. Microbial Biotechnology, 3 (2), 136–164.

Karthikeyan, R. and Bhandari, A., 2001. Anaerobic biotransformation of aromatic and polycyclic aromatic hydrocarbons in soil microcosms: a review. Journal of hazardous substance research, 3 (1), 3.

Kim, K.H., Jahan, S.A., Kabir, E., Brown, R.J., 2013. A review of airborne polycyclic aromatic hydrocarbons (PAHs) and their human health effects. Environment international, 60, 71–80.

Kristanti, R.A., Hadibarata, T., Al Farraj, D.A., Elshikh, M.S., Alkufeidy, R.M., 2018. Biodegradation mechanism of phenanthrene by halophilic *Hortaea* sp. B15. Water, Air, & Soil Pollution, 229 (10), 324.

Kumari, M. and Abraham, J., 2011. Biodegradation of diesel oil using yeast *Rhodosporidium toruloides*. Research Journal of Environmental Toxicology, 5 (6), 369.

Kuo, C.Y., Hsu, Y.W., Lee, H.S., 2003. Study of human exposure to particulate PAHs using personal air samplers. Archives of Environmental Contamination and Toxicology, 44 (4), 0454–0459.

Kuppusamy, S., Thavamani, P., Megharaj, M., Lee, Y.B., Naidu, R., 2016. Polyaromatic hydrocarbon (PAH) degradation potential of a new acid tolerant, diazotrophic P–solubilizing and heavy metal resistant bacterium *Cupriavidus*

sp. MTS–7 isolated from long–term mixed contaminated soil. Chemosphere, 162, 31–39.

Lanchun, S., Bochu, W., Zhiming, L., Chuanren, D., Chuanyun, D., Sakanishi, A., 2003. The research into the influence of low–intensity ultrasonic on the growth of *S. cerevisiaes*. Colloids and Surfaces B: Biointerfaces, 30 (1–2), 43–49.

Lannerö, E., Wickman, M., van Hage, M., Bergström, A., Pershagen, G., Nordvall, L., 2008. Exposure to environmental tobacco smoke and sensitisation in children. Thorax, 63 (2), 172–176.

Lawal, A.T., 2017. Polycyclic aromatic hydrocarbons. A review. Cogent Environmental Science, 3 (1), 1339841.

Li, P., Li, H., Stagnitti, F., Wang, X., Zhang, H., Gong, Z., Liu, W., Xiong, X., Li, L., Austin, C., Barry, D.A., 2005. Biodegradation of pyrene and phenanthrene in soil using immobilized fungi *Fusarium* sp. Bulletin of Environmental Contamination & Toxicology, 75 (3).

Li, C.H., Wong, Y.S., Tam, N.F.Y., 2010a. Anaerobic biodegradation of polycyclic aromatic hydrocarbons with amendment of iron (III) in mangrove sediment slurry. Bioresource Technology, 101 (21), 8083–8092.

Li, X., Lin, X., Zhang, J., Wu, Y., Yin, R., Feng, Y., Wang, Y., 2010b. Degradation of polycyclic aromatic hydrocarbons by crude extracts from spent mushroom substrate and its possible mechanisms. Current microbiology, 60 (5), 336–342.

Li, C.H., Wong, Y.S., Wang, H.Y., Tam, N.F.Y., 2015. Anaerobic biodegradation of PAHs in mangrove sediment with amendment of $NaHCO_3$. Journal of Environmental Sciences, 30, 148–156.

Li, C., Jia, T., Fu, M., Hou, N., Cao, H., Wang, Q., Li, D., 2017. Biodemulsifiers produced by *Achromobacter* sp. and their features in improving the biodegradation of phenanthrene. RSC advances, 7 (8), 4339–4347.

Li, J., Wang, Y., Zhou, W., Chen, W., Deng, M., Zhou, S., 2020. Characterization of a new biosurfactant produced by an effective pyrene–degrading *Achromobacter* species strain AC15. International Biodeterioration & Biodegradation, 152, 104959.

Lin, M., Hu, X., Chen, W., Wang, H., Wang, C., 2014. Biodegradation of phenanthrene by *Pseudomonas* sp. BZ–3, isolated from crude oil contaminated soil. International Biodeterioration & Biodegradation, 94, 176–181.

Liu, X.X., Hu, X., Cao, Y., Pang, W.J., Huang, J.Y., Guo, P., Huang, L., 2019. Biodegradation of phenanthrene and heavy metal removal by acid–tolerant *Burkholderia fungorum* FM–2. Frontiers in Microbiology, 10, 408.

Luo, L., Lin, S., Huang, H., Zhang, S., 2012. Relationships between aging of PAHs and soil properties. Environmental Pollution, 170, 177–182.

Luo, S., Chen, B., Lin, L., Wang, X., Tam, N.F.Y., Luan, T., 2014. Pyrene degradation accelerated by constructed consortium of bacterium and microalga: effects of degradation products on the microalgal growth. Environmental science & technology, 48 (23), 13917–13924.

Ma, J., Xu, L., Jia, L., 2013. Characterization of pyrene degradation by *Pseudomonas* sp. strain Jpyr–1 isolated from active sewage sludge. Bioresource Technology, 140, 15–21.

Ma, X.K., ling Wu, L., Fam, H., 2014. Heavy metal ions affecting the removal of polycyclic aromatic hydrocarbons by fungi with heavy–metal resistance. Applied microbiology and biotechnology, 98 (23), 9817–9827.

Ma, Z., Liu, J., Dick, R.P., Li, H., Shen, D., Gao, Y., Waigi, M.G., Ling, W., 2018. Rhamnolipid influences biosorption and biodegradation of phenanthrene by phenanthrene–degrading strain *Pseudomonas* sp. Ph6. Environmental Pollution, 240, 359–367.

Macaulay, B.M. and Rees, D., 2014. Bioremediation of oil spills: a review of challenges for research advancement. Annals of Environmental Science, 8, 9–37.

Majumdar, D., Rajaram, B., Meshram, S., Suryawanshi, P., Chalapati Rao, C.V., 2016. Worldwide distribution of polycyclic aromatic hydrocarbons in urban road dust. International journal of environmental science and technology, 14 (2), 397–420.

Mani, D. and Kumar, C., 2014. Biotechnological advances in bioremediation of heavy metals contaminated ecosystems: an overview with special reference to phytoremediation. International Journal of Environmental Science and Technology, 11 (3), 843–872.

Mao, J., Luo, Y., Teng, Y., Li, Z., 2012. Bioremediation of polycyclic aromatic hydrocarbon–contaminated soil by a bacterial consortium and associated microbial community changes. International Biodeterioration and Biodegradation, 70, 141–147.

Marco–Urrea, E., García–Romera, I., Aranda, E., 2015. Potential of non–ligninolytic fungi in bioremediation of chlorinated and polycyclic aromatic hydrocarbons. New biotechnology, 32 (6), 620–628.

Mallick, S., Chakraborty, J., Dutta, T.K., 2011. Role of oxygenases in guiding diverse metabolic pathways in the bacterial degradation of low–molecular–weight

polycyclic aromatic hydrocarbons: a review. Critical reviews in microbiology, 37 (1), 64–90.

McNally, D.L., Mihelcic, J.R., Lueking, D.R., 1999. Biodegradation of mixtures of polycyclic aromatic hydrocarbons under aerobic and nitrate–reducing conditions. Chemosphere, 38 (6), 1313–1321.

Megharaj, M., Ramakrishnan, B., Venkateswarlu, K., Sethunathan, N. and Naidu, R., 2011. Bioremediation approaches for organic pollutants: a critical perspective. Environment International, 37 (8), 1362–1375.

Mineki, S., Suzuki, K., Iwata, K., Nakajima, D., Goto, S., 2015. Degradation of polyaromatic hydrocarbons by fungi isolated from soil in Japan. Polycyclic Aromatic Compounds, 35 (1), 120–128.

Mnif, S., Chebbi, A., Mhiri, N., Sayadi, S., Chamkha, M., 2017. Biodegradation of phenanthrene by a bacterial consortium enriched from Sercina oilfield. Process Safety and Environmental Protection, 107, 44–53.

Mohan, S. V., Kisa, T., Ohkuma, T., Kanaly, R. A., Shimizu, Y., 2006. Bioremediation technologies for treatment of PAH–contaminated soil and strategies to enhance process efficiency. Reviews in Environmental Science and Bio/Technology, 5 (4), 347–374.

Moody, J.D., Freeman, J.P., Fu, P.P., Cerniglia, C.E., 2004. Degradation of benzo[a]pyrene by *Mycobacterium vanbaalenii* PYR–1. Applied and Environmental Microbiology, 70 (1), 340–345.

Nitayavardhana, S., Shrestha, P., Rasmussen, M.L., Lamsal, B.P., van Leeuwen, J.H., Khanal, S.K., 2010. Ultrasound improved ethanol fermentation from cassava chips in cassava–based ethanol plants. Bioresource Technology, 101 (8), 2741–2747.

Niti, C., Sunita, S., Kamlesh, K., Rakesh, K., 2013. Bioremediation: An emerging technology for remediation of pesticides. Research Journal of Chemical and Environmental, 17, 88–105.

Ojha, N., Mandal, S.K., Das, N., 2019. Enhanced degradation of indeno(1, 2, 3–cd)pyrene using *Candida tropicalis* NN4 in presence of iron nanoparticles and produced biosurfactant: a statistical approach. 3 Biotech, 9 (3), 1–13.

Okai, M., Kihara, I., Yokoyama, Y., Ishida, M., Urano, N., 2015. Isolation and characterization of benzo [a] pyrene–degrading bacteria from the Tokyo Bay area and Tama River in Japan. FEMS Microbiology Letters, 362 (18), 143.

Okerentugba, P.O., Ataikiru, T.L., Ichor, T., 2016. Isolation and characterization of hydrocarbon utilizing yeast (HUY) isolates from palm wine. American Journal of Molecular Biology, 6 (2), 63–70.

Okonkwo, F.O., Ejike, C.E., Berger, U., Schmaling, C., Schierl, R., Radon, K., 2014. Workplace exposure to polycyclic aromatic hydrocarbons (PAHs): A review and discussion of regulatory imperatives for Nigeria. Research Journal of Environmental Toxicology, 8 (3), 98.

Olsson, A.C., Fevotte, J., Fletcher, T., Cassidy, A., Mannetje, A.T., Zaridze, D., Szeszenia–Dabrowska, N., Rudnai, P., Lissowska, J., Fabianova, E., Mates, D., 2010. Occupational exposure to polycyclic aromatic hydrocarbons and lung cancer risk: a multicenter study in Europe. Occupational and environmental medicine, 67 (2), 98–103.

Ortega–Calvo, J.J., Tejeda–Agredano, M.C., Jimenez–Sanchez, C., Congiu, E., Sungthong, R., Niqui–Arroyo, J.L., Cantos, M., 2013. Is it possible to increase bioavailability but not environmental risk of PAHs in bioremediation?. Journal of Hazardous Materials, 261, 733–745.

Pan, F., Yang, Q., Zhang, Y., Zhang, S., Yang, M., 2004. Biodegradation of polycyclic aromatic hydrocarbons by *Pichia anomala*. Biotechnology letters, 26 (10), 803–806.

Partovinia, A. and Naeimpoor, F., 2013. Phenanthrene biodegradation by immobilized microbial consortium in polyvinyl alcohol cryogel beads. International Biodeterioration and Biodegradation, 85, 337–344.

Passarini, M.R., Rodrigues, M.V., da Silva, M., Sette, L.D., 2011. Marine–derived filamentous fungi and their potential application for polycyclic aromatic hydrocarbon bioremediation. Marine pollution bulletin, 62 (2), 364–370.

Peng, R.H., Xiong, A.S., Xue, Y., Fu, X.Y., Gao, F., Zhao, W., Tian, Y.S., Yao, Q.H., 2008. Microbial biodegradation of polyaromatic hydrocarbons. FEMS microbiology reviews, 32 (6), 927–955.

Ping, L., Zhang, C., Zhang, C., Zhu, Y., He, H., Wu, M., Tang, T., Li, Z., Zhao, H., 2014. Isolation and characterization of pyrene and benzo[a]pyrene–degrading *Klebsiella pneumonia* PL1 and its potential use in bioremediation. Applied microbiology and biotechnology, 98 (8), 3819–3828.

Ping, L., Zhang, C., Cui, H., Yuan, X., Cui, J., Shan, S., 2017. Characterization and application of a newly isolated pyrene–degrading bacterium, *Pseudomonas monteilii*. 3 Biotech, 7 (5), 309.

Pozdnyakova, N.N., 2012. Involvement of the ligninolytic system of white–rot and litter– decomposing fungi in the degradation of polycyclic aromatic hydrocarbons. Biotechnology Research International, 2012.

Priya, A., Manab Sarma, P., Lal, B., 2016. Isolation and characterization of *Candida vishwanathii* strain TERI MS1 for degradation of petroleum hydrocarbons in

marine environment. Desalination and Water Treatment, 57 (46), 22099–22106.

Ramadan, K.M., Azeiz, A.A., Hassanien, S.E., Eissa, H.F., 2012. Biodegradation of used lubricating and diesel oils by a new yeast strain *Candida viswanathii* KA–2011. African Journal of Biotechnology, 11 (77), 14166–14174.

Ravindra, K., Sokhi, R., Van Grieken, R., 2008. Atmospheric polycyclic aromatic hydrocarbons: source attribution, emission factors and regulation. Atmospheric Environment, 42 (13), 2895–2921.

Rigo, M., Alegre, R.M., Bezerra, J.R.M.V., Coelho, N., Bastos, R.G., 2010. Catechol biodegradation kinetics using *Candida parapsilopsis*. Brazilian Archives of Biology and Technology, 53 (2), 481–486.

Rodriguez–Morgado, B., Gomez, I., Parrado, J., Garcia, C., Hernandez, T., Tejada, M., 2015. Accelerated degradation of PAHs using edaphic biostimulants obtained from sewage sludge and chicken feathers. Journal of Hazardous Materials, 300, 235–242.

Salam, L., Ilori, M.O., Amund, O.O., 2017. Pyrene Biodegradation Potential of an Actinomycete, *Microbacterium Esteraromaticum* Isolated from Tropical Hydrocarbon–Contaminated Soil.

See, S.W., Karthikeyan, S., Balasubramanian, R., 2006. Health risk assessment of occupational exposure to particulate–phase polycyclic aromatic hydrocarbons associated with Chinese, Malay and Indian cooking. Journal of Environmental Monitoring, 8 (3), 369–376.

Seo, J.S., Keum, Y.S., Li, Q.X., 2009. Bacterial degradation of aromatic compounds. International journal of environmental research and public health, 6 (1), 278–309.

Shah, Y.T., Pandit, A.B., Moholkar, V.S., 1999. Sources and types of cavitation. In Cavitation reaction engineering, 1–14, Springer, Boston, MA.

Shahsavari, E., Schwarz, A., Aburto–Medina, A., Ball, A.S., 2019. Biological degradation of polycyclic aromatic compounds (PAHs) in soil: a current perspective. Current Pollution Reports, 5 (3), 84–92.

Simister, R.L., Poutasse, C.M., Thurston, A.M., Reeve, J.L., Baker, M.C., White, H.K., 2015. Degradation of oil by fungi isolated from Gulf of Mexico beaches. Marine pollution bulletin, 100 (1), 327–333.

Singh, P. and Tiwary, B.N., 2017. Optimization of conditions for polycyclic aromatic hydrocarbons (PAHs) degradation by *Pseudomonas stutzeri* P2 isolated from Chirimiri coal mines. Biocatalysis and agricultural biotechnology, 10, 20–29.

Sood, N., Patle, S., Lal, B., 2010. Bioremediation of acidic oily sludge–contaminated soil by the novel yeast strain *Candida digboiensis* TERI ASN6. Environmental Science and Pollution Research, 17 (3), 603–610.

Srogi, K., 2007. Monitoring of environmental exposure to polycyclic aromatic hydrocarbons: a review. Environmental Chemistry Letters, 5 (4), 169–195.

Stringfellow, W.T. and Aitken, M.D., 1995. Competitive metabolism of naphthalene, methylnaphthalenes, and fluorene by phenanthrene–degrading pseudomonads. Applied and environmental microbiology, 61 (1), 357–362.

Sun, K., Liu, J., Gao, Y., Jin, L., Gu, Y., Wang, W., 2014a. Isolation, plant colonization potential, and phenanthrene degradation performance of the endophytic bacterium *Pseudomonas* sp. Ph6–gfp. Scientific reports, 4, 5462.

Sun, M., Ye, M., Hu, F., Li, H., Teng, Y., Luo, Y., Jiang, X., Kengara, F.O., 2014b. Tenax extraction for exploring rate–limiting factors in methyl–β–cyclodextrin

enhanced anaerobic biodegradation of PAHs under denitrifying conditions in a red paddy soil. Journal of hazardous materials, 264, 505–513.

Tortella, G.R., Diez, M.C., Durán, N., 2005. Fungal diversity and use in decomposition of environmental pollutants. Critical reviews in microbiology, 31 (4), 197–212.

Ukiwe, L.N., Egereonu, U.U., Njoku, P.C., Nwoko, C.I., Allinor, J.I., 2013. Polycyclic aromatic hydrocarbons degradation techniques. International Journal of Chemistry, 5 (4).

Unwin, J., Cocker, J., Scobbie, E., Chambers, H., 2006. An assessment of occupational exposure to polycyclic aromatic hydrocarbons in the UK. Annals of Occupational Hygiene, 50 (4), 395–403.

Valentin, L., Nousiainen, A., Mikkonen, A., 2013. Introduction to organic contaminants in soil: concepts and risks. In Emerging Organic Contaminants in Sludges, Springer, Berlin, Heidelberg, 1–29.

Van Herwijnen, R., Wattiau, P., Bastiaens, L., Daal, L., Jonker, L., Springael, D., Govers, H.A.J., Parsons, J.R., 2003. Elucidation of the metabolic pathway of fluorene and cometabolic pathways of phenanthrene, fluoranthene, anthracene and dibenzothiophene by *Sphingomonas* sp LB126. Research in Microbiology, 154, 199–206.

Varjani, S.J., 2017. Microbial degradation of petroleum hydrocarbons. Bioresource Technology, 223, 277–286.

Verma, M., Brar, S.K., Tyagi, R.D., Surampalli, R.Y., 2007. Bioremediation with fungi. In Remediation Technologies for Soils and Groundwater, 259–289.

Vidali, M., 2001. Bioremediation. an overview. Pure and Applied Chemistry, 73 (7), 1163–1172.

Wagrowski, D. M. and Hites, R. A., 1997. Polycyclic aromatic hydrocarbon accumulation in urban, suburban, and rural vegetation. Environmental Science & Technology, 31 (1), 279–282.

Wang, X., Gong, Z., Li, P., Zhang, L., 2007. Degradation of pyrene in soils by free and immobilized yeasts, *Candida tropicalis*. Bulletin of environmental contamination and toxicology, 78, 522–526.

Wang, L., Lin, Y., Yang, L., Yu, P., Xie, Z., Luo, Y., 2011. *Candida tropicalis*: characterization of a strain capable of degrading high concentrations of phenol. Biotechnology letters, 33 (5), 943–946.

Wang, Y., Tian, Z., Zhu, H., Cheng, Z., Kang, M., Luo, C., Li, J., Zhang, G., 2012. Polycyclic aromatic hydrocarbons (PAHs) in soils and vegetation near an e–waste recycling site in South China: concentration, distribution, source, and risk assessment. Science of the Total Environment, 439, 187–193.

Wang, H., Lou, J., Gu, H., Luo, X., Yang, L., Wu, L., Liu, Y., Wu, J., Xu, J., 2016. Efficient biodegradation of phenanthrene by a novel strain *Massilia* sp. WF1 isolated from a PAH–contaminated soil. Environmental Science and Pollution Research, 23 (13), 13378–13388.

Wang, Z., Wang, W., Li, Y., Yang, Q., 2019. Co–metabolic degradation of naphthalene and pyrene by acclimated strain and competitive inhibition kinetics. Journal of Environmental Science and Health, Part B, 54 (6), 505–513.

WHO, 1983. Polynuclear aromatic compounds, Part 1, chemical, environmental and experimental data. IARC Monographs on the Evaluation of the Carcinogenic Risk of Chemicals to Man, IARC Scientific Publications, 32, 1–453.

Wu, Y.R., He, T.T., Lun, J.S., Maskaoui, K., Huang, T.W., Hu, Z., 2009. Removal of benzo[a]pyrene by a fungus *Aspergillus* sp. BAP14. World Journal of Microbiology and Biotechnology, 25 (8), 1395–1401.

Wu, F., Guo, C., Liu, S., Liang, X., Lu, G., Dang, Z., 2019. Pyrene Degradation by *Mycobacterium gilvum*: Metabolites and Proteins Involved. Water, Air, & Soil Pollution, 230 (3), 67.

Yan, J., Jianping, W., Hongmei, L., Suliang, Y., Zongding, H., 2005. The biodegradation of phenol at high initial concentration by the yeast *Candida tropicalis*. Biochemical Engineering Journal, 24 (3), 243–247.

Yan, J., Jianping, W., Jing, B., Daoquan, W., Zongding, H., 2006. Phenol biodegradation by the yeast *Candida tropicalis* in the presence of m–cresol. Biochemical Engineering Journal, 29 (3), 227–234.

Yang, X., Ye, J., Lyu, L., Wu, Q., Zhang, R., 2013. Anaerobic biodegradation of pyrene by *Paracoccus denitrificans* under various nitrate/nitrite–reducing conditions. Water, Air, & Soil Pollution, 224 (5), 1578.

Yuan, H., Yao, J., Masakorala, K., Wang, F., Cai, M., Yu, C., 2014. Isolation and characterization of a newly isolated pyrene–degrading *Acinetobacter* strain USTB–X. Environmental Science and Pollution Research, 21 (4), 2724–2732.

Zeng, G., Liu, Z., Zhong, H., Li, J., Yuan, X., Fu, H., Ding, Y., Wang, J., Zhou, M., 2011. Effect of monorhamnolipid on the degradation of n–hexadecane by *Candida tropicalis* and the association with cell surface properties. Applied microbiology and biotechnology, 90 (3), 1155–1161.

Zhao, H.P., Wu, Q.S., Wang, L., Zhao, X.T., Gao, H.W., 2009. Degradation of phenanthrene by bacterial strain isolated from soil in oil refinery fields in Shanghai China. Journal of hazardous materials, 164 (2–3), 863–869.

Zhao, Y., Ang, W.T., Xing, J., Zhang, J., Chen, J., 2012. Applications of ultrasound to enhance mycophenolic acid production. Ultrasound in medicine & biology, 38 (9), 1582–1588.

Zhao, Z., Zhang, L., Cai, Y., Chen, Y., 2014. Distribution of polycyclic aromatic hydrocarbon (PAH) residues in several tissues of edible fishes from the largest freshwater lake in China, Poyang Lake, and associated human health risk assessment. Ecotoxicology and Environmental Safety, 104, 323–331.

Zhong, Y., Zou, S., Lin, L., Luan, T., Qiu, R., Tam, N.F., 2010. Effects of pyrene and fluoranthene on the degradation characteristics of phenanthrene in the cometabolism process by *Sphingomonas* sp. strain PheB4 isolated from mangrove sediments. Marine pollution bulletin, 60 (11), 2043–2049.

Zhou, H., Wang, H., Huang, Y., Fang, T., 2016. Characterization of pyrene degradation by halophilic *Thalassospira* sp. strain TSL5–1 isolated from the coastal soil of Yellow Sea, China. International Biodeterioration & Biodegradation, 107, 62–69.

# CHAPTER 2

# Biodegradation of phenanthrene and pyrene using *Candida tropicalis*: Process optimization and kinetic study

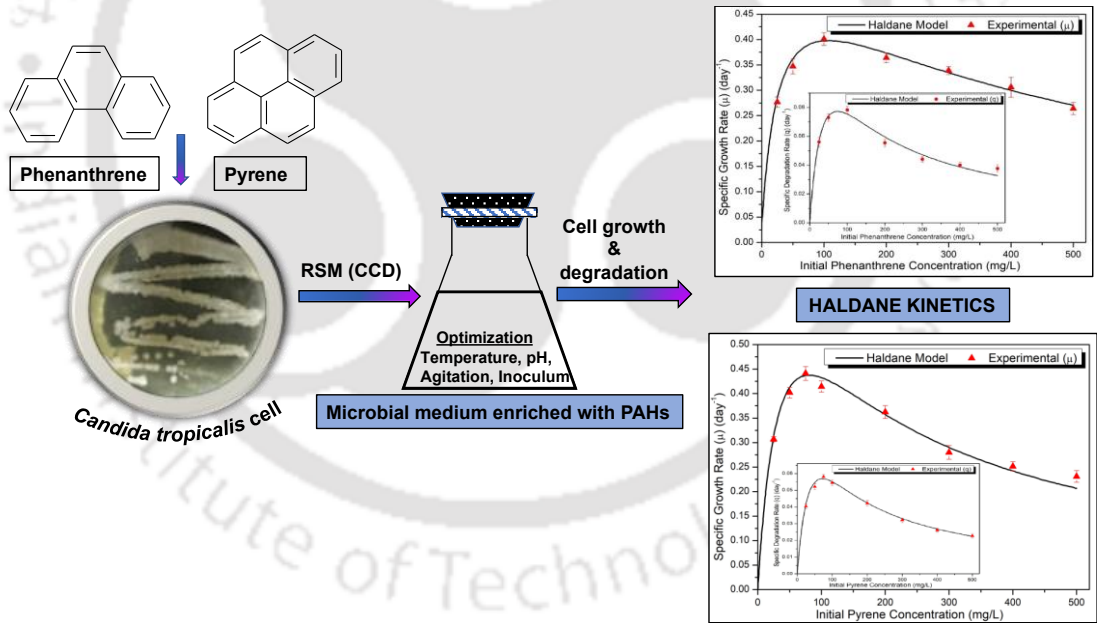

# CHAPTER 2

# Biodegradation of phenanthrene and pyrene using *Candida tropicalis*: Process optimization and kinetic study

## 2.1 INTRODUCTION

Among organic pollutants emerging from chemical and process industries, polycyclic aromatic hydrocarbons (PAHs) have gained noteworthy attention for decades owing to their extraordinary stability in terrestrial/aquatic environments, resistance to degradation through conventional advanced oxidation processes (AOPs) and harmful effects on ecosystem (Chebbi et al., 2017; Ortega–Calvo et al., 2013; Feng et al., 2012). PAHs like phenanthrene and pyrene are found ubiquitously and their ever–increasing concentrations is a serious threat to both mankind and environment (Hong et al., 2016; Srogi, 2007; Unwin et al., 2006). Effective degradation and

mineralization of PAHs has become major challenge for environmentalists worldwide. Bioremediation of PAHs using suitable microbial species has become a potential alternative to conventional oxidative processes. This technique has gained attention of research community, as it is cost–effective, safe and eco–friendly (Haritash and Kaushik 2009). Several fungi have been employed for bioremediation (Hidayat and Yanto 2018; Hadibarata and Tachibana 2010; Hesham et al., 2006; Pan et al., 2004). *Candida* sp. has been recognized as one of the commonly used non–ligninolytic fungi for bioremediation of different PAHs (Ojha et al., 2019; Hadibarata et al., 2017; Farag and Soliman, 2011). The degrading capability of microorganisms is a function of physical parameters like pH, carbon sources, temperature, and nutrients (Csutak et al., 2010). Biodegradation of PAHs can be enhanced by proper optimization of the physical process parameters (Umar et al., 2017). Analysis of the kinetics involved in any bioremediation process provides a clear picture of the various significant factors promoting and inhibiting degradation (Basak et al., 2014).

This chapter addresses the primary facet of a typical bioprocess, i.e. optimization of physical parameters and the kinetic analysis of microbial growth (with consumption of substrate – which essentially is the degradation of the pollutants in present context). The model system of present study comprises of PAHs (phenanthrene and pyrene) and *Candida tropicalis* MTCC 184. The physical parameters related to phenanthrene and pyrene biodegradation were optimized by response surface methodology using the central composite design of experiments. For the statistical optimization, four experimental parameters, viz. medium pH, % inoculum, temperature, and mechanical shaking were taken. Kinetic study was performed using different substrate inhibition models. The experimental profiles of biomass and substrate during bioremediation have been analyzed using kinetic models

that account for substrate inhibition. Both physical parameter optimization and kinetic parameter study is essential to have a fundamental knowledge and for the smooth functioning of the biodegradation process. The methodology and results obtained have been explained in subsequent sections.

## 2.2 MATERIALS AND METHODS

### 2.2.1 Microbial growth and maintenance

Yeast strain, *Candida tropicalis* MTCC 184, was acquired from the Institute of Microbial Technology (IMTECH), Chandigarh, India. The strain was conserved by sub–culturing on yeast extract peptone dextrose (YEPD) agar plates and storage at 4°C. *C. tropicalis* was grown on an incubator shaker (Make: Lab Companion; Model: SI–300R) at pH 7, 30°C and 150 rpm. Sub–culture was done every month and preserved at –80°C in glycerol (20% v/v). For the experiments on PAH biodegradation, the yeast was grown in Bushnell–Hass (BH) minimal salt medium with a composition of (g $L^{-1}$): $K_2HPO_4$ (1.0); $KH_2PO_4$ (1.0); $NH_4NO_3$ (1.0); $FeCl_3$ (0.05); $MgSO_4 \cdot 7H_2O$ (0.2) and $CaCl_2 \cdot 2H_2O$ (0.02). The biodegradation experiments were performed in BH medium with phenanthrene/pyrene as sole carbon source.

### 2.2.2 Chemicals, medium, and reagents

Phenanthrene and pyrene (sublimed grade, ≥ 99.5%) was procured from Sigma–Aldrich (India). Bushnell Haas (BH) medium was procured from Himedia (Mumbai, India). HPLC grade acetonitrile, acetone and n–hexane were purchased from Merck, India. The rest of the chemicals (analytical grade) used for analysis were acquired from Himedia (Mumbai, India).

### 2.2.3 Batch biodegradation experiments

In a typical experiment, the yeast culture was initially grown in YEPD

medium at 30°C, 150 rpm and pH 7. The pre–culture was incubated until it attained an optical density of 0.5 – 0.6 at 600 nm (OD600 nm). Successively, yeast biomass was separated through centrifugation, washed, and the pellets were suspended in BH medium. Next, the pre–culture was inoculated in the degradation medium with phenanthrene/pyrene as sole carbon source. Prior to degradation, BH medium was sterilized (autoclaved at 121°C, 20 min) followed by inoculation of seed culture. Due to low solubility in water, both the PAHs were dissolved in minimum acetone (2 – 3 mL) separately, and then the mixture was added to working volume of 100 mL BH medium in 250 mL Erlenmeyer flask. Un–inoculated controls flasks containing only BH medium and PAH were maintained to validate any abiotic loss. The experiments were carried out for 14 days, while samples were collected at regular intervals to monitor cell biomass growth and residual PAH.

After completion of 14 days, samples were initially extracted using an equal volume of n–hexane. The mixtures were vortex agitated, followed by 10 min centrifugation (10,000 rpm) to obtain residual PAH in the organic layer. The solution was allowed to settle, and the organic layer comprising n–hexane, and PAH was procured in vials. Samples with three replicates were prepared and were analyzed using high performance liquid chromatography (HPLC) (Agilent Technologies, 1220 Infinity LC) fitted with C18 reverse–phase column (3 mm × 150 mm and particle size of 3.5 μm). Acetonitrile: Milli–Q water (volume ratio 70:30) was taken as the mobile phase or eluent, 0.8 mL $min^{-1}$ flow rate with 20 μL injection volume. The compound was identified with a UV detector (254 nm), and retention time was compared against standards of phenanthrene and pyrene.

### 2.2.4 PAH tolerance of *C. tropicalis*

The tolerance of *C. tropicalis* strain towards phenanthrene and pyrene was examined through studying two important factors, viz. (1) biomass growth pattern and (2) degradation potential of the strain under different initial PAH concentrations ranging from 0 – 500 mg $L^{-1}$. Experiments were conducted where the pre–culture of *C. tropicalis* was inoculated in 100 mL liquid medium (BH medium) in 250 mL Erlenmeyer flask supplemented with different phenanthrene and pyrene concentrations separately. A control flask was also kept without any carbon (PAH source) to monitor any biomass growth in the absence of PAH. Every experiment including the control was conducted for 14 days and repeated three times for the assessment of reproducibility. Based on the tolerance of the strain, the concentration of phenanthrene and pyrene was fixed for the subsequent experiments.

### 2.2.5 Statistical optimization of physical parameters for PAH degradation

The physical parameters of PAH (phenanthrene and pyrene) biodegradation were optimized by response surface methodology using the central composite design (CCD) of experiments. Four experimental parameters, viz. medium pH, % inoculum, temperature, and agitation speed, were taken as the independent variables (or optimization parameters). Percentage degradation of both PAHs was the response (or dependent) variable. Two levels were chosen for each physical parameter, coded as (–1) for lower level and (+1) for higher level, as depicted in Table 2.1. The complete design of experiments was based on five coded levels ($-\alpha$, –1, 0, +1, $+\alpha$) of optimization parameters with zero as the central coded value. The complete design of experiments (devised using MINITAB, statistical software, release 15.1, PA, USA, Trial Version) comprised of a set of 31 individual experiments with permutation/combination of optimization parameters. The results of statistical

experimental design were studied using response surface methodology.

**Table 2.1.** Factors and levels of central composite experimental design (actual and coded values).

| Factors | Levels | |
|---|---|---|
| | Low (–1) | High (+1) |
| Medium pH ($X_1$) | 4 | 8 |
| Temperature (°C) ($X_2$) | 20 | 40 |
| Agitation speed (rpm) ($X_3$) | 130 | 170 |
| Inoculum size (%, v/v) ($X_4$) | 5 | 10 |

The experimental data acquired from central composite design was fitted to the quadratic equation with individual and interactive coefficients corresponding to operating parameters:

$$Y = \beta_0 + \sum_{i=1}^{k} \beta_i X_i + \sum_{i=1}^{k} \beta_{ii} X_i^2 + \sum\sum \beta_{ij} X_i X_j \quad (1)$$

Notation: $Y$ – dependent variable (% PAH degraded), k – number of factors, $\beta_0$, $\beta_i$, $\beta_{ii}$, $\beta_{ij}$ – regression coefficient acquired for constant, linear, quadratic, and interaction, respectively. The coded values (X) of the optimization variables are defined as: $X = (x_i - x_0)/\Delta x$, where $i$ = 1, 2, 3…, $x_i$ is a dimensionless value of the variables, $x_0$ is the value of $x_i$ at center point, and $\Delta x$ is the step change. Analysis of variance (ANOVA) with 95% confidence intervals was also done to identify the significant parameters of optimization (using the *F*– and *p*– values), the relative significance of interactions between these parameters and to determine the goodness of fit.

***Validation experiments:*** For validation of statistical optimization, biodegradation experiments with phenanthrene and pyrene (separately) were conducted in triplicates at optimum conditions (or parameters) predicted by the statistical experiments.

### 2.2.6 Kinetic analysis of PAH biodegradation

The previous literature (Basak et al., 2014) has reported significant substrate

inhibition effects during the growth of yeasts, such as *C. tropicalis* on organic pollutants. Substrate (PAH) utilization rate is written as:

$$\frac{dS}{dt} = -qX = -\left(\mu / Y_{x/s}\right) X \tag{2}$$

Notations are as follows: $S$ = PAH concentration (mg $L^{-1}$), $\mu$ = specific biomass (or cell) growth rate ($day^{-1}$), $t$ = incubation time (day), $X$ = dry cell weight (mg $L^{-1}$), $Y_{x/s}$ = growth yield coefficient (g $g^{-1}$), $q$ = specific degradation rate ($day^{-1}$). Yield factor for biomass, $Y_{x/s}$ (g dry biomass/g PAH) can be calculated as follows:

$$Y_{x/s} = -\frac{dX/dt}{dS/dt} = -\frac{dX}{dS} = -\frac{\left(X - X_0\right)}{\left(S - S_0\right)} \tag{3}$$

Profile of biomass involving growth and decay is written as:

$$\frac{dX}{dt} = \mu X - bX \tag{4}$$

where $b$ = biomass decay coefficient ($day^{-1}$). For the integration of equations 2 and 4, we have used the value of specific growth rate ($\mu$) corresponding to initial substrate concentration ($S = S_0$). Several kinetic models that account for substrate inhibition are available in the literature. The basic kinetic model for substrate inhibition is Haldane's kinetic model:

$$\mu = \left.\frac{\mu_{\max} S}{K_S + S + \left(S^2 / K_i\right)}\right|_{S=S_0} \tag{5}$$

where, $S$ = PAH concentration (mg $L^{-1}$), $\mu$ = specific biomass growth rate ($day^{-1}$), $\mu_{max}$ = maximum specific biomass growth rate ($day^{-1}$), $K_s$ = half saturation coefficient (mg $L^{-1}$), $K_i$ = inhibition coefficient (mg $L^{-1}$). However, other semi–empirical models reported in the literature are:

Aiba model: $$\mu = \left.\frac{\mu_{\max} S}{K_s + S} \exp\left(-S / K_i\right)\right|_{S=S_0} \tag{6}$$

Edward model: $$\mu = \left.\frac{\mu_{max} S}{S + K_s + \left(S^2/K_i\right)\left(1 + S/K_s\right)}\right|_{S=S_0} \quad (7)$$

Yano model: $$\mu = \left.\frac{\mu_{max} S}{S + K_s + \left(S^2/K_i\right)\left(1 + S/K\right)}\right|_{S=S_0} \quad (8)$$

The kinetic parameters in the above models were determined from the analysis of $\mu$ and $q$ over a wide range of initial substrate concentrations, viz. $S_0$ = 25 – 500 mg $L^{-1}$. The specific biomass growth rate ($\mu$) in the log or exponential phase of each experiment was obtained using basic relation: $dX/dt = -\mu X$ (i.e., equation 4 with decay coefficient assumed as zero), or as slope of the plot $\ln\left(X/X_i\right)$ versus $t$. The plot of $\mu$ versus $S_0$ was fitted to equations 5 to 8 using non–linear regression method in MATLAB R2018b to yield the growth coefficients $\mu_{max}$, $K$, $K_S$, and $K_i$. The best model for the analysis was selected on the basis of regression coefficient. For determination of specific degradation rate ($q$), a similar procedure was followed, in which the experimental values of $q$ (specific degradation rate) for varying initial substrate concentrations ($S_0$) were determined from the degradation profiles for the total period of experiment (14 days). This data was fitted to analogous expressions for $q$ (as a function of $S$ at $S = S_0$), as given in equations 5 to 8, to obtain parameters of $q_{max}$, $K'$, $K'_S$, $K'_i$.

## 2.3 RESULTS AND DISCUSSION

### 2.3.1 Tolerance of *C. tropicalis* to PAHs

The tolerance of the yeast strain to phenanthrene and pyrene separately was studied by performing batch experiments with different initial concentrations of the PAHs ranging from 0 – 500 mg $L^{-1}$. The trends of final biomass concentrations and residual phenanthrene and pyrene concentration are given in Fig. 2.1 (A and B). For

phenanthrene, the final biomass concentration in the mixture shows a maximum for initial concentration of 100 mg $L^{-1}$ and reduces thereafter. For pyrene, the final biomass concentration in the mixture shows a maximum for initial concentration of 75 mg $L^{-1}$ and reduces thereafter. This results demonstrate inhibition on growth of *C. tropicalis cells* after a certain initial concentration of the pollutant. The absolute phenanthrene and pyrene degradation rises with initial concentration in the mixture, but not proportionately, and this could be a manifestation of inhibition of biomass growth by both the PAHs.

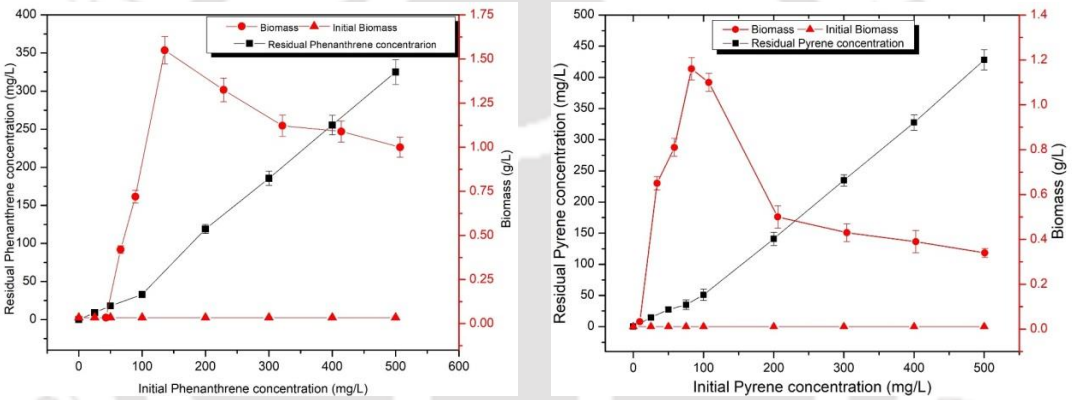


(A) (B)

**Figure 2.1.** PAHs tolerance of *C. tropicalis* cells: A. Biomass growth and phenanthrene degradation under different initial concentration of phenanthrene (0 – 500 mg $L^{-1}$) and B. Biomass growth and pyrene degradation under different initial concentration of pyrene (0 – 500 mg $L^{-1}$).

### 2.3.2 Statistical optimization of process parameters

#### 2.3.2.1 Statistical results of phenanthrene degradation parameters

The experimental data obtained from central composite design was fitted to a 2nd–order regression equation as:

$$Y = 45.857 - 0.812X_1 + 4.895X_2 + 1.312X_3 + 3.645X_4 - 9.792X_1^2 - 6.354X_2^2 - 0.354X_3^2 - 4.792X_4^2 + 2.406X_1X_2 + 0.031X_1X_3 + 2.343X_1X_4 - 0.218X_2X_3 - 0.656X_2X_4 + 1.593X_3X_4 \quad (9)$$

The notations for experimental parameters or factors and their levels with actual and coded values are provided in Table 2.1. The full CCD experimental design, along with the predicted and experimental values of response variable (i.e. percentage degradation) are shown in Table 2.2.

**Table 2.2.** Full factorial central composite design matrix of phenanthrene degradation parameters in coded and actual (in parentheses) values.

| Run order | Medium pH ($X_1$) | Temperature (°C) ($X_2$) | Agitation speed (rpm) ($X_3$) | Inoculum size (%, v/v) ($X_4$) | Phenanthrene degraded (%) | |
|---|---|---|---|---|---|---|
| | | | | | Experimental | Predicted |
| 1 | 0 (6) | –α (10) | 0 (150) | 0 (7.5) | 25.50±0.07 | 25.64 |
| 2 | 0 (6) | 0 (30) | 0 (150) | –α (2.5) | 34.00±0.16 | 34.39 |
| 3 | –1 (4) | +1 (40) | –1 (130) | +1 (10.0) | 40.50±0.09 | 40.85 |
| 4 | 0 (6) | 0 (30) | 0 (150) | 0 (7.5) | 61.00±0.30 | 60.85 |
| 5 | +1 (8) | +1 (40) | –1 (130) | +1 (10.0) | 48.50±0.19 | 48.66 |
| 6 | –1 (4) | +1 (40) | +1 (170) | +1 (10.0) | 46.00±0.09 | 46.16 |
| 7 | –1 (4) | –1 (20) | –1 (130) | –1 (5.0) | 36.00±0.28 | 36.02 |
| 8 | +1 (8) | +1 (40) | +1 (170) | +1 (10.0) | 54.00±0.03 | 54.10 |
| 9 | +1 (8) | –1 (20) | –1 (130) | +1 (10.0) | 34.50±0.06 | 34.93 |
| 10 | –1 (4) | –1 (20) | –1 (130) | +1 (10.0) | 37.00±0.16 | 36.75 |
| 11 | 0 (6) | 0 (30) | 0 (150) | 0 (7.5) | 61.00±0.28 | 60.85 |
| 12 | –1 (4) | +1 (40) | –1 (130) | –1 (5.0) | 43.00±0.17 | 42.75 |
| 13 | –1 (4) | +1 (40) | +1 (170) | –1 (5.0) | 42.00±0.10 | 41.68 |
| 14 | 0 (6) | 0 (30) | +α (190) | 0 (7.5) | 62.00±0.09 | 62.06 |
| 15 | –α (2) | (0 30) | 0 (150) | 0 (7.5) | 23.00±0.07 | 23.31 |
| 16 | +1 (8) | –1 (20) | +1 (170) | +1 (10.0) | 41.00±0.14 | 41.25 |
| 17 | +α (10) | 0 (30) | 0 (150) | 0 (7.5) | 20.50±0.19 | 20.06 |
| 18 | –1 (4) | –1 (20) | +1 (170) | +1 (10.0) | 43.00±0.23 | 42.93 |
| 19 | +1 (8) | –1 (20) | –1 (130) | –1 (5.0) | 25.00±0.38 | 24.83 |
| 20 | 0 (6) | 0 (30) | 0 (150) | 0 (7.5) | 60.50±0.21 | 60.85 |
| 21 | 0 (6) | 0 (30) | 0 (150) | 0 (7.5) | 61.00±0.13 | 60.85 |
| 22 | 0 (6) | 0 (30) | 0 (150) | 0 (7.5) | 61.00±0.09 | 60.85 |
| 23 | +1 (8) | –1 (20) | +1 (170) | –1(5.0) | 25.00±0.06 | 24.77 |
| 24 | 0 (6) | 0 (30) | 0 (150) | +α (12.5) | 49.50±0.09 | 48.97 |
| 25 | 0 (6) | +α (50) | 0 (150) | 0 (7.5) | 45.50±0.08 | 45.22 |
| 26 | +1 (8) | +1 (40) | +1 (170) | –1 (5.0) | 40.00±0.12 | 40.25 |
| 27 | 0 (6) | 0 (30) | –α (110) | 0 (7.5) | 57.00±0.17 | 56.81 |
| 28 | 0 (6) | 0 (30) | 0 (150) | 0 (7.5) | 60.50±0.15 | 60.85 |
| 29 | 0 (6) | 0 (30) | 0 (150) | 0 (7.5) | 61.00±0.26 | 60.85 |
| 30 | +1 (8) | +1 (40) | – 1 (130) | –1 (5.0) | 41.00±0.36 | 41.18 |
| 31 | –1 (4) | –1 (20) | +1 (170) | –1 (5.0) | 36.00±0.09 | 35.83 |

The values of the regression coefficients, viz. $R^2$ = 0.999, predicted $R^2$ = 0.998,

adjusted $R^2$ = 0.999 indicated that the model fits well to the experimental data. The coefficients of the quadratic response model (as given in equation 1) along with the *t*– and *p*– values of linear, quadratic and interaction coefficients are provided in Table 2.3(A). The ANOVA for the fitted model is displayed in Table 2.3(B).

**Table 2.3.** Statistical analysis of central composite experimental design for process parameter optimization of phenanthrene degradation.

(A) Model Coefficients, *t*– and *p*–values for each variable

| Model term | Coefficient | *t*–value | *p*–value |
|---|---|---|---|
| Intercept ($\beta_0$) | 45.857 | 335.990 | 0.000* |
| *Linear coefficients* | | | |
| Medium pH ($X_1$) | -0.812 | -11.023 | 0.000* |
| Temperature ($X_2$) | 4.895 | 66.421 | 0.000* |
| Agitation speed ($X_3$) | 1.312 | 17.806 | 0.000* |
| % Inoculum ($X_4$) | 3.645 | 49.462 | 0.000* |
| *Square coefficients* | | | |
| Medium pH ($X_1$) × Medium pH ($X_1$) | -9.792 | -145.014 | 0.000* |
| Temperature ($X_2$) × Temperature ($X_2$) | -6.354 | -94.109 | 0.000* |
| Agitation speed ($X_3$) × Agitation speed ($X_3$) | -0.354 | -5.256 | 0.000* |
| % Inoculum ($X_4$) × % Inoculum ($X_4$) | -4.792 | -70.970 | 0.000* |
| *Interaction coefficients* | | | |
| Medium pH ($X_1$) × Temperature ($X_2$) | 2.343 | 25.962 | 0.000* |
| Medium pH ($X_1$) × Agitation speed ($X_3$) | 0.031 | 0.346 | 0.734 |
| Medium pH ($X_1$) × % Inoculum ($X_4$) | 2.343 | 25.962 | 0.000* |
| Temperature ($X_2$) × Agitation speed ($X_3$) | -0.218 | -2.423 | 0.028* |
| Temperature ($X_2$) × % Inoculum ($X_4$) | -0.656 | -7.269 | 0.000* |
| Agitation speed ($X_3$) × % Inoculum ($X_4$) | 1.593 | 17.654 | 0.000* |

* Significant *p* values, $p \leq 0.05$; $R^2$= 0.999; Predicted $R^2$ = 0.998; Adjusted $R^2$ = 0.999

(B) ANOVA for quadratic model

| Source | DF | SS | MS | *F*–value | *p*–value |
|---|---|---|---|---|---|
| Regression | 14 | 5109.90 | 364.99 | 2799.15 | 0.000 |
| Linear | 4 | 951.46 | 237.86 | 1824.19 | 0.000 |
| Square | 4 | 3929.60 | 982.40 | 7534.06 | 0.000 |
| Interaction | 6 | 228.84 | 38.14 | 292.50 | 0.000 |
| Residual (error) | 16 | 2.09 | 0.13 | | |
| Lack of fit | 10 | 1.73 | 0.17 | 2.91 | 0.102 |
| Pure Error | 6 | 0.36 | 0.06 | | |
| Total | 30 | 5111.98 | | | |

DF – Degree of freedom; SS – Sum of squares; MS – Mean square

The *t*–, *F*– and *p*–values of the coefficients indicate the significance of the variables. Large *t*–value and *p*–value < 0.05 denotes the significance of coefficient

and the optimization variable to which the coefficient belongs. The relative *F*–values of linear interaction and quadratic coefficient indicate the significance of the individual effect of the variable and the magnitude of interaction between them. As per the ANOVA results displayed in Table 2.3B, the *F*–value of overall regression is 2799.15 and *F*–value of linear coefficient is 1824.19. The *p*–values of every linear, quadratic and interaction coefficient is < 0.05, which denotes their significance. The Lack of Fit *F*–value is 2.91 and *p*–value is 0.102, which implies that the Lack of Fit is not significant in comparison to the pure error, therefore, in other words, the model is significant. Nonetheless, it must be noted that the regression model is effective simply within the limits of optimization variables used in the experimental design. The global optimum values of variables (process parameters) corresponding to maximum response variable (phenanthrene degradation) were obtained as: medium pH = 6.2, temperature = 33.4°C, agitation speed = 190 rpm and % inoculum = 9.26 vol%. At optimum conditions, the maximum phenanthrene degradation predicted by the quadratic model was 65.19%. The desirability function plot showing optimum levels of process parameters is shown in Fig. 2.2.

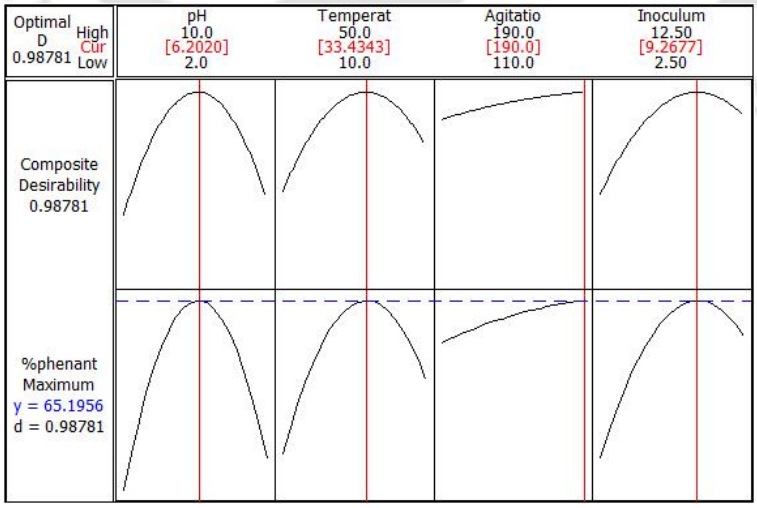


**Figure 2.2.** Desirability function plot for optimum levels of process parameters in phenanthrene degradation.

***Validation experiment*:** Validation of the statistical results obtained from optimization of physical operating parameters was done by performing phenanthrene degradation experiments using *C. tropicalis.* The experiments were performed using the results of CCD analyses as described in the preceding sections. For 100 mg $L^{-1}$ initial phenanthrene concentration, a residual concentration of 34 ± 2 mg $L^{-1}$ was obtained after 14 days, which corresponded to ~ 66% degradation. This result matched closely with the predictions of statistical experimental design.

**2.3.2.2 Statistical results of pyrene degradation parameters**

The experimental data obtained from CCD was fitted to a second–order regression equation. This equation in coded variables is depicted as:

$$Y = 53.028 + 0.541X_1 + 3.750X_2 + 2.000X_3 + 2.525X_4 - 8.267X_1^2 - 6.142X_2^2 - 1.517_3^2 - 5.642X_4^2 + 0.125X_1X_2 + 1.125X_1X_3 + 0.962X_1X_4 + 0.062X_2X_3 - 0.850X_2X_4 + 0.600X_3X_4 \quad (10)$$

Various notations for the experimental parameters or factors and their levels with actual and coded values are given in Table 2.1. The full CCD experimental design along with the predicted and experimental values of response variable (i.e. percentage pyrene degradation) are shown in Table 2.4. The coefficients of the quadratic response model along with the *t*– and *p*– values of linear, quadratic and interaction coefficients are provided in Table 2.5 (A). The ANOVA for the fitted model is displayed in Table 2.5 (B). The predicted values of pyrene degradation closely matched with the experimentally measured values. The *p*–values of every linear, quadratic and interaction coefficient is < 0.05, indicating their significance. The values of the regression coefficients, viz. $R^2$ = 0.999; Predicted $R^2$ = 0.999; Adjusted $R^2$ = 0.999 signify best fit of the model to the experimental data. The *F*–value of overall regression is 21306.11 and *F*–value of linear coefficient is 11254.80.

The Lack of Fit *F*–value is 3.09 and *p*–value is 0.090, which implies that the Lack of Fit is not significant in comparison to the pure error, therefore, in other words, the model is significant. Nonetheless, it must be noted that the regression model is effective simply within the limits of optimization variables used in the experimental design.

**Table 2.4.** Full factorial central composite design matrix of pyrene degradation parameters in coded and actual (in parentheses) values.

| Run order | Medium pH ($X_1$) | Temperature (°C) ($X_2$) | Agitation speed (rpm) ($X_3$) | Inoculum size (%, v/v) ($X_4$) | Pyrene degraded (%) | |
|---|---|---|---|---|---|---|
| | | | | | Experimental | Predicted |
| 1 | 0 (6) | 0 (30) | –α (110) | 0 (7.5) | 43.00±0.08 | 42.95 |
| 2 | –1 (4) | –1 (20) | –1 (130) | –1 (5.0) | 22.50±0.12 | 22.41 |
| 3 | +1 (8) | –1 (20) | –1 (130) | +1 (10.0) | 31.00±0.15 | 31.05 |
| 4 | –1 (4) | –1 (20) | +1 (170) | –1 (5.0) | 27.20±0.06 | 27.34 |
| 5 | 0 (6) | 0 (30) | 0 (150) | 0 (7.5) | 53.00±0.11 | 53.02 |
| 6 | –1 (4) | –1 (20) | +1 (170) | +1 (10.0) | 33.30±0.15 | 33.36 |
| 7 | –α (2) | 0 (30) | 0 (150) | 0 (7.5) | 19.00±0.22 | 18.87 |
| 8 | 0 (6) | +α (50) | 0 (150) | 0 (7.5) | 36.00±0.05 | 35.95 |
| 9 | 0 (6) | 0 (30) | +α (190) | 0 (7.5) | 51.00±0.24 | 50.95 |
| 10 | +1 (8) | +1 (40) | +1 (170) | +1 (10.0) | 40.00±0.10 | 40.05 |
| 11 | 0 (6) | 0 (30) | 0 (150) | 0 (7.5) | 53.20±0.26 | 53.02 |
| 12 | 0 (6) | 0 (30) | 0 (150) | 0 (7.5) | 53.00±0.32 | 53.02 |
| 13 | +1 (8) | +1 (40) | –1 (130) | –1 (5.0) | 33.00±0.10 | 32.90 |
| 14 | –1 (4) | –1 (20) | –1 (130) | +1 (10.0) | 26.00±0.13 | 26.04 |
| 15 | 0 (6) | 0 (30) | 0 (150) | +α (12.5) | 35.50±0.27 | 35.50 |
| 16 | –1 (4) | +1 (40) | +1 (170) | +1 (10.0) | 39.00±0.04 | 39.04 |
| 17 | 0 (6) | 0 (30) | 0 (150) | 0 (7.5) | 53.00±0.38 | 53.02 |
| 18 | 0 (6) | –α (10) | 0 (150) | 0 (7.5) | 21.00±0.19 | 20.95 |
| 19 | 0 (6) | 0 (30) | 0 (150) | –α (2.5) | 25.50±0.21 | 25.40 |
| 20 | +1 (8) | –1 (20) | +1 (170) | +1 (10.0) | 34.00±0.05 | 33.87 |
| 21 | +1 (8) | +1 (40) | –1 (130) | +1 (10.0) | 37.00±0.11 | 36.97 |
| 22 | +1 (8) | –1 (20) | –1 (130) | –1 (5.0) | 23.50±0.23 | 23.57 |
| 23 | +1 (8) | +1 (40) | +1 (170) | –1 (5.0) | 33.50±0.07 | 33.57 |
| 24 | 0 (6) | 0 (30) | 0 (150) | 0 (7.5) | 53.00±0.24 | 53.02 |
| 25 | +α (10) | 0 (30) | 0 (150) | 0 (7.5) | 21.00±0.12 | 21.04 |
| 26 | 0 (6) | 0 (30) | 0 (150) | 0 (7.5) | 53.00±0.09 | 53.02 |
| 27 | –1 (4) | +1 (40) | –1 (130) | +1 (10.0) | 31.50±0.35 | 31.46 |
| 28 | +1 (8) | –1 (20) | +1 (170) | –1 (5.0) | 24.00±0.18 | 24.00 |
| 29 | –1 (4) | +1 (40) | +1 (170) | –1 (5.0) | 36.50±0.06 | 36.41 |
| 30 | –1 (4) | +1 (40) | –1 (130) | –1 (5.0) | 31.00±0.13 | 31.24 |
| 31 | 0 (6) | 0 (30) | 0 (150) | 0 (7.5) | 53.00±0.19 | 53.02 |

**Table 2.5.** Statistical analysis of central composite experimental design for process parameter optimization of pyrene degradation.

(A) Model Coefficients, *t*− and *p*−values for each variable

| Model term | Coefficient | *t*-value | *p*-value |
|---|---|---|---|
| Intercept ($\beta_0$) | 53.028 | 1221.875 | 0.000* |
| *Linear coefficients* | | | |
| Medium pH ($X_1$) | 0.541 | 23.110 | 0.000* |
| Temperature ($X_2$) | 3.750 | 159.994 | 0.000* |
| Agitation speed ($X_3$) | 2.000 | 85.330 | 0.000* |
| % Inoculum ($X_4$) | 2.525 | 107.730 | 0.000* |
| *Square coefficients* | | | |
| Medium pH ($X_1$) × Medium pH ($X_1$) | -8.267 | -385.031 | 0.000* |
| Temperature ($X_2$) × Temperature ($X_2$) | -6.142 | -286.067 | 0.000* |
| Agitation speed ($X_3$) × Agitation speed ($X_3$) | -1.517 | -70.675 | 0.000* |
| % Inoculum ($X_4$) × % Inoculum ($X_4$) | -5.642 | -262.781 | 0.000* |
| *Interaction coefficients* | | | |
| Medium pH ($X_1$) × Temperature ($X_2$) | 0.125 | 4.354 | 0.000* |
| Medium pH ($X_1$) × Agitation speed ($X_3$) | -1.125 | -39.190 | 0.000* |
| Medium pH ($X_1$) × % Inoculum ($X_4$) | 0.962 | 33.530 | 0.000* |
| Temperature ($X_2$) × Agitation speed ($X_3$) | 0.062 | 2.177 | 0.045 |
| Temperature ($X_2$) × % Inoculum ($X_4$) | -0.850 | -29.611 | 0.000* |
| Agitation speed ($X_3$) × % Inoculum ($X_4$) | 0.600 | 20.902 | 0.000* |

* Significant *p* values, $p \leq 0.05$; $R^2$= 0.999; Predicted $R^2$ = 0.999; Adjusted $R^2$ = 0.999

(B) ANOVA for quadratic model

| Source | DF | SS | MS | *F*-value | *p*-value |
|---|---|---|---|---|---|
| Regression | 14 | 3932.75 | 280.91 | 21306.11 | 0.000 |
| Linear | 4 | 593.56 | 148.39 | 11254.80 | 0.000 |
| Square | 4 | 3286.49 | 821.62 | 62317.22 | 0.000 |
| Interaction | 6 | 52.70 | 8.78 | 666.25 | 0.000 |
| Residual (error) | 16 | 0.21 | 0.01 | | |
| Lack of fit | 10 | 0.18 | 0.02 | 3.09 | 0.090 |
| Pure Error | 6 | 0.03 | 0.01 | | |
| Total | 30 | 3932.96 | | | |

DF – Degree of freedom; SS – Sum of squares; MS – Mean square

The global optimum values of variables (process parameters) corresponding to maximum response variable (pyrene degradation) were obtained as: medium pH = 6.0, temperature = 33°C, agitation speed = 164 rpm and % inoculum = 8.07 vol%. At optimum conditions, the maximum pyrene degradation predicted by the quadratic model was 54.60%. The desirability function plot showing optimum levels of process parameters is shown in Fig. 2.3.

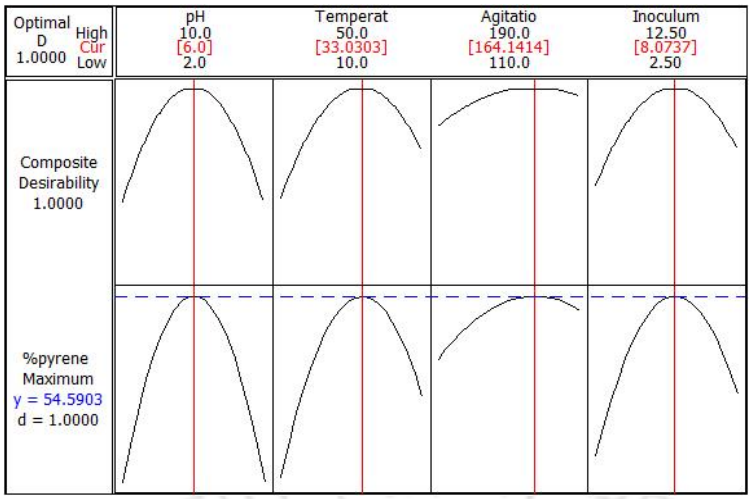


**Figure 2.3.** Desirability function plot for optimum levels of process parameters in pyrene degradation.

***Validation experiment*:** Validation of the statistical results obtained from optimization of physical operating parameters was done by performing pyrene degradation experiments using *C. tropicalis*. The experiments were performed using the results of CCD analyses as described in the preceding sections. For 75 mg $L^{-1}$ initial pyrene concentration, a residual concentration of 35 ± 1 mg $L^{-1}$ was obtained after 14 days, which corresponded to ~ 53% degradation. This result matched closely with the predictions of statistical experimental design. Table 2.6 presents a comparison of all the parameters of phenanthrene and pyrene degradation optimised through statistical process. Almost similar values were found for both the PAHs and this clearly indicates that a system designed for one PAH should work for the other as well.

**Table 2.6.** Comparison of the values of optimized parameters for phenanthrene and pyrene degradation.

| Physical parameter | Phenanthrene | Pyrene |
|---|---|---|
| Medium pH | 6.2 | 6.0 |
| Temperature (ºC) | 33.4 | 33 |
| Agitation speed (rpm) | 190 | 164 |
| % Inoculum (vol%) | 9.26 | 8.07 |

### 2.3.3 Results of kinetic analysis

#### 2.3.3.1 Kinetic analysis of growth and phenanthrene degradation

The profiles of $\mu$ (specific growth rate) and $q$ (specific degradation rate) for different initial concentrations of phenanthrene ($S_0$) are shown in Fig. 2.4.

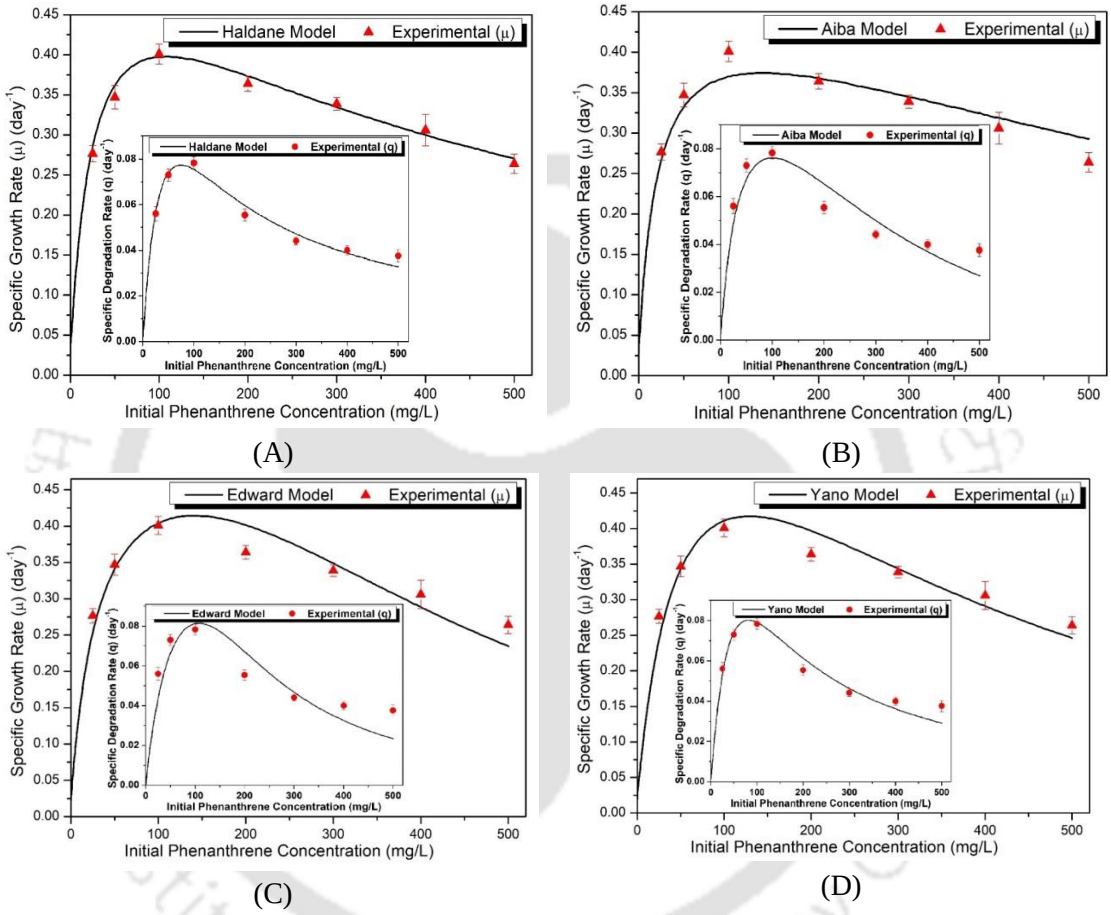


**Figure 2.4.** Experimental and predicted specific growth rate ($\mu$) and phenanthrene degradation rate ($q$) obtained from different models (A) Haldane model, (B) Aiba model, (C) Edward model, (D) Yano model.

These profiles were fitted to various substrate inhibition models using nonlinear regression method (MATLAB R2018b). The kinetic parameters in various models obtained after fitting the profiles are listed in Table 2.7. The Haldane model had the best fit for both profiles of $\mu$ and $q$ with the highest $R^2$ and the lowest RMSE. The kinetic parameters for Haldane model for biomass growth were: $\mu_{max}$ = 0.6 day$^{-1}$, $K_s$ =

27.54 mg $L^{-1}$, $K_i$ = 428.4 mg $L^{-1}$. The corresponding parameters for degradation profile were: $q_{max}$ = 0.18 $day^{-1}$, $K_s'$ = 46.89 mg $L^{-1}$, $K_i'$ = 117.5 mg $L^{-1}$. The profiles of both $\mu$ and $q$ in Fig. 2.4 show maxima at $S_0$ = 100 mg $L^{-1}$. Reduction in $\mu$ and $q$ after $S_0$ = 100 mg $L^{-1}$ is an indication of substrate inhibition at relatively higher concentrations of phenanthrene. Moreover, relatively faster reduction in $q$ with initial substrate concentration after $S_0$ = 100 mg $L^{-1}$ indicates greater influence of substrate inhibition on phenanthrene degradation pathway than biomass growth pathway. This is also reflected in terms of ~ 4× higher value of $K_i$ (inhibition constant for biomass growth) than $K_i'$ (inhibition constant for substrate degradation).

**2.3.3.2 Kinetic analysis of growth and pyrene degradation**

The profiles of $\mu$ (specific growth rate) and $q$ (specific degradation rate) for different initial concentrations of pyrene ($S_0$) are shown in Fig. 2.5. These profiles were fitted to various substrate inhibition models using nonlinear regression method (MATLAB R2018b). The kinetic parameters in various models obtained after fitting the profiles are listed in Table 2.8. The Haldane model had the best fit for both profiles of $\mu$ and $q$ with the highest $R^2$ and the lowest RMSE. The kinetic parameters for Haldane model for biomass growth were: $\mu_{max}$ = 0.9 $day^{-1}$, $K_s$ = 43.70 mg $L^{-1}$, $K_i$ = 153.0 mg $L^{-1}$. The corresponding parameters for degradation profile were: $q_{max}$ = 0.14 $day^{-1}$, $K_s'$ = 52.68 mg $L^{-1}$, $K_i'$ = 98.0 mg $L^{-1}$. The profiles of both $\mu$ and $q$ in Fig. 2.5 show maxima at $S_0$ = 75 mg $L^{-1}$. Reduction in $\mu$ and $q$ after $S_0$ = 75 mg $L^{-1}$ is an indication of substrate inhibition at relatively higher concentrations of phenanthrene. Moreover, relatively faster reduction in $q$ with initial substrate concentration after $S_0$ = 75 mg $L^{-1}$ indicates greater influence of substrate inhibition on pyrene degradation pathway than biomass growth pathway. This is also reflected

in terms of higher value of $K_i$ (inhibition constant for biomass growth) than $K_i'$ (inhibition constant for substrate degradation).

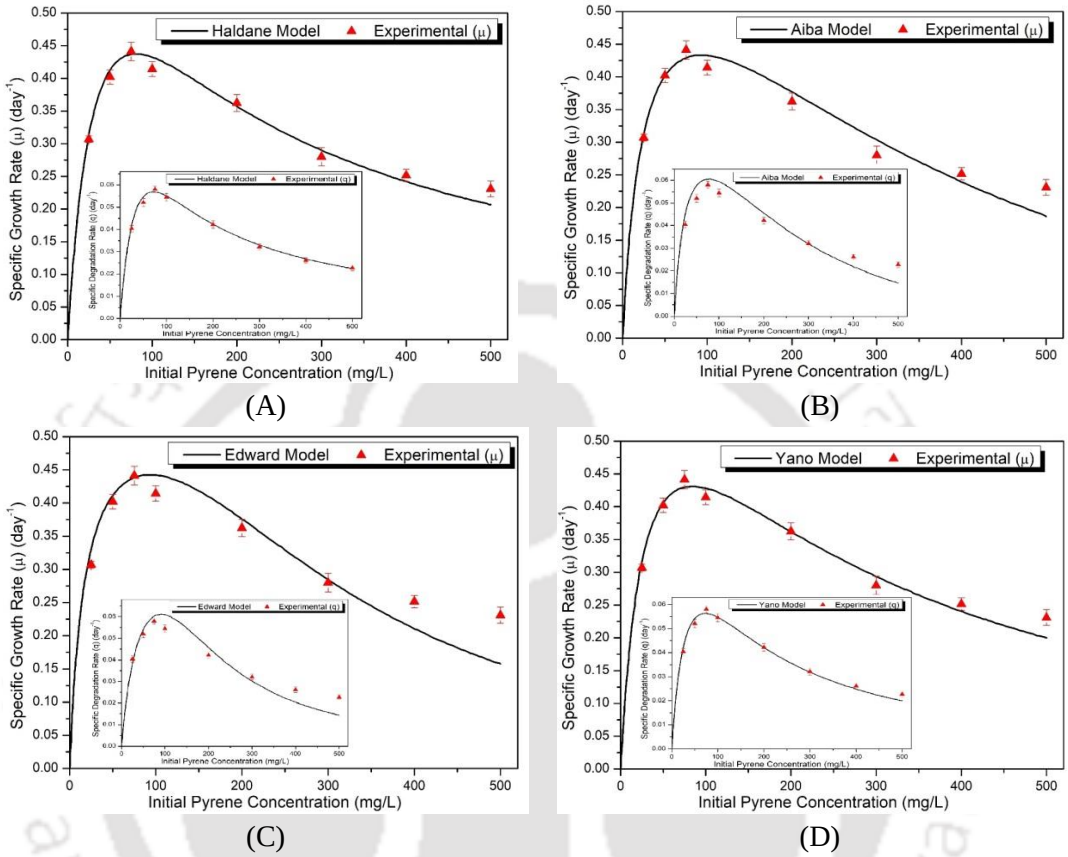


**Figure 2.5.** Experimental and predicted specific growth rate ($\mu$) and pyrene degradation rate ($q$) obtained from different models (A) Haldane model, (B) Aiba model, (C) Edward model, (D) Yano model.

## 2.4 CONCLUSION

This chapter reveals several important results regarding the optimum functioning of phenanthrene and pyrene degradation process by *C. tropicalis* cells. Physical operating parameters for degradation of phenanthrene and pyrene were optimized through central composite statistical design of experiments. The values of the optimised parameters were similar for both the PAHs. Under optimum conditions, ~ 66% of phenanthrene (100 mg $L^{-1}$) and ~ 53% of pyrene (75 mg $L^{-1}$) was degraded

in 14 days. The tolerance test revealed marked decrease in yeast cell growth after 100 and 75 mg $L^{-1}$ of phenanthrene and pyrene, respectively. In the kinetic analysis, profiles of specific growth rate ($\mu$) and specific degradation rate ($q$) versus initial substrate concentration fit best to Haldane substrate inhibition model. Both $\mu$ and $q$ showed maxima for initial concentration of 100 mg $L^{-1}$ for phenanthrene and 75 mg $L^{-1}$ for pyrene and strong substrate inhibition was displayed beyond these concentrations.

**Table 2.7.** Predicted kinetic parameters of phenanthrene degradation by *C. tropicalis* acquired from different models.

| | Mathematical model | Parameters for $\mu$ | | | | | | Parameters for $q$ | | | | | |
|---|---|---|---|---|---|---|---|---|---|---|---|---|---|
| | | $\mu_{max}$ | $K_s$ | $K_i$ | $K$ | $R^2$ | *RMSE* | $q_{max}$ | $K_s'$ | $K_i'$ | $K'$ | $R^2$ | *RMSE* |
| Haldane | $\mu = \left.\frac{\mu_{max} S}{K_s + S + \left(S^2 / K_i\right)}\right\|_{S=S_0}$ | 0.60 | 27.54 | 428.4 | – | 0.98 | 0.0082 | 0.18 | 46.89 | 117.5 | – | 0.98 | 0.0039 |
| Aiba | $\mu = \left.\frac{\mu_{max} S}{K_s + S} \exp\left(-S/K_i\right)\right\|_{S=S_0}$ | 0.49 | 21.00 | 1045.0 | – | 0.83 | 0.0275 | 0.16 | 52.00 | 293.5 | – | 0.90 | 0.0089 |
| Edward | $\mu = \left.\frac{\mu_{max} S}{S + K_s + \left(S^2/K_i\right)\left(1 + S/K_s\right)}\right\|_{S=S_0}$ | 0.55 | 31.47 | 6458.0 | – | 0.73 | 0.0349 | 0.16 | 71.00 | 659.3 | – | 0.83 | 0.0107 |
| Yano | $\mu = \left.\frac{\mu_{max} S}{S + K_s + \left(S^2/K_i\right)\left(1 + S/K\right)}\right\|_{S=S_0}$ | 0.71 | 50.00 | 449.0 | 786.0 | 0.74 | 0.0342 | 0.22 | 74.48 | 98.04 | 1817.0 | 0.95 | 0.0068 |

Notations are as follows: $S$ = phenanthrene concentration (mg $L^{-1}$), $\mu$ = specific biomass (or cell) growth rate ($day^{-1}$), $\mu_{max}$ = maximum specific biomass (or cell) growth rate ($day^{-1}$), $q$ = specific degradation rate ($day^{-1}$), $q_{max}$ = maximum specific degradation rate ($day^{-1}$). $K_s$, $K_i$, $K$ = half saturation coefficient, inhibition coefficient, constant respectively, applied to growth rate (mg $L^{-1}$), $K_s'$, $K_i'$, $K'$ = half saturation coefficient, inhibition coefficient, constant respectively, applied to specific degradation rate (mg $L^{-1}$).

**Table 2.8.** Predicted kinetic parameters of pyrene degradation by *C. tropicalis* acquired from different models.

| Mathematical model | | Parameters for $\mu$ | | | | | | Parameters for $q$ | | | | | |
|---|---|---|---|---|---|---|---|---|---|---|---|---|---|
| | | $\mu_{max}$ | $K_s$ | $K_i$ | $K$ | $R^2$ | *RMSE* | $q_{max}$ | $K_s'$ | $K_i'$ | $K'$ | $R^2$ | *RMSE* |
| Haldane | $\mu = \left.\frac{\mu_{max} S}{K_s + S + \left(S^2 / K_i\right)}\right\|_{S=S_0}$ | 0.90 | 43.70 | 153.0 | – | 0.95 | 0.0232 | 0.14 | 52.68 | 98.0 | – | 0.97 | 0.0036 |
| Aiba | $\mu = \left.\frac{\mu_{max} S}{K_s + S} \exp\left(-S/K_i\right)\right\|_{S=S_0}$ | 0.73 | 29.98 | 384.0 | – | 0.86 | 0.0355 | 0.12 | 35.00 | 248.0 | – | 0.83 | 0.0072 |
| Edward | $\mu = \left.\frac{\mu_{max} S}{S + K_s + \left(S^2/K_i\right)\left(1 + S/K_s\right)}\right\|_{S=S_0}$ | 0.57 | 18.00 | 5565.0 | – | 0.72 | 0.0550 | 0.11 | 46.00 | 905.0 | – | 0.82 | 0.0073 |
| Yano | $\mu = \left.\frac{\mu_{max} S}{S + K_s + \left(S^2/K_i\right)\left(1 + S/K\right)}\right\|_{S=S_0}$ | 0.74 | 31.11 | 256.0 | 1458.0 | 0.91 | 0.0362 | 0.12 | 39.04 | 152.0 | 1172.0 | 0.94 | 0.0047 |

Notations are as follows: $S$ = pyrene concentration (mg $L^{-1}$), $\mu$ = specific biomass (or cell) growth rate ($day^{-1}$), $\mu_{max}$ = maximum specific biomass (or cell) growth rate ($day^{-1}$), $q$ = specific degradation rate ($day^{-1}$), $q_{max}$ = maximum specific degradation rate ($day^{-1}$). $K_s$, $K_i$, $K$ = half saturation coefficient, inhibition coefficient, constant respectively, applied to growth rate (mg $L^{-1}$), $K_s'$, $K_i'$, $K'$ = half saturation coefficient, inhibition coefficient, constant respectively, applied to specific degradation rate (mg $L^{-1}$).

## REFERENCES

Basak, B., Bhunia, B., Dutta, S., Chakraborty, S., Dey, A., 2014. Kinetics of phenol biodegradation at high concentration by a metabolically versatile isolated yeast *Candida tropicalis* PHB5. Environmental Science and Pollution Research, 21 (2), 1444–1454.

Chebbi, A., Hentati, D., Zaghden, H., Baccar, N., Rezgui, F., Chalbi, M., Sayadi, S., Chamkha, M., 2017. Polycyclic aromatic hydrocarbon degradation and biosurfactant production by a newly isolated *Pseudomonas* sp. strain from used motor oil–contaminated soil. International Biodeterioration & Biodegradation, 122, 128–140.

Csutak, O., Stoica, I., Ghindea, R., Tanase, A.M., Vassu, T., 2010. Insights on yeast bioremediation processes. Romanian Biotechnological Letters, 15 (2), 5066–5071.

Farag, S. and Soliman, N.A., 2011. Biodegradation of crude petroleum oil and environmental pollutants by *Candida tropicalis* strain. Brazilian Archives of biology and Technology, 54 (4), 821–830.

Feng, T.C., Cui, C.Z., Dong, F., Feng, Y.Y., Liu, Y.D., Yang, X.M., 2012. Phenanthrene biodegradation by halophilic *Martelella* sp. AD–3. Journal of applied microbiology, 113 (4), 779–789.

Hadibarata, T. and Tachibana, S., 2010. Characterization of phenanthrene degradation by strain *Polyporus* sp. S133. Journal of Environmental Sciences, 22 (1), 142–149.

Hadibarata, T., Khudhair, A.B., Kristanti, R.A., Kamyab, H., 2017. Biodegradation of pyrene by *Candida* sp. S1 under high salinity conditions. Bioprocess and biosystems engineering, 40 (9), 1411–1418.

Haritash, A.K. and Kaushik, C.P., 2009. Biodegradation aspects of polycyclic aromatic hydrocarbons (PAHs): a review. Journal of hazardous materials, 169 (1–3), 1–15.

Hesham, A.E.L., Wang, Z., Zhang, Y., Zhang, J., Lv, W., Yang, M., 2006. Isolation and identification of a yeast strain capable of degrading four and five ring aromatic hydrocarbons. Annals of microbiology, 56 (2), 109.

Hidayat, A. and Yanto, D.H.Y., 2018. Biodegradation and metabolic pathway of phenanthrene by a new tropical fungus, *Trametes hirsuta* D7. Journal of Environmental Chemical Engineering, 6 (2), 2454–2460.

Hong, W., Jia, H., Ma, W.L., Sinha, R.K., Moon, H.B., Nakata, H., Minh, N.H., Chi, K.H., Li, W.L., Kannan, K., Sverko, E., 2016. Distribution, fate, inhalation exposure and lung cancer risk of atmospheric polycyclic aromatic hydrocarbons in some Asian countries. Environmental science & technology, 50 (13), 7163–7174.

Ojha, N., Mandal, S.K., Das, N., 2019. Enhanced degradation of indeno(1, 2, 3–cd)pyrene using *Candida tropicalis* NN4 in presence of iron nanoparticles and produced biosurfactant: a statistical approach. 3 Biotech, 9 (3), 1–13.

Ortega–Calvo, J.J., Tejeda–Agredano, M.C., Jimenez–Sanchez, C., Congiu, E., Sungthong, R., Niqui–Arroyo, J.L., Cantos, M., 2013. Is it possible to increase bioavailability but not environmental risk of PAHs in bioremediation?. Journal of Hazardous Materials, 261, 733–745.

Pan, F., Yang, Q., Zhang, Y., Zhang, S., Yang, M., 2004. Biodegradation of polycyclic aromatic hydrocarbons by *Pichia anomala*. Biotechnology letters, 26 (10), 803–806.

Srogi, K., 2007. Monitoring of environmental exposure to polycyclic aromatic hydrocarbons: a review. Environmental Chemistry Letters, 5 (4), 169–195.

Umar, Z.D., Aziz, N.A.A., Zulkifli, S.Z., Mustafa, M., 2017. Rapid biodegradation of polycyclic aromatic hydrocarbons (PAHs) using effective *Cronobacter sakazakii* MM045 (KT933253). MethodsX, 4, 104–117.

Unwin, J., Cocker, J., Scobbie, E., Chambers, H., 2006. An assessment of occupational exposure to polycyclic aromatic hydrocarbons in the UK. Annals of Occupational Hygiene, 50 (4), 395–403.

# CHAPTER 3

# Ultrasound-assisted biodegradation of phenanthrene and pyrene by *Candida tropicalis* and kinetic study

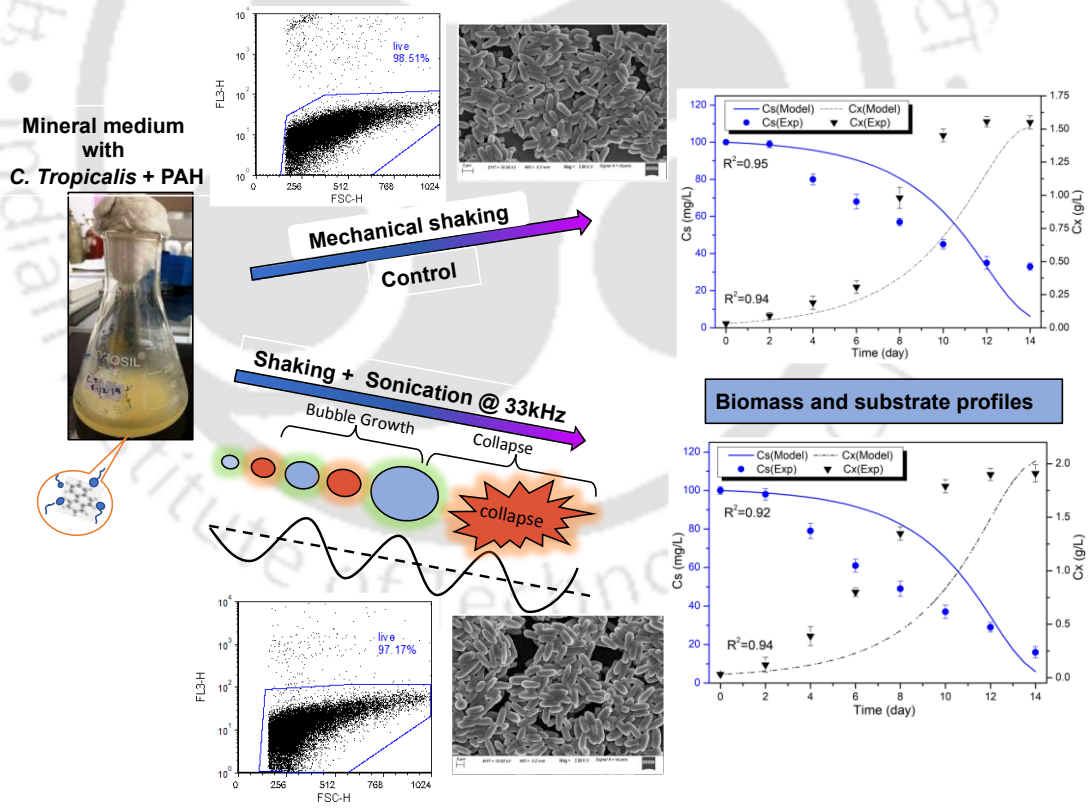

# CHAPTER 3

# Ultrasound-assisted biodegradation of phenanthrene and pyrene by *Candida tropicalis* and kinetic study

## 3.1 INTRODUCTION

As mentioned in the previous chapters, polycyclic aromatic hydrocarbons (PAHs) frequently pollute the ecosystem. A huge level of attention has been drawn for decades because of their prolonged existence, recalcitrance and potential mutagenic and carcinogenic properties (Aranda, 2016). Among various techniques for PAH remediation, the interest towards microbial degradation is increasing among environmentalists due to its eco–friendly nature, high efficiency and economic operation (Schmidt et al., 2010). Both fungi and bacteria have major roles in

biodegradation process of pollutants (Deeba et al., 2018; Ping et al., 2017). Fungi possess certain advantages over other microbes regarding biodegradation owing to their tolerance towards contaminants, penetration capability in soil through mycelia and fast colonization in solid substrates (Harms et al., 2011). Bioremediation can also be coupled with other techniques of process intensification. One of the contemporary techniques, for enhancing kinetics/yields of biochemical processes is ultrasound irradiation or sonication. Researchers have combined ultrasound with different biochemical processes to achieve augmentation of both kinetics and yield of the process (Batghare et al., 2020; May–Lozano et al., 2020; Sheydaei et al., 2019; Bhasarkar et al., 2015). Previous authors have also coupled sonication with inorganic catalysts for boosting the kinetics of degradation of organic pollutants (Khorasanizadeh et al., 2019; Monsef et al., 2018). Sonication of moderate intensity is known to augment the kinetics of the bioprocesses. Physical and chemical effects of sonication are responsible for intensification of the process. The phenomenon of cavitation (growth, nucleation, and the transient collapse of bubble) is responsible for the physical/chemical effects of sonication. The major physical effect produced by sonication is intense microturbulence in the system, and the chemical effect is formation of highly reactive radicals through thermal dissociation of gas and vapour molecules in the cavitation bubble.

In this study, we have attempted to investigate ultrasound–assisted biodegradation of PAHs (phenanthrene and pyrene) from a mechanistic viewpoint. The model system of present study comprises of PAHs and *Candida tropicalis* MTCC 184. This study starts with experimentations on optimization of sonication duty cycle followed by application of ultrasound in the log phase of yeast growth cycle. The kinetics involved in the biodegradation process in both test (ultrasound–treated) and

control was also analysed and parameters affecting the biomass growth and degradation were determined. Finally, the effect of sonication on cell viability and morphology was also assessed. Concurrent analysis of these studies has revealed interesting mechanistic aspects of ultrasound–induced enhancement of phenanthrene and pyrene biodegradation by *C. tropicalis* cells.

## 3.2 MATERIALS AND METHODS

### 3.2.1 Materials

The culture of *Candida tropicalis* MTCC 184 was obtained from the Institute of Microbial Technology (IMTECH), Chandigarh, India. Phenanthrene and pyrene (sublimed grade, ≥ 99.5%) was bought from Sigma–Aldrich (India). All the organic solvents (HPLC grade) were from Merck, India. Bushnell Haas (BH) medium and other chemicals (analytical grade) were procured from Himedia (Mumbai, India).

### 3.2.2 Growth and maintenance of *Candida tropicalis*

Freeze dried *C. tropicalis* cells were revived in agar plates of yeast extract peptone dextrose (YEPD) medium. The yeast was grown at 30°C, pH 7 and 150 rpm. The revived cells were stored at –4°C, and stocks in glycerol (20% v/v) were also made and kept at –80°C. BH medium with a composition of (g $L^{-1}$): $K_2HPO_4$ (1.0); $KH_2PO_4$ (1.0); $NH_4NO_3$ (1.0); $FeCl_3$ (0.05); $MgSO_4{\cdot}7H_2O$ (0.2) and $CaCl_2{\cdot}2H_2O$ (0.02) was used. Every experiment was carried out in BH medium supplemented with phenanthrene/pyrene as lone carbon source for the yeast strain.

### 3.2.3 Batch biodegradation experiments

As explained in the preceding section, *C. tropicalis* cells were initially grown in YEPD medium in order to perform biodegradation experiments. Sequentially, the cells were centrifuged and thoroughly washed. Then the yeast cells were inoculated

into the autoclaved (121°C, 20 min) BH medium. Since both the PAHs exhibits low water solubility, they were first dissolved completely in acetone and then introduced into the medium. Un–inoculated controls flasks comprising of only BH medium and pyrene were also kept to confirm any abiotic loss, i.e., to rule out the impact of any natural dissipation of PAH. The experiments were conducted for a period of 14 days and the operating parameters were taken as per the results of statistical analysis (discussed in Chapter 2). Dissolved oxygen (DO) of the degradation medium was monitored using Thermo Scientific DO meter (Eutech DO–700). The dissolved $O_2$ concentration in the culture continued to be close to saturation level (8 ± 0.25 ppm) throughout the 14–day batch biodegradation experiments.

### 3.2.4 Biomass and residual PAH estimation

Samples of reaction mixture were collected every 24 h (or 1 day) during the 14–day experiment for biomass estimation. The cell density in the sample (or growth profile) was examined at 600 nm. For assessment of biomass concentrations, samples were centrifuged and the resultant pellet was cleaned with water followed by drying at 105ºC for 24 h. The moisture–free pellet was weighed to analyse biomass growth. The batch experiments were performed in triplicates to assess the reproducibility of results.

Samples collected from the degradation medium (at intervals of 24 h) were analysed for residual PAH concentration. The collected samples were extracted in n–hexane and then mixed thoroughly followed by centrifugation (10 min, 10,000 rpm). As a result, the residual PAH present in the samples gets transferred to the organic layer. This layer was separated and analysed using high performance liquid chromatography (HPLC, Agilent Technologies, 1220 Infinity LC) with C18 reverse–phase column (3 mm × 150 mm and particle size: 3.5 $\mu$m). The mobile phase used

was Acetonitrile: Milli–Q water mixture (70:30). 20 $\mu$L sample volume was injected and the mobile phase flow rate was kept at 0.8 mL $min^{-1}$. A UV detector (254 nm) was used for identification of both the PAHs.

### 3.2.5 Ultrasound–assisted biodegradation of PAH (test experiments)

Ultrasound–assisted biodegradation of phenanthrene was conducted in an ultrasonic bath (PCi Analytics, India, dimensions – 30 cm × 15 cm × 10 cm, volume – 3.5 L, rated power 100 W, frequency 33 kHz). Before experiments, ultrasonic bath was calibrated with calorimetric technique to determine the ultrasound pressure amplitude and the actual power input. The pressure amplitude of ultrasonic waves in the medium corresponding to calorimetrically measured acoustic intensity of 0.66 W $cm^{-2}$ was 1.4 bar (or 140 kPa). The water temperature in ultrasound bath was kept at 32° ± 2°C. Moreover, location of the Erlenmeyer flask in the bath was maintained same in every experiment to prevent artifacts due to spatial variation of ultrasound intensity (Moholkar et al., 2000).

In biodegradation test experiments, all physical parameters (except mechanical shaking) were at their optimum values, as obtained in validation experiments from Chapter 2. Mechanical shaking in control experiments was replaced with a combination of mechanical shaking and sonication at 10% duty cycle (1 min ON and 9 min OFF in every 10 min of process). The important process parameter (duty cycle) was optimized by flow cytometry analysis explained in the following section. It must be noted that in the OFF period of the duty cycle, mechanical agitation was applied to the reaction mixture. Sonication was applied to the broth during log phase of yeast cells (total four days from day 4 to day 8) for 12 h/day @ 10% duty cycle. For the remaining 12 h/day of log phase, the reaction mixture was subjected to mechanical shaking. Thus, the total period of sonication in each day was 0.1 × 12 h × 60 min = 72

min. The duration of all biodegradation experiments was 14 days. The experimental protocol of control (mechanical shaking) and test (mechanical shaking + sonication @ 10% duty cycle) experiments is explained in Fig. 3.1.

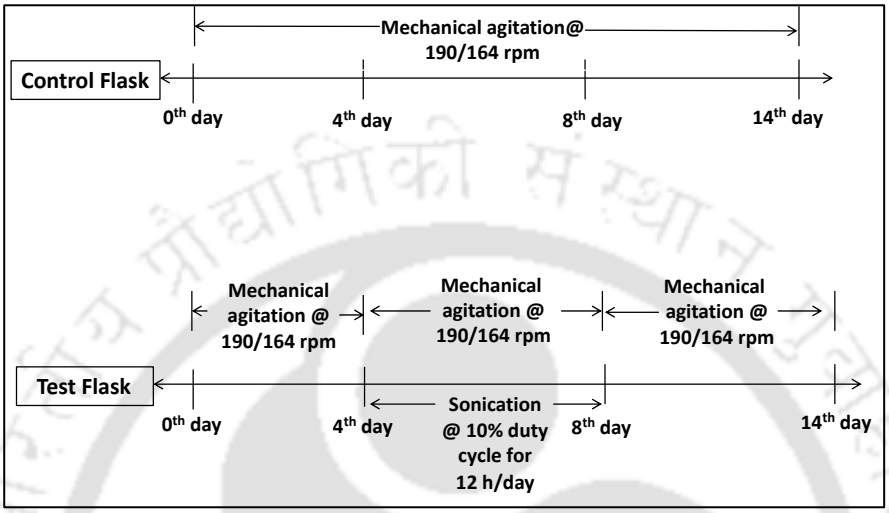


**Figure 3.1.** Schematic of the experimental protocol for control (mechanical agitation) and test (sonication at 10% duty cycle) experiments.

### 3.2.6 Optimization of sonication duty cycle

Constant exposure to sonication can result in adverse effects like disruption or damage to microbial cells because of the shock waves created by the cavitation bubbles. This adverse effect can be avoided by applying sonication in pulsed mode (intermittently), characterized by the parameter duty cycle (fractional durations of ultrasound and silent mode per unit time of treatment) (Dikshit et al., 2018).

For optimization of this parameter, three duty cycles (10, 20 and 30%) of sonication were given to the yeast strain to study the cell viability. The yeast cells were grown in YEPD medium and then exposed to ultrasound at different duty cycles for 12 h/day for 48 h. A control experiment (without sonication) was also performed and compared with the test experiments. After incubation, the cells were centrifuged and separated followed by dilution with phosphate buffer saline (PBS). The viability

and morphological variations on the yeast strain from both control and test samples were analyzed by Flow cytometry using a multi–parametric BD FACS Calibur (Becton Dickson, Calibur$^{TM}$ Flow Cytometer, USA). Microbial cells after completion of experiment were examined with 488 nm laser and 530 nm emission filter using propidium iodide (PI). The changes in cell morphology during sonication were assessed on the basis of SSC (Side Scatter) and FSC (Forward Scatter). Side–scattered light (SSC) is proportional to cell complexity or granularity, and forward–scattered light (FSC) is proportional to cell size or surface area.

### 3.2.7 FE–SEM analysis and chemical oxygen demand (COD) measurement

The *C. tropicalis* cells in both control and test experiments were analysed with FE–SEM (Field Emission Scanning Electron Microscope, Make: Zeiss, Model: Sigma 300) micrographs to spot any visible differences in morphological and phenotypic characters. Initially, the cells were centrifuged for 10 min at 5,000 rpm, and the resultant pellet was washed thrice with phosphate buffer saline (PBS, pH 7). Further, the pellet was fixed with 2.5% formaldehyde for 1 h and again washed thrice with PBS, followed by a dehydration step using ethanol at different concentration range (10, 30, 50. 70, 90, 100% ethanol) for 30 min. At last, the samples were drop cast on the FE–SEM grid and allowed to dry at 37°C. The grids were coated with gold powder and observed under FE–SEM at magnification of 2.00 KX.

The extent of PAH biodegradation was also assessed in terms of reduction in chemical oxygen demand (COD). It is an indicative measurement of soluble and particulate organic material in waste water. Samples from control and test experiments were centrifuged for 5 min at 10,000 rpm, and the aqueous supernatant was taken for COD analysis. COD of the samples was quantified using HACH COD

reagents and measured in DR900 calorimeter (Hach, USA). The percentage reduction of COD was calculated from initial COD and final COD values.

### 3.2.8 Kinetics of PAHs biodegradation (control and test experiments)

As mentioned in the previous chapter, significant substrate inhibition effects occur during the growth of *C. tropicalis* on PAHs (Basak et al., 2014). Substrate (PAH) utilization rate can be written as:

$$\frac{dS}{dt} = -qX = -\left(\mu / Y_{x/s}\right) X \tag{1}$$

Notations are as follows: $S$ = PAH concentration (mg $L^{-1}$), $\mu$ = specific biomass (or cell) growth rate ($day^{-1}$), $t$ = incubation time (day), $X$ = dry cell weight (mg $L^{-1}$), $Y_{x/s}$ = growth yield coefficient (g $g^{-1}$), $q$ = specific degradation rate ($day^{-1}$). Yield factor for biomass, $Y_{x/s}$ (g dry biomass/g PAH) can be calculated as follows:

$$Y_{x/s} = -\frac{dX/dt}{dS/dt} = -\frac{dX}{dS} = -\frac{\left(X - X_0\right)}{\left(S - S_0\right)} \tag{2}$$

Profile of biomass involving growth and decay is written as:

$$\frac{dX}{dt} = \mu X - bX \tag{3}$$

where $b$ = biomass decay coefficient ($day^{-1}$). For the integration of equations 1 and 3, we have used the value of specific growth rate ($\mu$) corresponding to initial substrate concentration ($S = S_0$). Among the different kinetic models that account for substrate inhibition, Haldane model was found to fit best as shown in Chapter 2. The basic kinetic model for substrate inhibition is Haldane model:

$$\mu = \left.\frac{\mu_{\max} S}{K_S + S + \left(S^2 / K_i\right)}\right|_{S=S_0} \tag{4}$$

where, $S$ = phenanthrene concentration (mg $L^{-1}$), $\mu$ = specific biomass growth rate ($day^{-1}$), $\mu_{max}$ = maximum specific biomass growth rate ($day^{-1}$), $K_s$ = half saturation

coefficient (mg $L^{-1}$), $K_i$ = inhibition coefficient (mg $L^{-1}$).

The kinetic parameters of $b$ (decay coefficient) and $Y_{X/S}$ (biomass yield coefficient) in Eqs. 1 and 3 were obtained by fitting experimental profiles of biomass and substrate to Eqs. 1 and 3 using Genetic Algorithm in MATLAB (R2018b). These equations were simultaneously solved using Runge–Kutta 4$^{th}$ order method (as initial value problem) to obtain the simulated profiles of substrate and biomass. The simulated profiles were compared against the experimental profiles (mean values of biomass and substrate concentrations in the triplicate experimental runs). The sum of RMSE (root mean square error) between the two profiles was minimized by adjusting the numerical values of kinetic parameters in the model within specified bounds (Tizazu et al., 2018). For this purpose, experiments (both control and test) were conducted at optimum conditions obtained from statistical experiments. The initial substrate concentration (corresponding to maximum $q$ and $\mu$) for these experiments was obtained from analysis of substrate inhibition kinetics as described in the previous chapter.

## 3.3 RESULTS AND DISCUSSION

### 3.3.1 Optimization of sonication duty cycle

The findings of flow cytometry analysis for identification of any significant alterations stimulated in *C. tropicalis* cells by sonication treatment at duty cycles of 10, 20 and 30% are shown in Fig. 3.2. The results were compared with the control experiment. Live and dead cells have been categorised from their distinctive staining property with PI stain. When the FSC and SSC of the cells in control and 10% duty cycle experiments were compared, no significant alteration was observed. Acquisition dot plots between FL3 and FSC shown in Figs. 3.2 (B and E) indicate the live cell

percentage existing in control and 10% duty cycle samples. Both samples displayed live cell percentage in the same range, which indicated a constancy in cellular structure and morphology even after 10% duty cycle treatment. The histograms given in Figs. 3.2 (C and F) displayed similar dead cell percentage in control (1.40%) and 10% duty cycle (2.13%) experiments. The flow cytometry analysis results of samples exposed to 20 and 30% duty cycles sonication are exhibited in Fig. 3.2. The dot plots displayed substantial alterations, as compared to the control experiment. A small percentage (35.50%) of live cells was indicated after 20% duty cycle treatment. For 30% duty cycle treatment, the live cell percentage was negligible (1.17%). This clearly indicates that exposure to 20 and 30% duty cycle sonication results in major alterations in the cellular morphology, and induces adverse effects in cell viability and activity. The histograms PI + cells revealed a high percentage of dead cells for both the duty cycles as displayed in Figs. 3.2 (I and L). Therefore, among the different duty cycles, 10% did not stimulate any change in the morphology of the yeast cells. Therefore, the optimal duty cycle for the intensification (test) experiment was fixed at 10%.

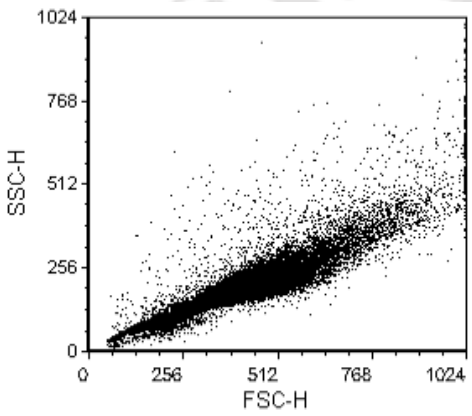


(A)

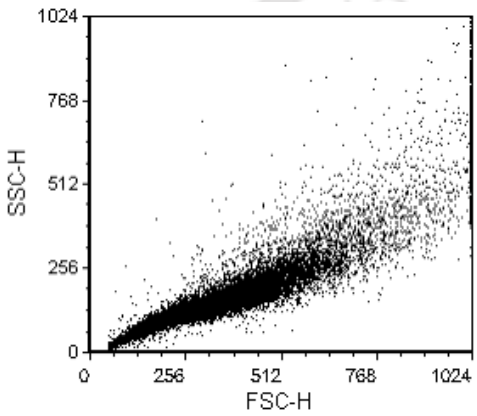


(D)

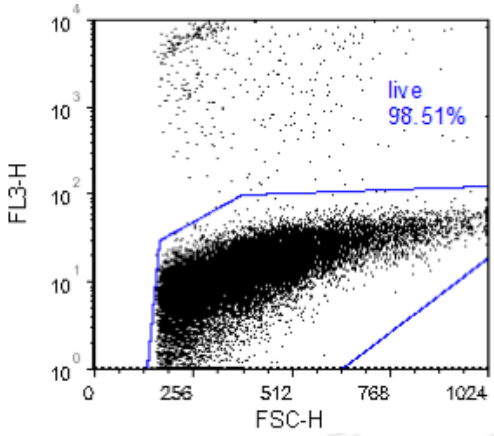


(B)

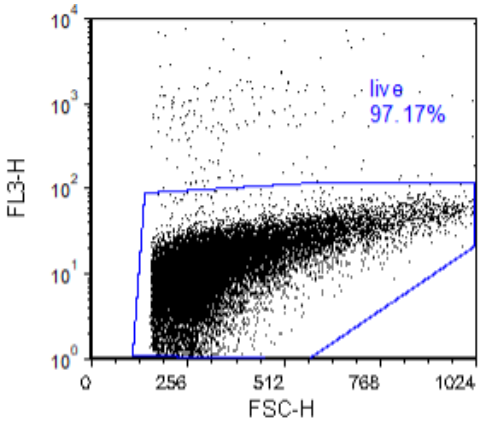


(E)

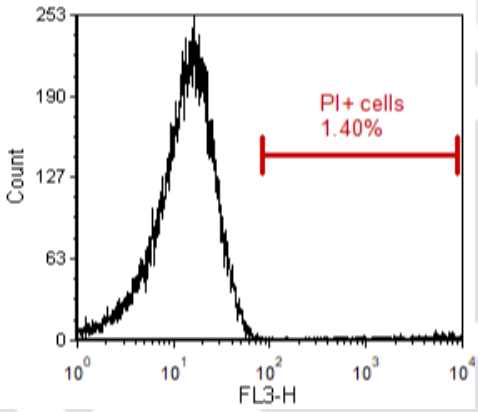


(C)

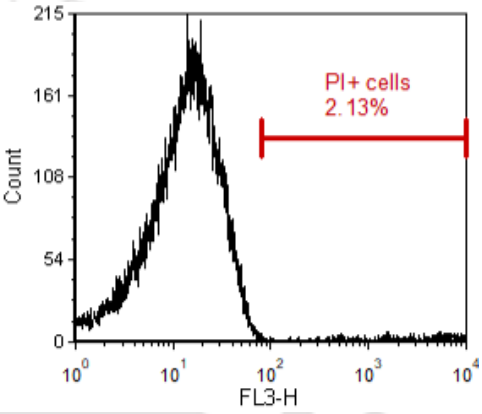


(F)

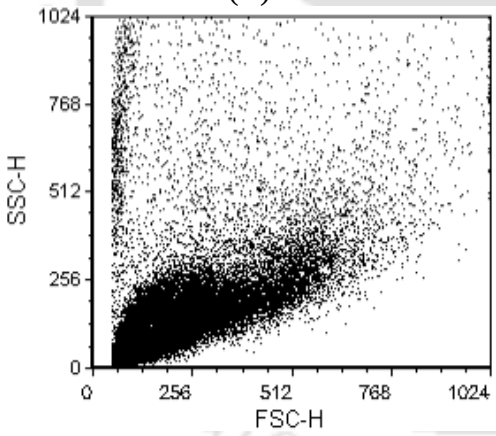


(G)

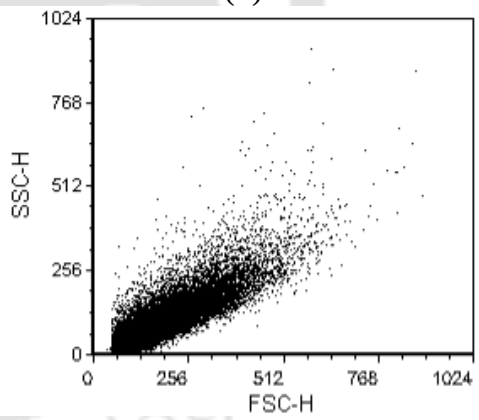


(J)

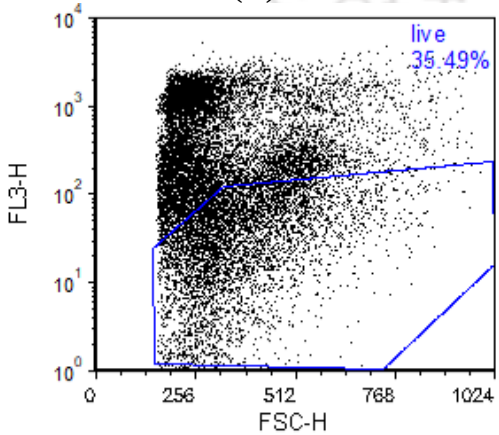


(H)

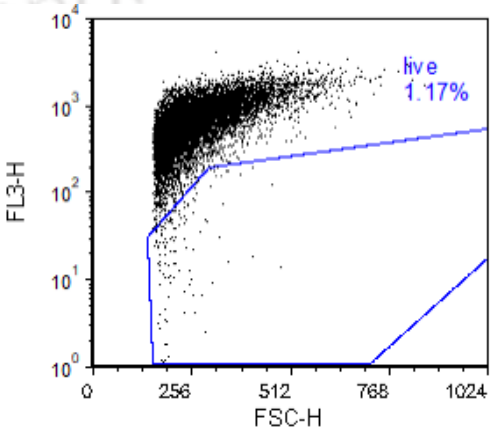


(K)

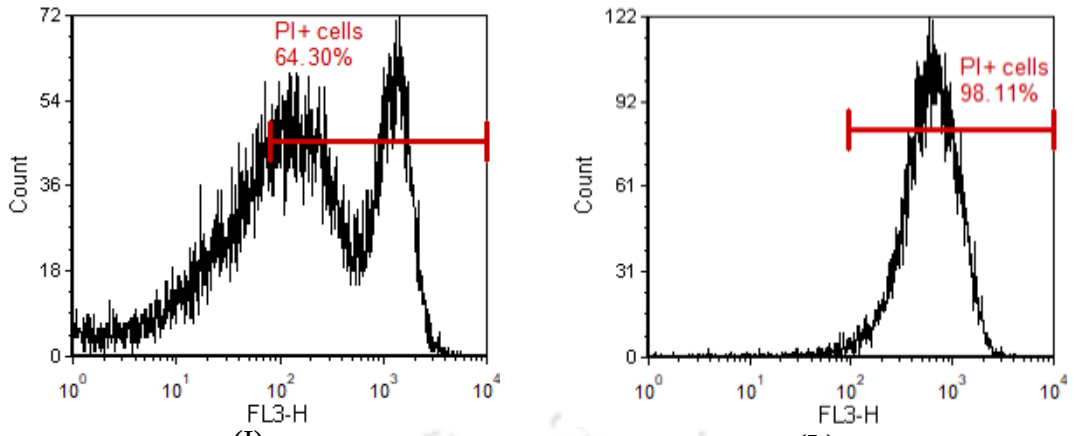


(I) (L)

**Figure 3.2.** Flow cytometric analysis for detection of morphological changes in *C. tropicalis* cells (A, D, G, J): Acquisition dot plots (FSC vs. SSC) for control, 10, 20 and 30% duty cycle experiments, respectively. (B, E, H, K): Acquisition dot plots (FSC vs. FL3) showing percentage of live cells present for control, 10, 20 and 30% duty cycle experiments, respectively. (C, F, I, L): Histogram plots (FL3 vs. count) showing dead *C. tropicalis* cells in control, 10, 20 and 30% duty cycle experiments, respectively.

### 3.3.2 PAH degradation experiment: control and test

For both control and test experiments, the initial concentration of phenanthrene and pyrene was fixed at 100 and 75 mg $L^{-1}$, respectively. This was based on the results obtained from the tolerance test of *C. tropicalis* cells which was performed in the previous chapter. The results of phenanthrene degradation under control (mechanical shaking), and test (combination of sonication @ 10% duty cycle and mechanical shaking) conditions are shown in Figs. 3.3 (A and B). For 100 mg $L^{-1}$ initial phenanthrene concentration, a residual concentration of 34 ± 2 mg $L^{-1}$ was obtained after 14 days in the control experiments, which corresponded to ~ 66% degradation. In test experiments, a residual concentration of 16 ± 2 mg $L^{-1}$ was obtained, which corresponded to ~ 84% degradation. Pyrene degradation under control and test conditions are shown in Figs. 3.4 (A and B). For 75 mg $L^{-1}$ initial pyrene concentration, a residual concentration of 35 ± 2 mg $L^{-1}$ was obtained after 14 days in the control experiments, which corresponded to ~ 53% degradation. In test

experiments, a residual concentration of 22 ± 2 mg $L^{-1}$ was obtained, which corresponded to ~ 70% degradation.

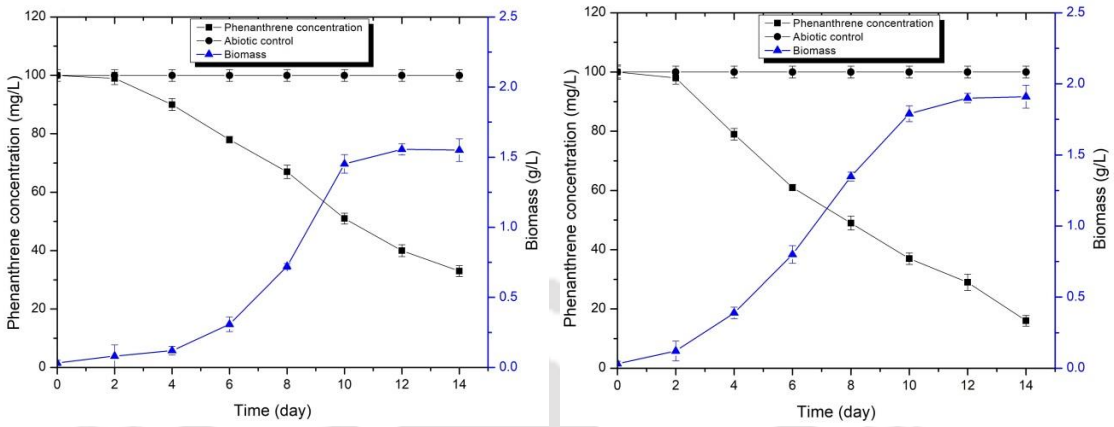


**Figure 3.3.** (A) Experimental profiles of phenanthrene degradation in control experiment. (B) Experimental profiles of phenanthrene degradation in test experiment (mechanical agitation with sonication at 10% duty cycle). Abiotic control (●) profiles are also shown.

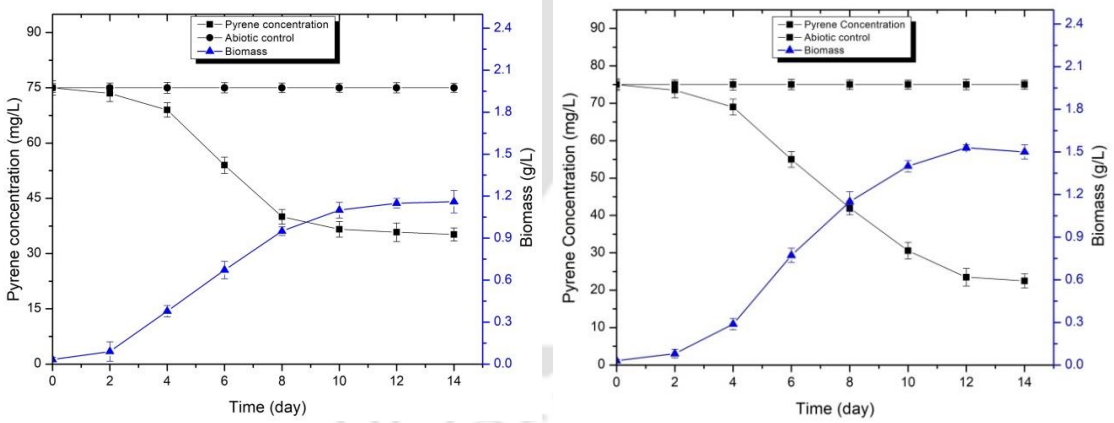


**Figure 3.4.** (A) Experimental profiles of pyrene degradation in control experiment. (B) Experimental profiles of pyrene degradation in test experiment (mechanical agitation with sonication at 10% duty cycle). Abiotic control (●) profiles are also shown.

### 3.3.3 FE–SEM analysis and chemical oxygen demand (COD) removal

The FE–SEM micrographs of *C. tropicalis cells* are shown in Fig. 3.5. Figs.

3.5 (A and B) represent the micrographs of phenanthrene degradation in control and test experiment, respectively. Figs. 3.5 (C and D) represent the micrographs of pyrene degradation in control and test experiment, respectively. A comparison of these micrographs does not show any significant difference in morphology and topography of the cells. The micrographs for test experiment also do not show any visible cell damage, rupture, or debris, indicating that the cells remained intact during exposure to sonication. Thus, the results of FE–SEM analysis were in concurrence with the results of flow cytometry.

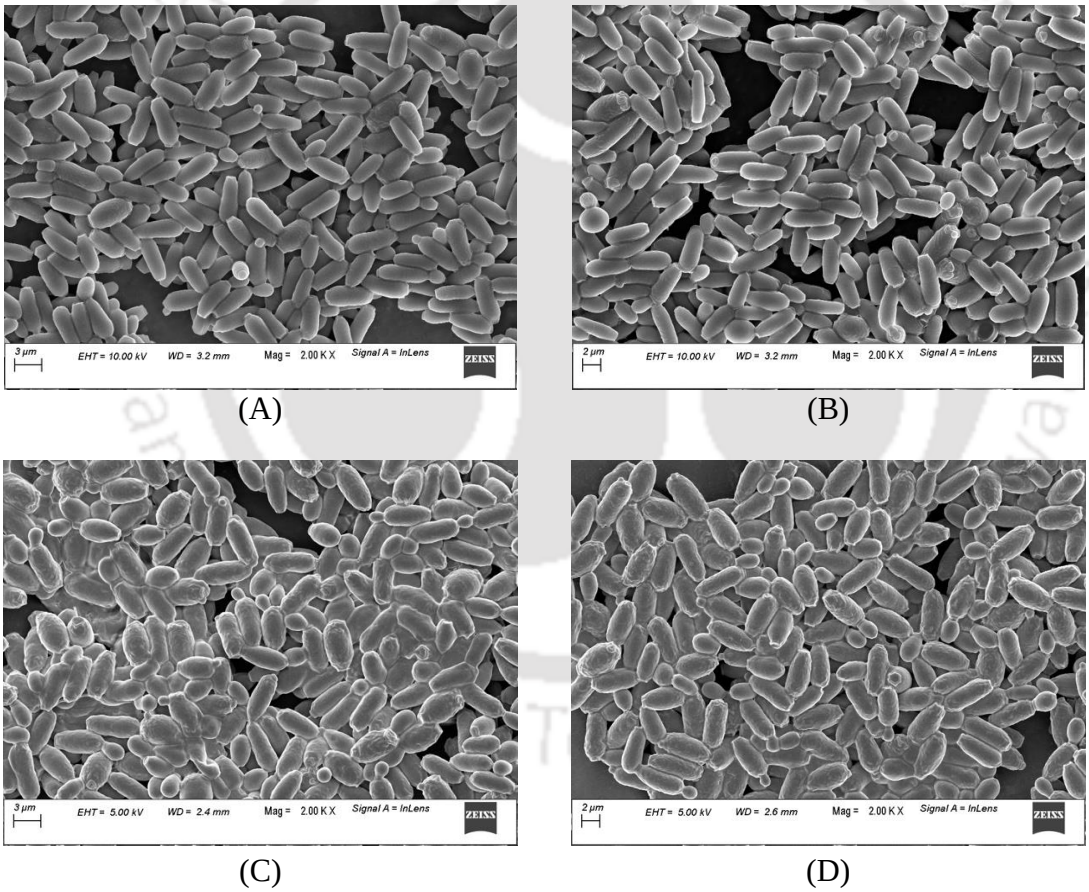


**Figure 3.5.** FE–SEM micrographs: Control (A) and Test (B) samples from phenanthrene degradation. Control (C) and Test (D) samples from pyrene degradation.

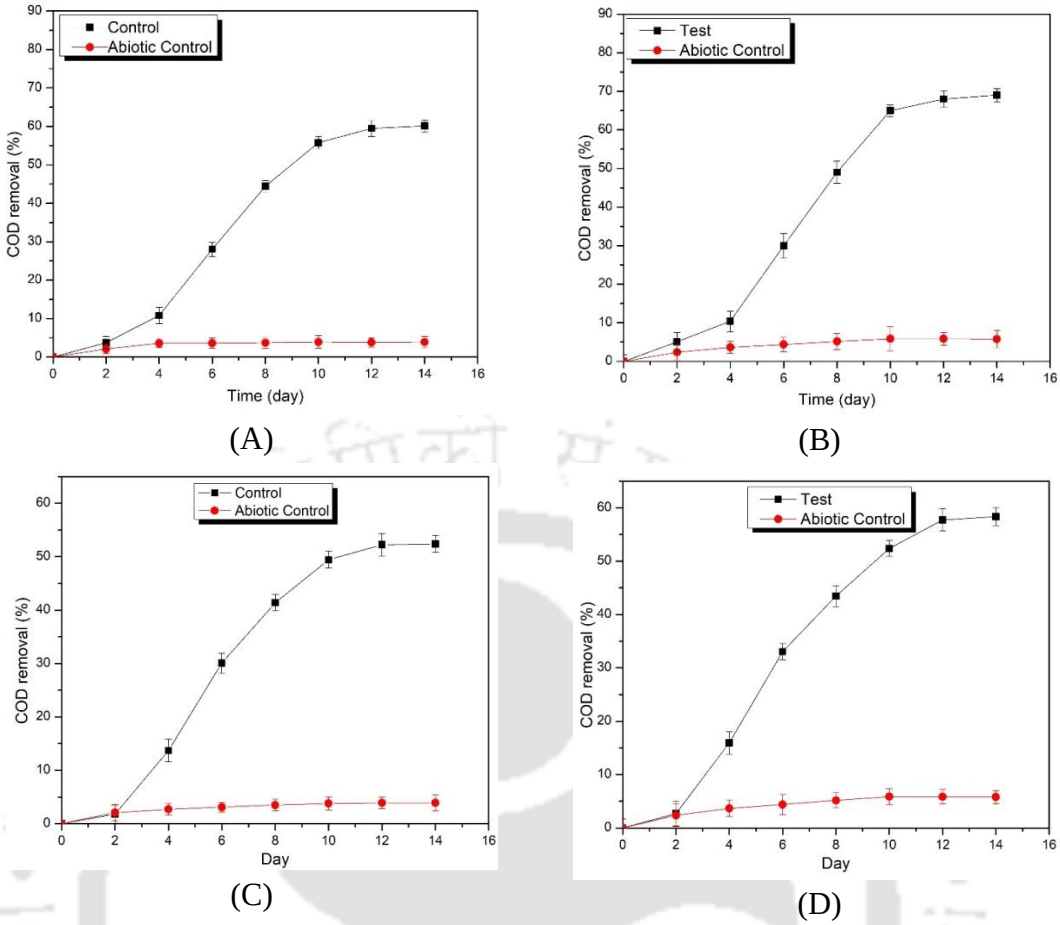


**Figure 3.6.** Percentage removal of COD after biodegradation experiment. (A) Control and (B) Test for phenanthrene. (C) Control and (B) Test for pyrene.

The COD reduction in both control and test samples was continuously monitored. For phenanthrene, it was observed that 60% COD removal was achieved in control experiments, while 69% COD removal was achieved in test experiments. Relatively higher reduction in COD is attributed to enhancement of phenanthrene biodegradation by sonication. For pyrene, final COD removal in control and ultrasound–treated samples was 52 and 58%, respectively. On comparing the reduction in COD with PAH removal in both experiments shows a marked discrepancy. The removal of both the PAH (phenanthrene and pyrene) enhanced by ~ 30% with application of sonication, while the rise in COD removal was quite marginal, ~ 10%. This essentially reveals the exact role of sonication in the

biodegradation process. Ultrasound aids in the creation of water–soluble products from the reactions between pyrene and •OH radicals. Thus, ultrasound only leads to transformation of pyrene to simpler metabolites and not complete degradation of pyrene. Moreover, only 3 – 5 % of COD was degraded in the abiotic samples. The figures of COD analysis are shown in Fig. 3.6.

### 3.3.4 Kinetic of PAHs biodegradation (control and test experiments)

The experimental time profiles of concentrations (substrate and biomass) were fitted using numerical solutions coupled with Genetic algorithm. Fig. 3.7 (A and B) depicts the experimental and stimulated time profiles of biomass and substrate concentration in control and test experiments of phenanthrene degradation. While, Fig. 3.8 (A and B) depicts the experimental and stimulated time profiles of biomass and substrate concentration in control and test experiments of pyrene degradation. The regressions coefficients $R^2$ for all profiles are > 0.9, indicating good match between simulations and experimental profiles. The final results of both phenanthrene and pyrene degradation are tabulated in Table 3.1 and 3.2, which depicts the kinetic parameters (b and $Y_{X/S}$). The phenanthrene degradation shows ~ 25% rise under test conditions. The biomass yield coefficient ($Y_{X/S}$) also shows 25% rise in test experiments, while the decay coefficient (b) reduces ~ 21%. The pyrene degradation shows ~ 30% rise under test conditions. The biomass yield coefficient ($Y_{X/S}$) also shows 25% rise in test experiments, while the decay coefficient (b) reduces ~ 10%.

**Table 3.1**. Kinetic parameters for biomass and substrate concentration profiles.

| Initial phenanthrene concentration (mg $L^{-1}$) | b ($day^{-1}$) | $Y_{X/S}$ (g $g^{-1}$) |
|---|---|---|
| 100 (Control) | 0.087 | 0.004 |
| 100 (Test) | 0.069 | 0.005 |

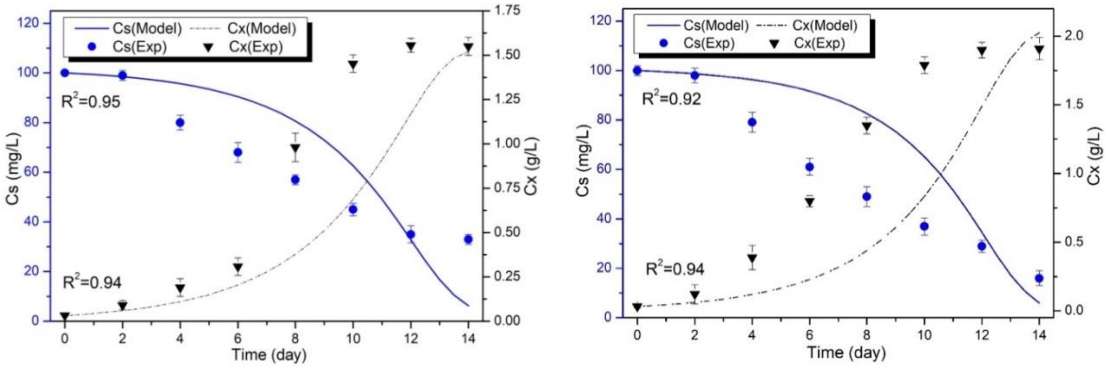


(A) (B)

**Figure 3.7.** Experimental and stimulated time profiles of biomass concentration ($C_x$) and substrate concentration ($C_s$) in control (mechanical shaking) [A] and test (sonication at 10% duty cycle) experiments [B].

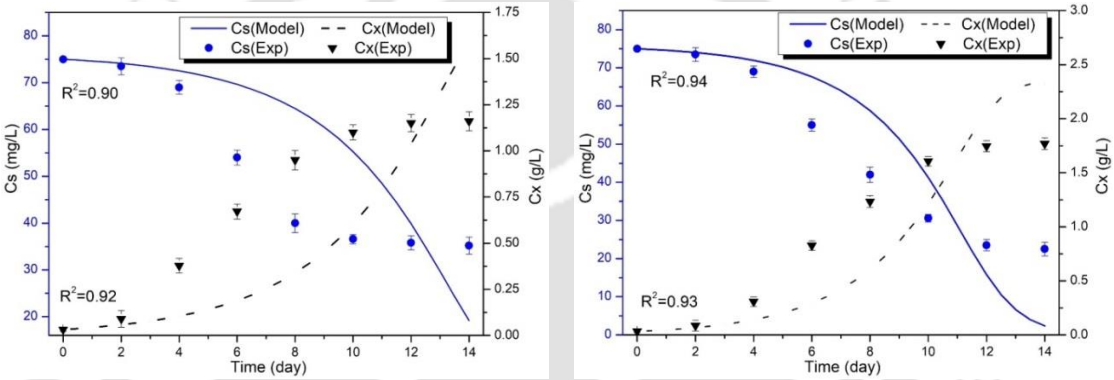


(A) (B)

**Figure 3.8.** Experimental and stimulated time profiles of biomass concentration ($C_x$) and substrate concentration ($C_s$) in control (mechanical shaking) [A] and test (sonication at 10% duty cycle) experiments [B].

**Table 3.2.** Kinetic parameters for biomass and substrate concentration profiles.

| Initial pyrene concentration (mg $L^{-1}$) | b ($day^{-1}$) | $Y_{X/S}$ (g $g^{-1}$) |
|---|---|---|
| 75 (Control) | 0.073 | 0.004 |
| 75 (Test) | 0.067 | 0.005 |

Enhanced phenanthrene and pyrene degradation with higher yeast cell growth in test experiments can be attributed to several beneficial effects of sonication on reaction system as follows:

(1) intense microturbulence generated by sonication enhances the cell membrane

permeability, which facilitates quicker cellular transport of nutrients, substrate, and other metabolites (Huang et al., 2017; Chemat and Khan, 2011).

(2) microturbulence also causes deagglomeration of cell clusters, which helps better access to nutrients and substrate in broth (Avhad and Rathod, 2015).

(3) microturbulence also causes dilution of toxic substances produced during substrate utilization, which helps in reducing cell death and enhancing cell growth.

## 3.4 CONCLUSION

This work demonstrated a potential ultrasonic bioremediation process for degradation of phenanthrene and pyrene by the yeast, *C. tropicalis*. A mechanistic analysis of sonication–induced enhancement of PAH removal using the yeast strain has revealed several interesting facets of the bioremediation process. A marked rise of ~ 25% in phenanthrene removal and ~ 30% in pyrene removal was seen with the application of sonication (10% duty cycle) as compared to the conventional biodegradation process. Kinetic analysis revealed that the biomass yield coefficient increased while the decay coefficient of the cells reduced in presence of sonication. However, COD removal rate with sonication was only marginally higher (~ 10%). Thus, sonication was effective in transforming pyrene to simpler intermediates. The FE–SEM micrographs did not reveal any noteworthy alteration in the cellular morphology and topography, thereby signifying that the yeast remained undamaged after the ultrasound treatment. We believe that the results of this study could form useful inputs for further research in ultrasound–assisted biodegradation of PAHs using yeast strains.

## REFERENCES

Aranda, E., 2016. Promising approaches towards biotransformation of polycyclic aromatic hydrocarbons with Ascomycota fungi. Current opinion in biotechnology, 38, 1–8.

Avhad, D.N. and Rathod, V.K., 2015. Ultrasound assisted production of a fibrinolytic enzyme in a bioreactor. Ultrasonics Sonochemistry, 22, 257 – 264.

Basak, B., Bhunia, B., Dutta, S., Chakraborty, S., Dey, A., 2014. Kinetics of phenol biodegradation at high concentration by a metabolically versatile isolated yeast *Candida tropicalis* PHB5. Environmental Science and Pollution Research, 21 (2), 1444–1454.

Batghare, A.H., Roy, K., Khaire, K.C., Moholkar, V.S., 2020. Mechanistic investigations in ultrasound–induced intensification of fermentative riboflavin production. Bioresource Technology Reports, 9, 100380.

Bhasarkar, J.B., Dikshit, P.K., Moholkar, V.S., 2015. Ultrasound assisted biodesulfurization of liquid fuel using free and immobilized cells of *Rhodococcus rhodochrous* MTCC 3552: A mechanistic investigation. Bioresource Technology, 187, 369–378.

Chemat, F. and Khan, M.K., 2011. Applications of ultrasound in food technology: processing, preservation and extraction. Ultrasonics sonochemistry, 18 (4), 813–835.

Deeba, F., Pruthi, V., Negi, Y.S., 2018. Aromatic hydrocarbon biodegradation activates neutral lipid biosynthesis in oleaginous yeast. Bioresource technology, 255, 273–280.

Dikshit, P.K., Kharmawlong, G.J., Moholkar, V.S., 2018. Investigations in sonication–induced intensification of crude glycerol fermentation to

dihydroxyacetone by free and immobilized *Gluconobacter oxydans*. Bioresource technology, 256, 302–311.

Harms H., Schlosser D., Wick L.Y., 2011. Untapped potential: exploiting fungi in bioremediation of hazardous chemicals. Nature Reviews Microbiology, 9 (3) , 177–192.

Huang, G., Chen, S., Dai, C., Sun, L., Sun, W., Tang, Y., Xiong, F., He, R., Ma, H., 2017. Effects of ultrasound on microbial growth and enzyme activity. Ultrasonics Sonochemistry, 37, 144–149.

Khorasanizadeh, M.H., Monsef, R., Amiri, O., Amiri, M., Salavati–Niasari, M., 2019. Sonochemical–assisted route for synthesis of spherical shaped holmium vanadate nanocatalyst for polluted waste water treatment. Ultrasonics Sonochemistry, 58, 104686.

May–Lozano, M., Lopez–Medina, R., Escamilla, V.M., Rivadeneyra–Romero, G., Alonzo–Garcia, A., Morales–Mora, M., González–Díaz, M.O., Martinez–Degadillo, S.A., 2020. Intensification of the Orange II and Black 5 degradation by sonophotocatalysis using Ag–graphene oxide/TiO2 systems. Chemical Engineering and Processing–Process Intensification, 108175.

Moholkar, V.S., Sable, S.P., Pandit, A.B., 2000. Mapping the cavitation intensity in an ultrasonic bath using the acoustic emission. AIChE journal, 46 (4), 684–694.

Monsef R., Ghiyasiyan–Arani M., Salavati–Niasari M., 2018. Application of ultrasound–aided method for the synthesis of NdVO4 nano–photocatalyst and investigation of eliminate dye in contaminant water. Ultrasonics Sonochemistry, 42, 201–211.

Ping, L., Zhang, C., Cui, H., Yuan, X., Cui, J., Shan, S., 2017. Characterization and

application of a newly isolated pyrene–degrading bacterium, *Pseudomonas monteilii*. 3 Biotech, 7 (5), 309.

Schmidt, S.N., Christensen, J.H., Johnsen, A.R., 2010. Fungal PAH–Metabolites Resist Mineralization by Soil Microorganisms. Environmental Science and Technology, 44 (5), 1677–1682.

Sheydaei, M., Zangouei, M., Vatanpour, V., 2019. Coupling visible light sono–photocatalysis and sono–enhanced ultrafiltration processes for continuous flow degradation of dyestuff using N–doped titania nanoparticles. Chemical Engineering and Processing–Process Intensification, 143, 107631.

Tizazu, B.Z., Roy, K., Moholkar, V.S., 2018. Mechanistic investigations in ultrasound–assisted xylitol fermentation. Ultrasonics sonochemistry, 48, 321–328.

# CHAPTER 4

# Identification of metabolic pathway and intermediates in phenanthrene and pyrene biodegradation

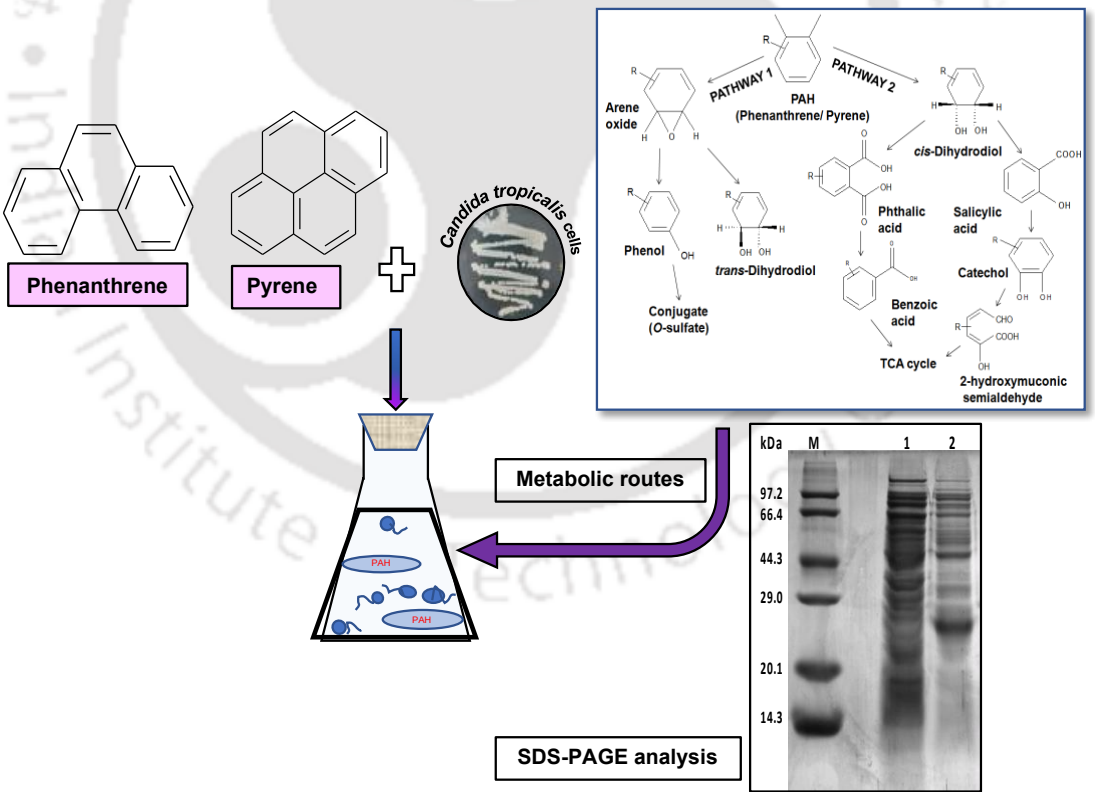

# CHAPTER 4

# Identification of metabolic pathway and intermediates in phenanthrene and pyrene biodegradation

## 4.1 INTRODUCTION

Pollution caused by polycyclic aromatic compounds (PAHs) is a daunting threat to ecosystems and environment. PAHs like naphthalene, phenanthrene, anthracene, pyrene, etc. are components of petroleum ubiquitous in the environment. These PAHs pose risk to public health because of their carcinogenic, mutagenic and teratogenic characteristics (Gou et al., 2020; Huang and Batterman, 2014). Bioremediation of different PAHs has emerged as a potential alternative to conventional oxidative removal processes. Several ligninolytic or non–ligninolytic

fungi have been employed for bioremediation (Anita et al., 2019; Yanto et al., 2019; Hidayat and Yanto, 2018; Yanto and Tachibana, 2014). However, for bioremediation of wastewater, non–ligninolytic fungi have proved to be comparatively more suitable, as the ligninolytic fungi have habitat limitation of growth (Marco–Urrea et al., 2015). Most common non–ligninolytic fungi (yeast) species which known as hydrocarbons degraders belong to genera of *Candida*, *Debaryomyces*, *Leucosporidium*, *Lodderomyces*, *Pichia*, *Rhodosporidium*, *Rhodotorula*, *Sporidiobolus*, *Sporobolomyces*, *Stephanoascus*, *Trichosporon* and *Yarrowia* (Hashem et al., 2018; Hadibarata et al., 2017; Okerentugba et al., 2016; Gargouri et al., 2015; Kumari and Abraham, 2011; Csutak et al., 2010). The microbial degradation route of PAHs by non–ligninolytic fungi normally comprises of three phases, viz. (a) activation of aromatic ring, (b) dearomatization, (c) transformation of ring fission products into tricarboxylic acid (TCA) cycle metabolites. A normal pathway of metabolic cleavage of PAH comprises of dihydroxylation of benzene ring into catechol derivative and then ring fission via *ortho* (intradiol) or *meta* (extradiol) oxidation route. Catechol undergoes oxidation by cleavage enzyme catechol 1,2– dioxygenase (C1,2–D) to form *cis*, *cis*–muconic acid through *ortho*– route. Alternatively, catechol may also be oxidised by cleavage enzyme catechol 2,3–dioxygenase (C2,3–D) through *meta*–route resulting in formation of 2–hydroxymuconic semialdehyde (HMSA) (Deeba et al., 2018).

The aim of this chapter was to get an in–depth insight into the biomechanism involved in degradation of phenanthrene and pyrene by *Candida tropicalis*. The experiments were performed with a 3–fold approach, viz. (1) Identification of the enzymes triggering the degradation process, (2) Identification of metabolites/intermediates formed during the degradation process and (3) Elucidation

of the pathway followed during degradation. The predominant metabolic pathway followed during PAH degradation has been identified for both mechanical shaking (control) and sonication (test) experiments through enzymatic analysis. Moreover, the expression of overall cellular proteins formed during the process was also examined using SDS–PAGE analysis. The attempt of metabolic pathway identification though intermediate metabolites was done by GC–MS spectroscopy.

## 4.2 MATERIALS AND METHODS

### 4.2.1 Materials

*Candida tropicalis* MTCC 184 was obtained from the Institute of Microbial Technology (IMTECH), Chandigarh, India. Phenanthrene, pyrene and all the chemicals used for enzymatic analysis (sublimed grade, ≥ 99.5%) were bought from Sigma–Aldrich (India). The organic solvents (HPLC grade) were from Merck, India. Bushnell Haas (BH) medium and other chemicals (analytical grade) were procured from Himedia (Mumbai, India).

### 4.2.2 Batch biodegradation experiments

As explained in the preceding chapters, *C. tropicalis* cells were initially grown in YEPD medium in order to perform biodegradation experiments. Sequentially, the cells were centrifuged and thoroughly washed. Then the yeast cells were inoculated into the autoclaved (121°C, 20 min) BH medium. Since both PAHs (phenanthrene and pyrene) exhibits low water solubility, they were first dissolved completely in acetone and then introduced into the medium. The degradation experiments were performed at optimised physical operating conditions with phenanthrene/pyrene as sole carbon source. Test experiments at 10% duty cycle sonication were also performed as described in the previous chapter. Both control and test experiments

were conducted for a period of 14 days.

### 4.2.3 Protein extraction and expression (SDS–PAGE analysis)

The expression and size of crude proteins present in the samples were established by running SDS–PAGE (sodium dodecyl sulfate polyacrylamide gel electrophoresis). Samples of broth (control and test experiments) were collected and *C. tropicalis* cells were separated by centrifugation at 10,000 rpm for 5 min. The resulting cell pellets were suspended in lysis buffer (5% SDS, 8 M urea, 0.1 mM EDTA, 40 mM Tris–HCl pH 7.5) (Datta et al., 2016). Further, the cells were ruptured using a sonicator probe (Sonics & Materials VCX 500) @ 50% duty cycle (30 s on and 30 s off) to extract intracellular proteins. The samples were further centrifuged for 30 min at 10,000 rpm and at 4ºC and supernatant were separated. To confirm the expression of proteins, SDS–PAGE (sodium dodecyl sulfate polyacrylamide gel electrophoresis) analysis was done. 40 µL of the sample was mixed with SDS loading buffer and reducing agent, and then resolved on a 12% SDS–polyacrylamide gel (PAGE). The SDS gel was stained with coomassie brilliant blue dye and was observed in Gel Doc (Bio–RAD, USA) with Image Lab 5.2.1 software. The protein bands were examined according to their respective molecular weights. The total protein content present in samples was estimated by Lowry method with bovine serum albumin (BSA) as standard (Lowry et al., 1951).

### 4.2.4 Identification of metabolic pathway through analysis of enzyme activity

The PAHs degradation pathway by *C. tropicalis* (either *ortho*– or *meta*–cleavage route) under test and control conditions was identified. The principal enzymes involved in the pathway, viz. catechol 1,2–dioxygenase (C1,2–D) and catechol 2,3–dioxygenase (C2,3–D), are responsible for catechol ring fission through *ortho* or *meta* route. The predominant degradation pathway can be identified by

conducting an assay of catechol dioxygenase enzyme activity.

Activities of the two enzymes in the metabolic pathway, C1,2–D, and C2,3–D, were assessed by growing *C. tropicalis* in BH medium with phenanthrene as sole carbon source. $7^{th}$ and $14^{th}$ day samples of control and test experiments were used for enzyme activity assay. Catechol dioxygenase activity in the extract was determined according to the standard procedure (Mahiudddin and Fakhruddin, 2012).

### 4.2.5 Analysis of catechol 1,2–dioxygenase activity

The catechol 1,2–dioxygenase activity is a signature of the *ortho*–cleavage reaction of catechol leading to *cis,cis*–muconic acid formation. This activity can be quantified using spectrophotometric measurements. The reaction mixture for assessment of C1,2–D activity was added in a quartz cuvette with following composition (total 3 mL): 0.1 mL 2–mercaptoethanol (100 mM), 0.7 mL distilled water, 2 mL Tris–HCl buffer (50 mM, pH 8), 0.1 mL cell–free sample. After thorough mixing, 0.1 mL catechol (0.1 mM) was added. The absorbance of this solution at 260 nm was monitored for 5 min. The rise in absorbance of solution was an indicator of *cis–cis* muconic acid production (Shetty and Shetty, 2016).

### 4.2.6 Analysis of catechol 2,3–dioxygenase activity

The presence of catechol 2,3–dioxygenase activity signifies the *meta*–cleavage reaction of catechol with the formation of 2–hydroxymuconic semialdehyde (HMSA). The reaction mixture for assessment of the activity consisted of 0.2 mL cell–free sample, 2 mL Tris–HCl buffer (pH 7.5), and 0.6 mL distilled water. Catechol (100 mM) was added after thorough mixing, and then absorbance was monitored at 375 nm for 5 min. A rise in absorbance essentially signifies formation of HMSA (Shetty and Shetty, 2016).

### 4.2.7 Calculation of enzyme activity

The enzymatic activity of one unit (U) can be defined as the quantity of enzyme converting one μmol of the substrate into the product in one minute under specific reaction conditions and can be estimated as:

$$\text{Activity (U mL}^{-1}) = \frac{\Delta E \cdot V_f \cdot 1000}{\Delta t \cdot V_s \cdot L \cdot E_m} \quad (1)$$

where, $\Delta E$ = change in absorbance, $V_f$ = final volume, $V_s$ = cell–free extract volume, $\Delta t$ = time of reaction (5 min), $E_m$ = molar extinction coefficient of the formed product and $L$ = path length (1 cm for standard cuvette). Specific activities of the samples were expressed as units per milligram of protein.

### 4.2.8 Extraction and identification of metabolites

To identify the intermediate metabolites of PAH degradation, cultures were sampled and the organic fraction (comprising of intermediate metabolites and residual PAH) was extracted. The samples were acidified by adding 2–3 drops of HCl and then extraction was done twice by using ethyl acetate in equal volumes. The solvent was then removed using a rotary evaporator and the extracted residue was dissolved in methanol and filtered through membrane filter (0.2 micron). Finally, the extracts were analyzed using a gas chromatograph coupled with mass spectrometer (GC–MS). The GC–MS consisted of a gas chromatograph (Clarus 680, Perkin Elmer, USA) equipped with capillary column Elite–5MS (dimensions: 60 m × 0.25 mm × 0.25 μm with stationary phase: 95% dimethylpolysiloxane and 5% diphenyl) and a mass spectrometer (Clarus 600C, Perkin Elmer, USA). Mass spectra of the samples were acquired in Electron Impact positive (EI+) mode at 70 eV. Mass range (i.e. m/z range) of 50–600 amu was considered. Interpretation and identification of the peaks in the GC spectra was done by library search using the database software of National

Institute Standard and Technology (NIST) 2008, and the compounds corresponding to peaks were identified with name, molecular weight, empirical formula etc.

## 4.3 RESULTS AND DISCUSSION

### 4.3.1 SDS–PAGE analysis of protein expressions

The intracellular proteins present in the samples of control and test experiments were extracted and resolved on a 12% SDS–polyacrylamide gel (PAGE) by electrophoresis and stained with coomassie brilliant blue. The protein ladder marker used in the experiment was protein molecular weight marker (Low) (97.2 kDa to 14.3 kDa) (Company: Takara, Code no:3450) (Verma et al., 2019). Figs. 4.1 (A and B) shows the gel image of SDS–PAGE analysis of protein expression in control and test degradation experiments of both phenanthrene and pyrene, respectively. Comparing the protein bands in lane 1 (test) and lane 2 (control) reveals much higher expression of the proteins in test experiments. This is clear evidence of enhanced metabolism that results in faster degradation.

Bands of different sizes were visible in the lanes of both control and test samples. Among various proteins that facilitate PAHs degradation, catechol 2,3–dioxygenase (C2,3–D), possessing a size of 35.0 kDa (Takeo et al., 2007), is a key enzyme in the *meta*–route of degradation. SDS–PAGE analysis of both test and control samples revealed that it contained a protein band (Fig. 4.1), whose size was in good agreement with that of C2,3–D (35.0 kDa). Moreover, the protein bands were more expressed in test samples (lane 1), indicating higher production of this protein under the influence of sonication (Huang et al., 2017).

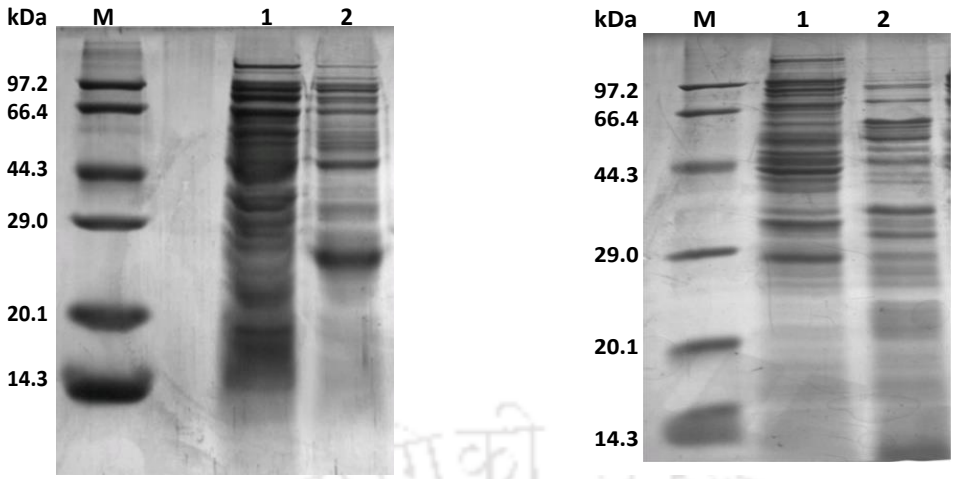


(A) (B)

**Figure 4.1.** Lane M shows the protein molecular weight marker (Low) (97.2 kDa to 14.3 kDa), Lane 1 and Lane 2 shows the bands of test (sonicated) and control samples respectively indicating the sizes of proteins. (A) Phenanthrene and (B) Pyrene.

### 4.3.2 Identification of metabolic pathway through analysis of enzyme activity

Biodegradation of PAHs is known to occur via catechol degradation pathway. Catechol is a common intermediate in polycyclic aromatic biodegradation (Salam et al., 2017; Shetty and Shetty, 2016). It is further degraded through *ortho*– or *meta*–cleavage route. As noted earlier, the *ortho*–cleavage route leads to *cis,cis*–muconic acid, whereas the *meta* route results in HMSA formation. Contributions of both *meta* and *ortho* pathways can be discerned by quantification of the characteristic enzymes, C2,3–D for *meta* pathway, and C1,2–D for *ortho* pathway (Mahiuddin and Fakhruddin, 2012; Banerjee and Ghoshal, 2010). To identify the impact of sonication on catechol ring cleavage route, enzymatic assay for C1,2–D and C2,3–D was carried out on $7^{th}$ and $14^{th}$ day of degradation in both control and test experiments for both phenanthrene and pyrene. There was no rise in absorbance at 260 nm during C1,2–D assay in control and test experiments, i.e. no C1,2–D activity and no *cis,cis*–muconic acid production. During C2,3–D assay for $7^{th}$ and $14^{th}$ day of degradation, rise in absorbance at 375 nm was observed in both control and test experiments signifying

strong activity of C2,3–D enzyme. Absorbance profiles of C2,3–D enzyme in control and test experiments are shown in Fig. 4.2. The absorbance values for test experiments were higher than control for both days, which indicates greater enzyme production and faster metabolism in test experiments.

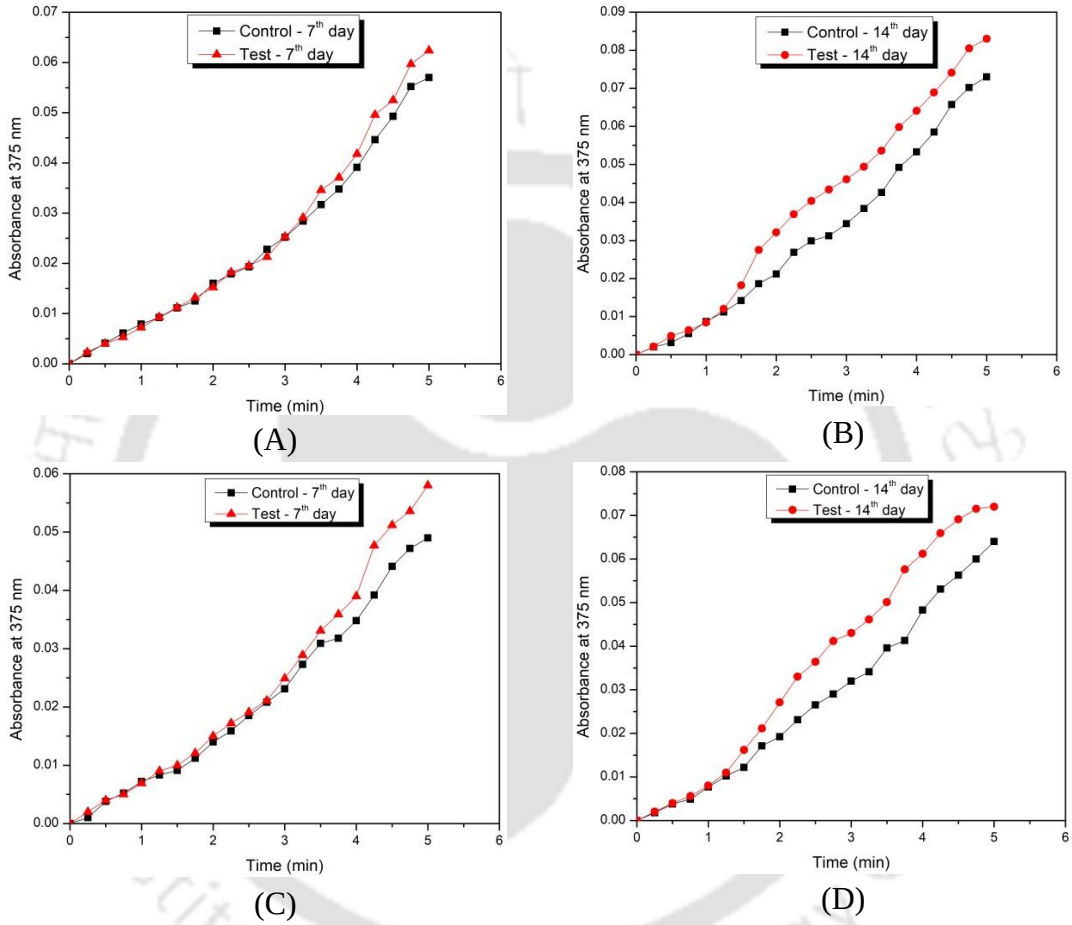


**Figure 4.2.** Change of absorbance with respect to time during catechol 2,3–dioxygenase assay. (A and B) indicates increase in absorbance of control and test experiments of phenanthrene degradation in 7$^{th}$ and 14$^{th}$ day respectively, and (C and D) indicates increase in absorbance of control and test experiments of pyrene degradation in 7$^{th}$ and 14$^{th}$ day respectively.

### 4.3.3 Catechol 2, 3–dioxygenase enzyme activity

The activities (U mL$^{-1}$) and the specific activities (mol min$^{-1}$ mg$^{-1}$) of the C2,3–D enzyme are given in Table 4.1 and 4.2. The activities were determined for

both phenanthrene and pyrene. 2–hydroxymuconic semialdehyde (HMSA) possessed molar extinction coefficient of 36,000 $M^{-1}$ $cm^{-1}$ (Arai et al., 2000).

**Table 4.1.** Catechol 2,3–dioxygenase activity of the control and test (Phenanthrene)

| Sample | Activity (U $mL^{-1}$) | Protein concentration (mg $mL^{-1}$) | Specific activity (mol $min^{-1}$ $mg^{-1}$) |
|---|---|---|---|
| Control ($7^{th}$ day) | 0.00475 | $28.90 \times 10^{-4}$ | $1.64 \times 10^{-6}$ |
| Control ($14^{th}$ day) | 0.00612 | $47.51 \times 10^{-4}$ | $1.28 \times 10^{-6}$ |
| Test ($7^{th}$ day) | 0.00520 | $30.76 \times 10^{-4}$ | $1.69 \times 10^{-6}$ |
| Test ($14^{th}$ day) | 0.00693 | $51.83 \times 10^{-4}$ | $1.34 \times 10^{-6}$ |

**Table 4.2.** Catechol 2,3–dioxygenase activity of the control and test (Pyrene)

| Sample | Activity (U $mL^{-1}$) | Protein concentration (mg $mL^{-1}$) | Specific activity (mol $min^{-1}$ $mg^{-1}$) |
|---|---|---|---|
| Control ($7^{th}$ day) | 0.00408 | $24.20 \times 10^{-4}$ | $1.68 \times 10^{-6}$ |
| Control ($14^{th}$ day) | 0.00533 | $40.25 \times 10^{-4}$ | $1.32 \times 10^{-6}$ |
| Test ($7^{th}$ day) | 0.00483 | $28.03 \times 10^{-4}$ | $1.72 \times 10^{-6}$ |
| Test ($14^{th}$ day) | 0.00600 | $44.00 \times 10^{-4}$ | $1.36 \times 10^{-6}$ |

From both the tables, it was clear that the C2,3–D activity in samples of test experiments was higher than the corresponding samples of control experiments. This essentially points to relatively lesser inhibition and inactivation of the cellular enzymes in test experiments. A plausible cause underlying this effect could be enhanced cellular transport induced by microturbulence generated during sonication. Another possible cause leading to higher activity of enzymes in test experiments, as demonstrated in previous literature (Agarwal et al., 2016) is alterations in secondary structure of enzyme produced due to sonication. These alterations include reduction in the rigid α–helix content leading to unfolding of proteins that exposes inner hydrophobic group and substrate–binding sites. These changes in secondary structure leads to faster metabolism. The metabolic pathway of degradation is not influenced by

sonication, as both the PAHs are degraded through *meta*– cleavage pathway in both control and test experiments.

### 4.3.4 Identification of intermediate metabolites of biodegradation

The metabolites formed during the degradation of phenanthrene and pyrene were analyzed using GC–MS on $6^{th}$, $10^{th}$ and $12^{th}$ day of degradation, which corresponded to the mid and end of log phase as per the growth curve of *C. tropicalis*. As no independent carbon source – other than phenanthrene and pyrene – was provided in the experiments, there is no possibility of interference from independent metabolites produced by *C. tropicalis* cells. Representative GC–MS spectra of some metabolites formed during biodegradation of phenanthrene and pyrene are provided in Appendix I. These metabolites are also provided in tables attached in the Appendix I. Similar types of metabolites were also found during PAHs biodegradation in (Kamyabi et al., 2018; Guntupalli et al., 2016). It can be referred that the metabolites for both substrates mainly comprised of mixture of alkanes, aldehydes, aromatic compounds, fatty/ carboxylic acids and epoxy derivatives of PAHs. In addition, other compounds such as sulfates, alcohol derivatives and diol/triol derivatives were also detected. The presence of epoxy derivative metabolites in the medium, viz. oxiraneundecanoic acid, 3–pentyl–, methyl ester, *cis*–, elucidates the initiation of PAHs oxidation to epoxide (arene oxide) mediated by the intracellular enzyme cytochrome P450 monooxygenase of *C. tropicalis*. These epoxides undergo rearrangement (non–enzymatically) resulting in formation of phenol detected in pyrene degradation. This is followed by conversion of phenols to conjugates of sulfates. For phenanthrene as substrate, the sulfates detected were as follows: 4'–Methylphenyl–1c–sulfonyl–β–d–galactoside and dodecane, 1,1'–thiobis. For pyrene as substrate, the sulfates detected in GC–MS analysis were:

thiazole–5–carboxylic acid, 2–tert–butylthio–4–methyl. Moreover, a diol derivative, viz. 1–naphthalene propanol, α–ethyl decahydro–5 was also detected during pyrene degradation.

In an alternate metabolic pathway, the intracellular enzymes dioxygenase and dehydrogenase can covert PAHs to *cis*–dihydrodiol and diols to catechol, respectively. Phenols can also be oxidized to catechol by mono–oxygenase. Catechol can subsequently undergo *ortho*– or *meta*– ring cleavage to produce succinate, acetaldehyde and pyruvate. Menthyl salicylate was detected as a metabolite in phenanthrene degradation. Salicyclic acid in different forms has reported as an important metabolite in previous literature (Feng et al., 2012; Prabhu and Phale, 2003). The presence of 1,2–benzenedicarboxylic acid (phthalic acid) as the metabolite for both phenanthrene and pyrene as substrate proves that both PAHs followed the phthalate pathway of degradation (Wu et al., 2019; Hou et al., 2018). PAHs are eventually converted into products like simple hydrocarbon alkanes that form from complete cleavage of aromatic ring. The accumulation of alkanes (hexadecane, decane, dodecane and tetradecane) in the culture medium is a clear indication of PAHs breakdown into simple hydrocarbons. These products undergo further oxidation to produce alcohols and fatty acids. Fatty acids such as n–hexadecanoic acid, eicosanoic acid, octadecanoic acid, and alcohols such as oleyl alcohol, octadecadien–1–ol, have been detected as metabolites. These metabolites can undergo complete mineralization by entering into TCA cycle. It may be noted that for both phenanthrene and pyrene degradation, a key intermediate of TCA cycle, viz. oxalic acid, has been detected.

### 4.3.5 Proposed degradation pathway elucidation

From the metabolites identified by GC–MS analysis (as discussed in previous

section), it can be inferred that multiple pathways (Hidayat and Yanto, 2018; Hou et al., 2018; Swaathy et al., 2014) were involved in phenanthrene and pyrene degradation by *C. tropicalis*. One possible pathway is the conversion of PAHs to epoxides by intracellular microbial monoxygenase enzymes followed by either formation of *trans*–dihydrodiols catalyzed by epoxide hydrolase, or non–enzymatic rearrangements leading to formation of conjugation products, like sulfates, glucuronides, xylosides and glucosides. Another possible pathway is the oxidation of PAHs by dioxygenases to produce *cis*–dihydrodiols. These enzymes facilitate further oxidative degradation of *cis*–dihydrodiols through two possible pathways: phthalate route or salicylate route. The initial step of both pathways is double hydroxylation of the PAHs ring (Cerniglia and Sutherland, 2001; Cerniglia, 1997).

Fig. 4.3 depicts the proposed degradation pathway on the basis of metabolites identified in GC–MS analysis. Both substrates of present study, viz. phenanthrene and pyrene, may be degraded in multiple ways as described below:

***Pathway 1:*** In this pathway 1, the primary step is attack of intracellular cytochrome P450 monooxygenase enzyme on substrate PAH (either phenanthrene or pyrene) to form arene oxide followed the formation of *trans*–dihydrodiols catalyzed by epoxide hydrolase. The presence of phenol indicates non–enzymatic conversion of arene oxide (epoxides) to sulfates conjugates. Sulfate conjugates were detected as intermediate metabolites in degradation of both PAHs.

***Pathway 2***: This pathway suggests the transformation of PAHs to *cis*–dihyrodiols due to hydroxylation of the ring via dioxygenase enzyme, which then follows either phthalate or salicylate routes. The presence of 1,2–benzenedicarboxylic acid (phthalic acid) as metabolites proves that both PAHs followed the phthalate pathway that eventually ended up in TCA cycle. Moreover, the presence of menthyl salicylate

(methyl ester of salicyclic acid) suggests that PAHs degradation may also occur via salicylate route. In the previous section, catechol,2,3–dioxygenase enzyme was detected in the cells of *C. tropicalis* MTCC 184, which support the inference that PAHs could be degraded by salicylate route. This enzyme leads to the further breakdown of catechol via *meta*–pathway to 2–hydroxy muconic semialdehyde (2–HMSA) which enters the TCA cycle.

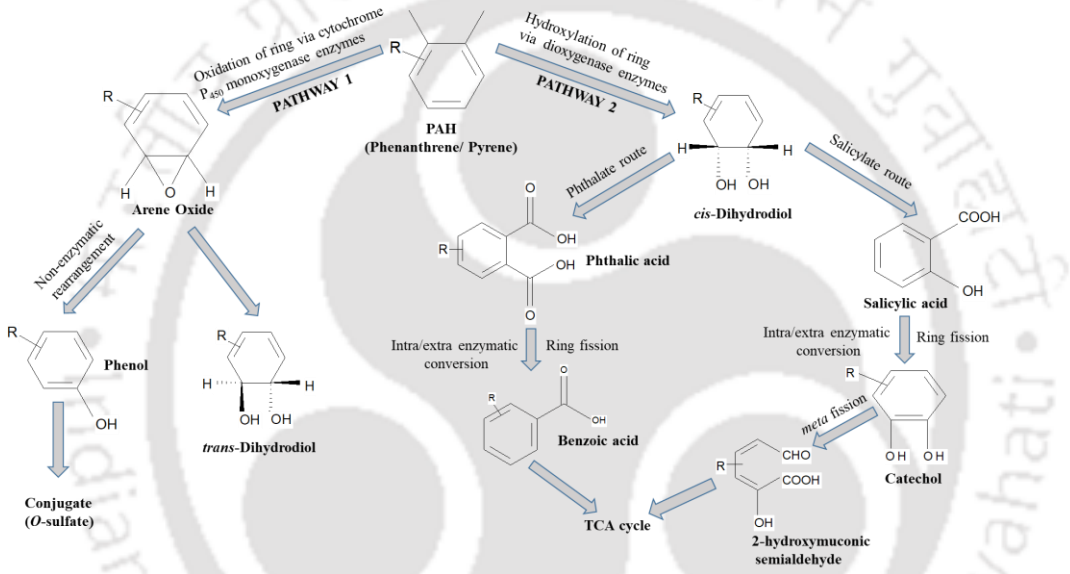


**Figure 4.3.** Proposed degradation pathway of phenanthrene and pyrene by *C. tropicalis* (Cerniglia and Sutherland, 2001; Cerniglia, 1997).

From practical point of view, involvement of multiple parallel metabolic pathways in biodegradation of PAH leads to faster and effective degradation. In this case, the degradation can proceed through alternate routes, even if one or more routes are ceased or blocked due to inhibition.

## 4.4 CONCLUSION

In this chapter, we have attempted to elucidate the enzymes, intermediates and

pathway followed in the degradation of phenanthrene and pyrene by *C. tropicalis*. It was found that same route of degradation (*meta*– pathway) was followed in both test and control experiments, thereby signifying that ultrasound did not alter the route of degradation. The total protein expression analysis by SDS–PAGE revealed higher expression in the test samples as compared to control samples. Enzyme activity in the test samples was also higher as compared to the control samples. GC–MS analysis of intermediate metabolites revealed two parallel pathways of degradation, first triggered by intracellular cytochrome P450 monooxygenase enzyme, and second initiated by dioxygenase enzymes. The former pathway yielded sulfate conjugate and dihydrodiols, while the latter resulted in acids and aldehydes that enters the TCA cycle. We believe that these results could form useful inputs for further research regarding the cellular proteins and metabolic pathway involved in PAH biodegradation by yeast strains.

## REFERENCES

Agarwal, M., Dikshit, P.K., Bhasarkar, J.B., Borah, A.J., Moholkar, V.S., 2016. Physical insight into ultrasound–assisted biodesulfurization using free and immobilized cells of *Rhodococcus rhodochrous* MTCC 3552. Chemical Engineering Journal, 295, 254–267.

Anita, S.H., Sari, F.P., Yanto, D.H.Y., 2019. Decolorization of synthetic dyes by ligninolytic enzymes from *Trametes hirsuta* D7. Makara Journal of Science, 44–50.

Arai, H., Ohishi, T., Chang, M.Y., Kudo, T., 2000. Arrangement and regulation of the genes for meta–pathway enzymes required for degradation of phenol in *Comamonas testosteroni* TA441. Microbiology, 146 (7), 1707–1715.

Banerjee, A. and Ghoshal, A.K., 2010. Phenol degradation by Bacillus cereus: pathway and kinetic modeling. Bioresource Technology, 101 (14), 5501–5507.

Cerniglia, C.E., 1997. Fungal metabolism of polycyclic aromatic hydrocarbons: past, present and future applications in bioremediation. Journal of industrial microbiology & biotechnology, 19.

Cerniglia, C.E. and Sutherland, J.B., 2001, November. Bioremediation of polycyclic aromatic hydrocarbons by ligninolytic and non–ligninolytic fungi. In British Mycological Society Symposium Series, 23, 136–187.

Csutak, O., Stoica, I., Ghindea, R., Tanase, A.M., Vassu, T., 2010. Insights on yeast bioremediation processes. Romanian Biotechnological Letters, 15 (2), 5066–5071.

Datta, K.K., Patil, A.H., Patel, K., Dey, G., Madugundu, A.K., Renuse, S., Kaviyil, J.E., Sekhar, R., Arunima, A., Daswani, B.; Kaur, I., 2016. Proteogenomics of

*Candida tropicalis*—An opportunistic pathogen with importance for global health. Omics: a journal of integrative biology, 20 (4), 239–247.

Feng, T.C., Cui, C.Z., Dong, F., Feng, Y.Y., Liu, Y.D., Yang, X.M., 2012. Phenanthrene biodegradation by halophilic *Martelella* sp. AD–3. Journal of applied microbiology, 113 (4), 779–789.

Gargouri, B., Mhiri, N., Karray, F., Aloui, F., Sayadi, S., 2015. Isolation and characterization of hydrocarbon–degrading yeast strains from petroleum contaminated industrial wastewater. BioMed research international, 2015.

Gou, Y., Zhao, Q., Yang, S., Qiao, P., Cheng, Y., Song, Y., Sun, Z., Zhang, T., Wang, L., Liu, Z., 2020. Enhanced degradation of polycyclic aromatic hydrocarbons in aged subsurface soil using integrated persulfate oxidation and anoxic biodegradation. Chemical Engineering Journal, 125040.

Guntupalli, S., Thunuguntla, V.B.S.C., Reddy, K.S., Newton, M.I., Rao, C.V., Bondili, J.S., 2016. Enhanced degradation of carcinogenic PAHs Benzo (a) Pyrene and Benzo (k) Fluoranthene by a Microbial Consortia. Indian Journal of Science and Technology, 9, 35.

Hadibarata, T., Khudhair, A.B., Kristanti, R.A., Kamyab, H., 2017. Biodegradation of pyrene by *Candida* sp. S1 under high salinity conditions. Bioprocess and biosystems engineering, 40 (9), 1411–1418.

Hashem, M., Alamri, S.A., Al–Zomyh, S.S., Alrumman, S.A., 2018. Biodegradation and detoxification of aliphatic and aromatic hydrocarbons by new yeast strains. Ecotoxicology and environmental safety, 151, 28–34.

Hidayat, A. and Yanto, D.H.Y., 2018. Biodegradation and metabolic pathway of phenanthrene by a new tropical fungus, *Trametes hirsuta* D7. Journal of Environmental Chemical Engineering, 6 (2), 2454–2460.

Hou, N., Zhang, N., Jia, T., Sun, Y., Dai, Y., Wang, Q., Li, D., Luo, Z., Li, C., 2018. Biodegradation of phenanthrene by biodemulsifier–producing strain *Achromobacter* sp. LH–1 and the study on its metabolisms and fermentation kinetics. Ecotoxicology and environmental safety, 163, 205–214.

Huang, L. and Batterman, S.A., 2014. Multimedia model for polycyclic aromatic hydrocarbons (PAHs) and nitro–PAHs in Lake Michigan. Environmental science & technology, 48 (23), 13817–13825.

Huang, G., Tang, Y., Sun, L., Xing, H., Ma, H., He, R., 2017. Ultrasonic irradiation of low intensity with a mode of sweeping frequency enhances the membrane permeability and cell growth rate of *Candida tropicalis*. Ultrasonics Sonochemistry, 37, 518–528.

Kamyabi, A., Nouri, H., Moghimi, H., 2018. Characterization of pyrene degradation and metabolite identification by *Basidioascus persicus* and mineralization enhancement with bacterial–yeast co–culture. Ecotoxicology and Environmental Safety, 163, 471–477.

Kumari, M. and Abraham, J., 2011. Biodegradation of diesel oil using yeast *Rhodosporidium toruloides*. Research Journal of Environmental Toxicology, 5 (6), 369.

Lowry, O.H., Rosebrough, N.J., Farr, A.L., Randall, R.J., 1951. Protein measurement with the Folin phenol reagent. Journal of Biological Chemistry, 193, 265–275.

Mahiudddin, M. and Fakhruddin, A.N.M., 2012. Degradation of phenol via meta cleavage pathway by *Pseudomonas fluorescens* PU1. Isrn Microbiology, 2012.

Marco–Urrea, E., García-Romera, I., Aranda, E., 2015. Potential of non–ligninolytic fungi in bioremediation of chlorinated and polycyclic aromatic hydrocarbons. New biotechnology, 32 (6), 620–628.

Okerentugba, P.O., Ataikiru, T.L., Ichor, T., 2016. Isolation and characterization of hydrocarbon utilizing yeast (HUY) isolates from palm wine. American Journal of Molecular Biology, 6 (2), 63–70.

Prabhu, Y. and Phale, P.S., 2003. Biodegradation of phenanthrene by *Pseudomonas* sp. strain PP2: novel metabolic pathway, role of biosurfactant and cell surface hydrophobicity in hydrocarbon assimilation. Applied microbiology and biotechnology, 61 (4), 342–351.

Salam, L., Ilori, M.O., Amund, O.O., 2017. Pyrene Biodegradation Potential of an Actinomycete, *Microbacterium Esteraromaticum* isolated from Tropical Hydrocarbon–Contaminated Soil. Journal of Microbiology, Biotechnology and Food Sciences, 6, 995–1000.

Shetty, G.R. and Shetty, V.K., 2016. Pathway identification, enzyme activity and kinetic study for the biodegradation of phenol by *Nocardia hydrocarbonoxydans* NCIM 2386. Desalination and Water Treatment, 57 (19), 8789–8801.

Swaathy, S., Kavitha, V., Pravin, A.S., Mandal, A.B., Gnanamani, A., 2014. Microbial surfactant mediated degradation of anthracene in aqueous phase by marine *Bacillus licheniformis* MTCC 5514. Biotechnology Reports, 4, 161–170.

Takeo, M., Nishimura, M., Shirai, M., Takahashi, H., Negoro, S., 2007. Purification and characterization of catechol 2, 3–dioxygenase from the aniline degradation pathway of *Acinetobacter* sp. YAA and its mutant enzyme, which resists substrate inhibition. Bioscience, biotechnology, and biochemistry, 71, 1688–1675.

Verma, K., Saha, G., Kundu, L.M., Dubey, V.K., 2019. Biochemical characterization of a stable azoreductase enzyme from *Chromobacterium violaceum*: application in industrial effluent dye degradation. International journal of biological macromolecules, 121, 1011–1018.

Wu, F., Guo, C., Liu, S., Liang, X., Lu, G., Dang, Z., 2019. Pyrene Degradation by *Mycobacterium gilvum*: Metabolites and Proteins Involved. Water, Air, & Soil Pollution, 230 (3), 67.

Yanto, D.H.Y. and Tachibana, S., 2014. Potential of fungal co-culturing for accelerated biodegradation of petroleum hydrocarbons in soil. Journal of hazardous materials, 278, 454–463.

Yanto, D.H.Y., Krishanti, N.P.R.A., Ardiati, F.C., Anita, S.H., Nugraha, I.K., Sari, F.P., Laksana, R.P.B., Sapardi, S., Watanabe, T., 2019. Biodegradation of styrofoam waste by ligninolytic fungi and bacteria. In IOP Conference Series: Earth and Environmental Science, 308, 012001, IOP Publishing.

# CHAPTER 5

# Investigations on co-biodegradation of phenanthrene and pyrene by *Candida tropicalis* and kinetic study

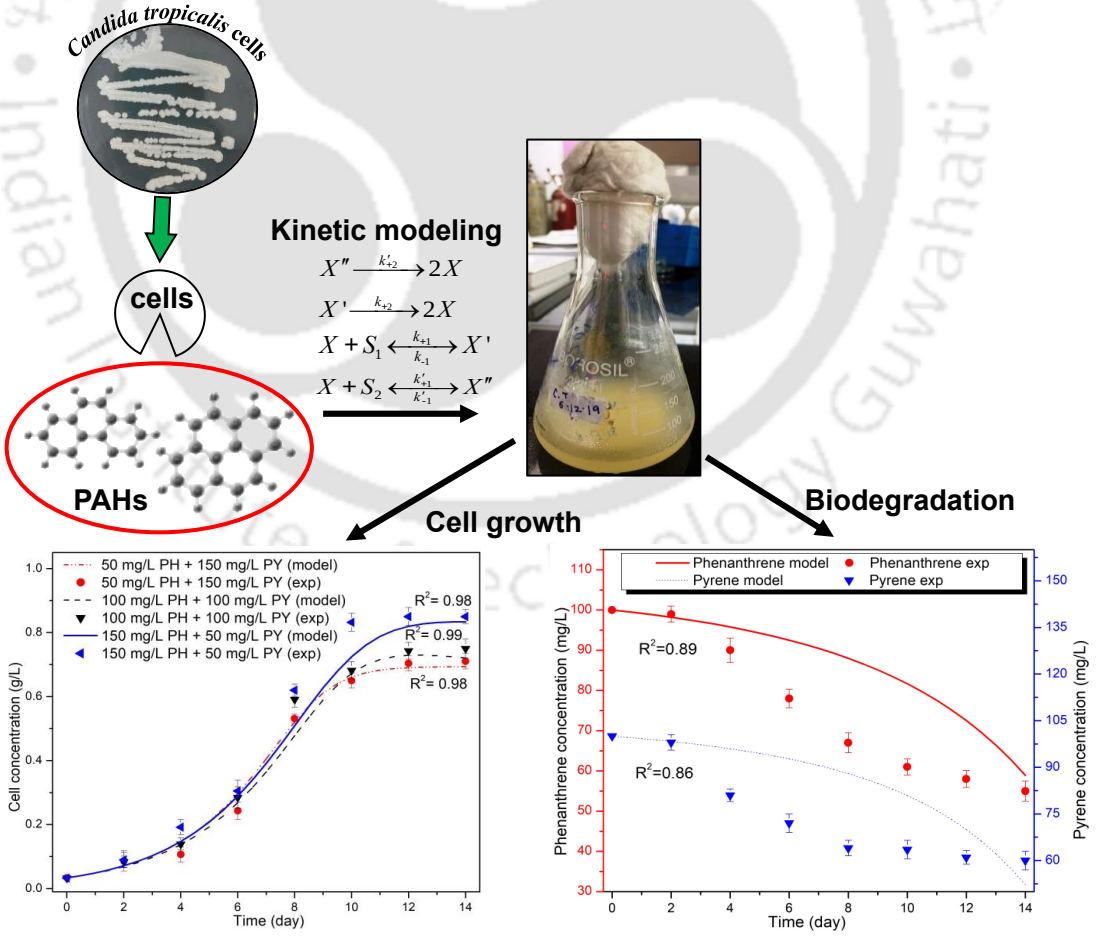

# CHAPTER 5

# Investigations on co-biodegradation of phenanthrene and pyrene by *Candida tropicalis* and kinetic study

## 5.1 INTRODUCTION

An efficient technique for effective degradation and mineralization of PAHs in both aquatic and terrestrial ecosystems is bioremediation using suitable microbial species. This technique has gained attention of research community, as it is safe, cost effective and eco-friendly (Xu et al., 2016; Ali and Tarek, 2009). Various microbial strains (both fungi and bacteria) have been reported by previous authors for effective degradation of different PAHs, for example *Mycobacterium* sp. (Mahanty et al., 2008), *Pseudomonas* sp. (Singh and Tiwary, 2017), *Candida* sp. (Hadibarata et al.,

2017; Farag and Soliman, 2011) *Burkholderia* sp. (Chen et al., 2013) and *Enterobacter* sp. (Umar et al., 2018). Most of the previous literature has employed single substrate while studying biodegradation of PAHs. However, in practical situations, several PAHs existing in eco–systems are simultaneously consumed by microbial species. Previous authors have employed either binary or multi-substrate systems for bioremediation study of the PAHs (Wang et al., 2019; Jiang et al., 2018a; Jiang et al., 2018b; Dutta et al., 2017; Ma et al., 2013). Moreover, there has also been reports of biomass growth inhibition for initial substrate concentrations higher than a particular limit due to substrate toxicity (Basak et al., 2014; Juang and Tsai, 2006). This inhibition results in lowering of biomass growth rate, and also reduction in biomass yield. In multi–substrate systems, in addition to self–inhibition, cross–inhibition is also possible, where degradation rate of one substrate is hampered by the other. Similar to self–inhibition, cross–inhibition also results in reduction of both biomass growth rate and yield. Moreover, the formation of toxic intermediates by nonspecific enzymes also augment inhibition effect. The interactions among the substrates is rather complex, not just by virtue of their toxicity, but also competition for common enzyme and co–factors in their individual metabolic routes. Previous literature has reported both kinds of substrate interaction patterns, viz. competitive inhibition and noncompetitive inhibition, in various multi–substrate degradation system (mentioned in Chapter 1). Optimization of the physical conditions such as pH, inoculum volume, temperature and agitation is essential for enhancement of biodegradation rate.

The principal objective of this chapter is to study co–bioremediation of two ubiquitous PAHs in the environment, viz. phenanthrene (PH) and pyrene (PY). Both of these PAHs are on the priority list of pollutants declared by US Environmental

Protection Agency (EPA). The microbial strain used in this study is yeast strain, *Candida tropicalis*. In the present study, we report for the first time use of *C. tropicalis* for co–biodegradation of two ubiquitous PAHs, viz. phenanthrene and pyrene. Another novel feature of the methodology adopted in this work is to couple experiments with a mathematical model (which accounts for both self– and cross–inhibition), so as to quantify the cell growth and degradation parameters of co–biodegradation of PH and PY. The kinetics of degradation has also been studied with varying initial concentrations of the two substrates. This analysis has provided insight into interactive effects among the two substrates in co–degradation of PH and PY.

## 5.2 MATERIALS AND METHODS

### 5.2.1 Culture growth and cultivation condition

*C. tropicalis* MTCC 184 was procured from the Institute of Microbial Technology (IMTECH), Chandigarh, India. Regular sub–culturing of the strain was done using yeast extract peptone dextrose (YEPD) medium agar plates comprising: yeast extract (3 g $L^{-1}$), peptone (10 g $L^{-1}$), dextrose (20 g $L^{-1}$) and agar (15 g $L^{-1}$) and storage at 4°C. Glycerol (20% v/v) stocks of the strain were also prepared and stored at –80°C. The yeast strain was grown at pH 7, 30°C, and 150 rpm agitation. Bushnell–Hass (BH) minimal salt medium having composition of (g $L^{-1}$): $K_2HPO_4$ (1.0); $KH_2PO_4$ (1.0); $NH_4NO_3$ (1.0); $FeCl_3$ (0.05); $MgSO_4{\cdot}7H_2O$ (0.2) and $CaCl_2{\cdot}2H_2O$ (0.02) was used in the degradation experiments. The experiments were conducted using BH medium supplemented with either PH or PY for single substrate experiments and both PH and PY as dual substrate for dual substrate experiments.

### 5.2.2 Chemicals

Phenanthrene and pyrene (sublimed grade, ≥ 99.5%) were purchased from Sigma–Aldrich (India). All organic solvents (HPLC grade) were from Merck, India. Bushnell Haas (BH) medium and other chemicals (analytical grade) required in the experiments were purchased from Himedia (Mumbai, India).

### 5.2.3 Inoculum development and experimentation

Acclimatization experiments were performed to familiarize the yeast strain to PAH environment. Two PAHs: PH and PY were degraded using yeast strain *C. tropicalis* MTCC 184 by taking a wide range of PH concentration upto 500 mg $L^{-1}$ and PY upto 250 mg $L^{-1}$. PAHs exhibit negligible solubility in water, so first it is dissolved in minimum acetone (2–3 mL) and then introduced in BH medium. Yeast strain was acclimatized using glucose (2%) to facilitate proper growth of the yeast in BH medium comprising of substrate (PH/PY). The yeast culture was acclimatized by exposing it to PAHs in a batch of Erlenmeyer flasks (250 mL) containing working volume (100 mL). Glucose concentration was reduced slowly while the concentration of PAHs was increased in the medium for 60 days. The developed inoculum was used in every biodegradation experiment pH 7 and incubator temperature of 30°C were maintained throughout the entire experimentation process.

The experiments were carried out with either single substrate or dual (or mixed) substrates. For all experiments, Erlenmeyer flasks (250 mL) containing working volume (100 mL) was used. The physical (or operating) parameters of the system were optimized (in Chapter 2) using statistical techniques. The time period of every experiment was fixed as 14 days. Biodegradation experiments with single substrate employed either PH or PY as only source of carbon and energy. In these experiments, the substrate concentration was varied over a large range, viz. 25–500 mg $L^{-1}$ for PH

and 25–250 mg $L^{-1}$ for PY. These concentrations were decided on the basis of preliminary experiments of *C. tropicalis* growth on both PAHs as single substrate. These experiments were conducted to assess tolerance of *C. tropicalis* cells towards both substrates as sole carbon source. The cell growth started declining after a typical initial threshold concentration for both substrates, viz. PH = 250 mg $L^{-1}$ and PY = 125 mg $L^{-1}$. In view of this result, the upper limit of initial substrate concentration was decided as 2× the threshold concentration, i.e. PH = 500 mg $L^{-1}$ and PY = 250 mg $L^{-1}$.

In biodegradation experiments with dual substrates, different initial concentration combinations of PH and PY used were as follows: PH = 100 mg $L^{-1}$ & PY = 100 mg $L^{-1}$, PH = 50 mg $L^{-1}$ & PY = 150 mg $L^{-1}$, and PH = 150 mg $L^{-1}$ & PY = 50 mg $L^{-1}$. Thus, the total initial PAHs concentration in all biodegradation experiments with dual substrate was 200 mg $L^{-1}$. The combination of initial concentrations of PH and PY were selected on the basis of maximum cell growth in single substrate experiments. In these experiments, maximum cell growth was observed at initial concentrations of 100 and 75 mg $L^{-1}$ for PH and PY, respectively. Thus, in dual substrate experiments, the total initial concentration of the two PAHs was maintained at ~ 200 mg $L^{-1}$, i.e. close to sum total of individual PH and PY concentrations corresponding to maximum growth. Higher total initial concentration of the two PAHs may lead to complete inhibition of growth as observed in our preliminary trials in dual substrate system.

Two important parameters that influence biodegradation are: (1) pH of the solution, and (2) dissolved $O_2$ concentration in the solution. Formation of intermediates during degradation (some of which are of acidic nature) leads to lowering of solution pH. However, these intermediates are rather unstable and their instantaneous concentration is expected to be too low to cause major variation in

solution pH. Prior to main experiments, we conducted preliminary trials, in which we found that final pH of solution (at the end of 14–day experiment) changed only marginally from 6.2 to 5.8 – which is ~ 6% variation. In the preliminary trials, we also checked intermittently the dissolved $O_2$ concentration of the solution. For conditions of flask covered with cotton plug and shaking speed of > 150 rpm, the dissolved $O_2$ concentration of the medium remained close to saturation level of ~ 8 ppm. This effect is possibly attributed to induction and dissolution of headspace air into the solution due to surface agitation. Moreover, the microbial cells also adsorb onto the surface of solution (which essentially is air–water interface) and access the $O_2$ in headspace air.

### 5.2.4 Biomass estimation and PAHs concentration in samples

2 mL samples of liquid mixture in each experimental flask were taken every 24 h for quantification of biomass and residual substrate concentrations. Samples extraction by using equal volumes of n–hexane followed by vortex agitation and then centrifugation (10,000 rpm) for 10 min. This procedure essentially transferred the residual PAHs (PH and PY) in the samples into the organic layer. Then the organic portion containing n–hexane (with dissolved PAHs) was collected and analysed. Three samples of the organic layer were analysed using high performance liquid chromatography (HPLC, Agilent Technologies, 1220 Infinity LC) fitted with C18 reverse–phase column (3 mm × 150 mm and particle size of 3.5 $\mu$m). The mobile phase (or eluent) used was acetonitrile: Milli–Q water mixture (70:30 volume ratio). Sample injection volume was 20 $\mu$L and flow rate of mobile phase was maintained.at 0.8 mL $min^{-1}$. PH and PY was identified using UV detector at 254 nm. The cell density was monitored by turbidity at 600 nm. To determine the biomass concentrations, samples were centrifuged (15 min) at 10,000 rpm and resulting pellet

was washed with water. After washing, the pellet was placed in a filter paper and was dried to a constant mass through heating for 24 h at 105ºC. The dry biomass pellet was then weighed for study of biomass growth. To assess reproducibility of results, each batch experiment was conducted in three parallel flasks under identical conditions and analysis was done using procedure outlined above. Average values of biomass concentration and residual PAHs concentrations were used for construction of time profiles of biomass growth and substrate consumption.

### 5.2.5 Kinetic model

#### 5.2.5.1 Kinetic model of cell growth

The biokinetic model for cell growth and substrate (PAH) degradation used in the present study is based on earlier works (Kumar et al., 2013; Bai et al., 2007; Wang and Loh, 2001; Yoon et al., 1977). This model comprises of total 14 reactions in dual substrate system (7 reactions for each substrate). These reactions essentially represent substrate consumption, cell growth, self–inhibition and cross–inhibition in a dual substrate system. The cross–inhibition reactions take into account the interactive effects of the two substrates. This model also incorporates kinetic parameters for single–substrate system, which have been determined using Haldane type kinetic model (James and David, 1986). In view of results of preliminary trials (mentioned in previous section), the pH and dissolved $O_2$ concentration of the solution are assumed to be constant. The temperature of the solution is also assumed constant.

The reactions of the model are listed in Table 5.1. Reactions 1 to 7 correspond to first substrate (represented as $S_1$) as main substrate, while reactions 8 to 14 correspond to second substrate (represented as $S_2$) as main substrate. In the analysis, hereafter, we have designated phenanthrene (PH) as $S_1$ and pyrene (PY) as $S_2$.

**Table 5.1.** Reaction scheme for cell growth in a dual substrate system

| No. | Reaction (for substrate $S_1$) | Nature | No. | Reaction (for substrate $S_2$) | Nature |
|---|---|---|---|---|---|
| 1. | $X + S_1 \underset{k_{-1}}{\overset{k_{+1}}{\longleftrightarrow}} X'$ | Substrate consumption | 8. | $X + S_2 \underset{k'_{-1}}{\overset{k'_{+1}}{\longleftrightarrow}} X''$ | Substrate consumption |
| 2. | $X' \xrightarrow{k_{+2}} 2X$ | Biomass growth | 9. | $X'' \xrightarrow{k'_{+2}} 2X$ | Biomass growth |
| 3. | $X' + S_1 \underset{k_{-3}}{\overset{k_{+3}}{\longleftrightarrow}} X'S_1$ | Self-inhibition* | 10. | $X'' + S_1 \underset{k'_{-3}}{\overset{k'_{+3}}{\longleftrightarrow}} X''S_1$ | Cross-inhibition* |
| 4. | $X' + S_2 \underset{k_{-4}}{\overset{k_{+4}}{\longleftrightarrow}} X'S_2$ | Cross-inhibition* | 11. | $X'' + S_2 \underset{k'_{-4}}{\overset{k'_{+4}}{\longleftrightarrow}} X''S_2$ | Self-inhibition* |
| 5. | $X'S_1 + S_1 \underset{k_{-5}}{\overset{k_{+5}}{\longleftrightarrow}} X'S_1^2$ | Self-inhibition# | 12. | $X''S_1 + S_1 \underset{k'_{-5}}{\overset{k'_{+5}}{\longleftrightarrow}} X''S_1^2$ | Cross-inhibition# |
| 6. | $X'S_2 + S_2 \underset{k_{-6}}{\overset{k_{+6}}{\longleftrightarrow}} X'S_2^2$ | Cross-inhibition# | 13. | $X''S_2 + S_2 \underset{k'_{-6}}{\overset{k'_{+6}}{\longleftrightarrow}} X''S_2^2$ | Self-inhibition# |
| 7. | $X'S_1 + S_2 \underset{k_{-7}}{\overset{k_{+7}}{\longleftrightarrow}} X'S_1S_2$ | Cross-inhibition# | 14. | $X''S_1 + S_2 \underset{k'_{-7}}{\overset{k'_{+7}}{\longleftrightarrow}} X''S_1S_2$ | Cross-inhibition# |

***Note:*** * = reaction leading to secondary complex formation; # = reaction leading to ternary complex formation. Primary complexes = $X'$, $X''$; Secondary complexes = $X'S_1$, $X'S_2$, $X''S_1$, $X''S_2$; Ternary complexes = $X'S_1^2$, $X'S_2^2$, $X'S_1S_2$, $X''S_1^2$, $X''S_2^2$, $X''S_1S_2$

The reactions listed in Table 5.1 can be divided into four categories: (1) formation of primary complexes through substrate consumption (reactions 1 for $S_1$ and 8 for $S_2$), (2) biomass growth (reactions 2 for $S_1$ and reaction 9 for $S_2$), (3) self–inhibition by substrate (reactions 3 & 5 for $S_1$ and 11 & 13 for $S_2$), (4) cross–inhibition between two substrates (reactions 4, 6, 7 for $S_1$ and reactions 10, 12, 14 for $S_2$). Different intermediate species in the reaction scheme presented in Table 5.1. Reactions representing the metabolism of first substrate (viz. 1, 3–7), and second substrate (viz. 8, 10–14) are assumed to be first order and reversible with respect to both reactants and products. Reactions 2 and 9 representing biomass growth with first and second substrate, respectively, are considered as irreversible. The complexes (or the intermediates) formed during metabolism can have two possible fates, viz. they may split back into the constituent species due to reversible reaction or they may decompose into stable products. Whatever the fate of complexes may be, the lifespan of these intermediates is very small due to their instability and high reactivity.

Accurate measurement of their real–time profile is rather difficult. However, their instantaneous concentration in the reaction mixture at any time during the degradation process is expected to be very miniscule. In view of this, an assumption of pseudo–steady state can be made, and any inhibitory effect induced by these species on biodegradation process can be ignored. Pseudo–steady state essentially means that the rate of formation of these species is equal to rate of disappearance, and thus, their concentration in the reaction mixture stays constant. The hypothesis of pseudo–steady state also helps in devising the mathematical model (comprising of ordinary differential equations for the mass balances of biomass and substrate) for the kinetics of biomass growth and substrate degradation.

The mass balances for the primary complexes, viz. $X'$ and $X''$, are written as:

$$\frac{d[X']}{dt} = k_{+1}[X][S_1] - k_{-1}[X'] - k_{+2}[X'] + k_{+3}[S_1][X'] - k_{-3}[X'S_1] + k_{+4}[X'][S_2] - k_{-4}[X'S_2] \quad (1)$$

$$\frac{d[X'']}{dt} = k'_{+1}[X][S_2] - k'_{-1}[X''] - k'_{+2}[X''] + k'_{+3}[S_1][X''] - k'_{-3}[X''S_1] + k'_{+4}[S_2][X''] - k'_{-4}[X''S_2] \quad (2)$$

Under assumption of pseudo–steady state for the secondary and ternary complexes for both substrates these equations reduce as:

$$\frac{d[X']}{dt} = k_{+1}[X][S_1] - k_{-1}[X'] - k_{+2}[X'] = 0 \quad (3)$$

$$\frac{d[X'']}{dt} = k'_{+1}[X][S_2] - k'_{-1}[X''] - k'_{+2}[X''] = 0 \quad (4)$$

The concentrations of the primary complexes are written in terms of $[X]$, $[S_1]$ and $[S_2]$ as:

$$[X'] = \frac{k_{+1}}{k_{-1} + k_{+2}}[X][S_1] \quad (5)$$

$$[X''] = \frac{k'_{+1}}{k'_{-1} + k'_{+2}}[X][S_2] \tag{6}$$

The pseudo–steady state mass balances for other species and their steady state concentrations have been given in the Appendix II. The total cell mass concentration $X_T$, in either native (free) or complexed form is:

$$\begin{aligned} X_T = {} & [X] + [X'] + [X'S_1] + [X'S_2] + [X'S_1^2] + [X'S_2^2] + [X'S_1S_2] + [X''] + \\ & [X''S_1] + [X''S_2] + [X''S_1^2] + [X''S_2^2] + [X''S_1S_2] \end{aligned} \tag{7}$$

Substituting the pseudo–steady state concentrations of the primary, secondary and ternary complexes (as derived in Appendix II) gives:

$$\begin{aligned} X_T = {} & [X] + \frac{k_{+1}}{k_{-1} + k_{+2}}[X][S_1] + \frac{k_{+3}}{k_{-3}}\frac{k_{+1}}{k_{-1} + k_{+2}}[X][S_1]^2 + \frac{k_{+4}}{k_{-4}}\frac{k_{+1}}{k_{-1} + k_{+2}}[X][S_1][S_2] + \\ & \frac{k_{+5}}{k_{-5}}\frac{k_{+3}}{k_{-3}}\frac{k_{+1}}{k_{-1} + k_{+2}}[X][S_1]^3 + \frac{k_{+6}}{k_{-6}}\frac{k_{+4}}{k_{-4}}\frac{k_{+1}}{k_{-1} + k_{+2}}[X][S_1][S_2]^2 + \frac{k_{+7}}{k_{-7}}\frac{k_{+3}}{k_{-3}}\frac{k_{+1}}{k_{-1} + k_{+2}}[X][S_1]^2[S_2] + \\ & \frac{k'_{+1}}{k'_{-1} + k'_{+2}}[X][S_2] + \frac{k'_{+3}}{k'_{-3}}\frac{k'_{+1}}{k'_{-1} + k'_{+2}}[X][S_2][S_1] + \frac{k'_{+4}}{k'_{-4}}\frac{k'_{+1}}{k'_{-1} + k'_{+2}}[X][S_2]^2 + \\ & \frac{k'_{+5}}{k'_{-5}}\frac{k'_{+3}}{k'_{-3}}\frac{k'_{+1}}{k'_{-1} + k'_{+2}}[X][S_2][S_1]^2 + \frac{k'_{+6}}{k'_{-6}}\frac{k'_{+4}}{k'_{-4}}\frac{k'_{+1}}{k'_{-1} + k'_{+2}}[X][S_2]^3 + \frac{k'_{+7}}{k'_{-7}}\frac{k'_{+3}}{k'_{-3}}\frac{k'_{+1}}{k'_{-1} + k'_{+2}}[X][S_2]^2[S_1] \end{aligned} \tag{8}$$

We now make following substitutions for the ratios of various kinetic constants:

$$\begin{aligned} & \frac{1}{K_{S1}} = \frac{k_{+1}}{(k_{-1} + k_{+2})}, \frac{1}{K_{S2}} = \frac{k'_{+1}}{k'_{-1} + k'_{+2}}, \frac{1}{K_{i1}} = \frac{k'_{+3}}{k'_{-3}}, \frac{1}{K_{i2}} = \frac{k'_{+4}}{k'_{-4}}, \frac{1}{g'} = \frac{k'_{+6}}{k'_{-6}}, \frac{1}{m} = \frac{k_{+4}}{k_{-4}}, \\ & \frac{1}{n} = \frac{k_{+5}}{k_{-5}}, \frac{1}{m'} = \frac{k'_{+4}}{k'_{-4}}, \frac{1}{n'} = \frac{k'_{+5}}{k'_{-5}}, \frac{1}{g} = \frac{k_{+6}}{k_{-6}}, \frac{1}{g'} = \frac{k'_{+6}}{k'_{-6}}, \frac{1}{h} = \frac{k_{+7}}{k_{-7}}, \frac{1}{h'} = \frac{k'_{+7}}{k'_{-7}} \end{aligned}$$

Thus, the total biomass concentration is now expressed as:

$$X_T = [X]\left(\begin{array}{l} 1 + \frac{[S_1]}{K_{S1}} + \frac{[S_1]^2}{K_{i1}K_{S1}} + \frac{[S_1][S_2]}{mK_{S1}} + \frac{[S_1]^3}{nK_{i1}K_{S1}} + \frac{[S_1][S_2]^2}{gmK_{S1}} + \frac{[S_1]^2[S_2]}{hK_{i1}K_{S1}} + \\ \frac{[S_2]}{K_{S2}} + \frac{[S_2][S_1]}{m'K_{S2}} + \frac{[S_2]^2}{K_{i2}K_{S2}} + \frac{[S_2][S_1]^2}{n'm'K_{S2}} + \frac{[S_2]^3}{g'K_{i2}K_{S2}} + \frac{[S_2]^2[S_1]}{h'm'K_{S2}} \end{array}\right) \tag{9}$$

The cell growth in a single substrate system can be assumed to follow first order kinetics as:

$d[X]/dt = \mu[X]$, where $\mu$ is specific cell growth rate. Analogously, the total biomass growth rate in presence of mixed substrate is written as: $d[X_T]/dt = \mu_T[X_T]$, where $\mu_T$ is the resultant total specific growth rate in the dual substrate system. Further, the biomass growth rate in a dual substrate system is also written as:

$$\frac{d[X_T]}{dt} = \mu_{x1}[X_T] + \mu_{x2}[X_T] \tag{10}$$

where, $\mu_{x1}$ and $\mu_{x2}$ represent the contributions to total growth from individual substrates $S_1$ and $S_2$, respectively, in the presence of the other. However, as per the reaction scheme presented in Table 5.1.

$$\frac{d[X_T]}{dt} = k_{+2}[X'] + k'_{+2}[X''] \tag{11}$$

Comparing Eqs 10 and 11 yields following relations: $\mu_{x1} = k_{+2}[X']/[X_T]$, and $\mu_{x2} = k'_{+2}[X'']/[X_T]$. Denoting $k_{+2} = \mu_{m,S1}$, $k'_{+2} = \mu_{m,S2}$ and $f = K_{s1}/K_{s2}$, and substituting Eq. 9 for $[X_T]$ in equations for $\mu_{x1}$ and $\mu_{x2}$ gives following:

$$\mu_{x1} = \frac{\mu_{m,S1}[S_1]}{\left\{\begin{array}{l} K_{S1} + [S_1] + \frac{[S_1]^2}{K_{i1}} + \frac{[S_1][S_2]}{m} + \frac{[S_1]^3}{nK_{i1}} + \frac{[S_1][S_2]^2}{gm} + \frac{[S_1]^2[S_2]}{hK_{i1}} + \\ f[S_2] + \frac{f[S_1][S_2]}{m'} + \frac{f[S_2]^2}{K_{i2}} + \frac{f[S_1]^2[S_2]}{n'm'} + \frac{f[S_2]^3}{g'K_{i2}} + \frac{f[S_1][S_2]^2}{h'm'} \end{array}\right\}} \tag{12}$$

$$\mu_{x2} = \frac{\mu_{m,S2}[S_2]}{\left\{\begin{array}{l} K_{S2} + \frac{[S_1]}{f} + \frac{[S_1]^2}{K_{i1}f} + \frac{[S_1][S_2]}{mf} + \frac{[S_1]^3}{nK_{i1}f} + \frac{[S_1][S_2]^2}{gmf} + \frac{[S_1]^2[S_2]}{hK_{i1}f} + \\ [S_2] + \frac{[S_1][S_2]}{m'} + \frac{[S_2]^2}{K_{i2}} + \frac{[S_1]^2[S_2]}{n'm'} + \frac{[S_2]^3}{g'K_{i2}} + \frac{[S_1][S_2]^2}{h'm'} \end{array}\right\}} \tag{13}$$

The values of specific growth rate, Monod constant and inhibition constants for single substrate, viz. $\mu_{m,S1}$, $K_{S1}$, $K_{i1}$ for the first substrate $S_1$, and $\mu_{m,S2}$, $K_{S2}$, $K_{i2}, K'_{i2}$ for the second substrate $S_2$, can be acquired independently from the individual cell growth

kinetics with either PH or PY as only carbon and energy source (described and discussed in next section). Substituting Eqs. 12 and 13 in Eq. 10 gives:

$$\frac{d[X_T]}{dt} = \left( \begin{array}{l} \dfrac{\mu_{m,S1}[S_1]}{\left\{ K_{S1} + [S_1] + \dfrac{[S_1]^2}{K_{i1}} + \dfrac{[S_1][S_2]}{m} + \dfrac{[S_1]^3}{nK_{i1}} + \dfrac{[S_1][S_2]^2}{gm} + \dfrac{[S_1]^2[S_2]}{hK_{i1}} + f[S_2] \right.} \\ \left. + \dfrac{f[S_1][S_2]}{m'} + \dfrac{f[S_2]^2}{K_{i2}} + \dfrac{f[S_1]^2[S_2]}{n'm'} + \dfrac{f[S_2]^3}{g'K_{i2}} + \dfrac{f[S_1][S_2]^2}{h'm'} \right\} \\ + \dfrac{\mu_{m,S2}[S_2]}{\left\{ K_{S2} + \dfrac{[S_1]}{f} + \dfrac{[S_1]^2}{K_{i1}f} + \dfrac{[S_1][S_2]}{mf} + \dfrac{[S_1]^3}{nK_{i1}f} + \dfrac{[S_1][S_2]^2}{gmf} + \dfrac{[S_1]^2[S_2]}{hK_{i1}f} \right.} \\ \left. + [S_2] + \dfrac{[S_1][S_2]}{m'} + \dfrac{[S_2]^2}{K_{i2}} + \dfrac{[S_1]^2[S_2]}{n'm'} + \dfrac{[S_2]^3}{g'K_{i2}} + \dfrac{[S_1][S_2]^2}{h'm'} \right\} \end{array} \right) [X_T] \quad (14)$$

The terms in the denominators are rearranged as follows (Wang et al., 1996):

$$\frac{d[X_T]}{dt} = \left( \begin{array}{l} \dfrac{\mu_{m,S1}[S_1]}{\left\{ K_{S1} + [S_1] + \dfrac{[S_1]^2}{K_{i1}} + I_{a,1}[S_2] + I_{b,1}[S_1][S_2] \right\}} \\ + \dfrac{\mu_{m,S2}[S_2]}{\left\{ K_{S2} + [S_2] + \dfrac{[S_2]^2}{K_{i2}} + I_{a,2}[S_1] + I_{b,2}[S_1][S_2] \right\}} \end{array} \right) [X_T] \quad (15)$$

The significance of different terms in the denominator of eq. 15 is as follows: (1) $I_{a,1}$ signifies $S_1$ degradation inhibition in presence of $S_2$; (2) $I_{a,2}$ signifies $S_2$ degradation inhibition in presence of $S_1$; (3) $I_{b,1}$ signifies inhibition to degradation of $S_1$ by both $S_1$ and $S_2$; (4) $I_{b,2}$ signifies inhibition to degradation of $S_2$ by both $S_1$ and $S_2$. Thus, $I_{a,1}$, $I_{a,2}$, $I_{b,1}$ and $I_{b,2}$ can be considered as interactive parameters of substrate inhibition in dual substrate system. Inspecting Eqs.14 and 15, these parameters in dual substrate system are written as:

$$I_{a,1} = f + \frac{f[S_2]}{K_{i2}} + \frac{f[S_2]^2}{g'K_{i2}} \quad (16)$$

$$I_{b,1} = \frac{1}{m} + \frac{[S_1]^2}{nK_{i1}[S_2]} + \frac{[S_2]}{gm} + \frac{[S_1]}{hK_{i2}} + \frac{f}{m'} + \frac{f[S_1]}{n'm'} + \frac{f[S_2]}{h'm'} \quad (17)$$

$$I_{a,2} = \frac{1}{f} + \frac{[S_1]}{K_{i1}f} + \frac{[S_1]^2}{nK_{i1}f} \quad (18)$$

$$I_{b,2} = \frac{1}{mf} + \frac{[S_2]}{gmf} + \frac{[S_1]}{hK_{i1}f} + \frac{1}{m'} + \frac{[S_1]}{n'm'} + \frac{[S_2]}{h'm'} \quad (19)$$

### 5.2.5.2 Kinetic model for PAH degradation

The substrate consumed by microorganism is utilized for three purposes: (1) product formation, (2) biomass growth and (3) cell maintenance. On this basis, the mass balance for the substrate is written as:

$$\frac{d[S]}{dt} = \frac{1}{Y_{X/S}}\frac{d[X]}{dt} + m_c[X] + \frac{1}{Y_{P/S}}\frac{d[P]}{dt} \quad (20)$$

Product formation may occur in either log phase (cell growth) or stationary phase. Therefore, $d[P]/dt = \alpha\, d[X]/dt + \beta[X]$, where $\alpha$ is the coefficient for growth associated product formation while $\beta$ represents the production formation in stationary phase. Substitution of $d[P]/dt$ in Eq. 20, and combining common terms yields the following relation:

$$\frac{d[S]}{dt} = \left(\frac{1}{Y_{X/S}} + \frac{\alpha}{Y_{P/S}}\right)\frac{d[X]}{dt} + \left(m_c + \frac{\beta}{Y_{P/S}}\right)[X] \quad (21)$$

$$\frac{d[S]}{dt} = A\frac{d[X]}{dt} + B[X] \quad (22)$$

Dividing Eq. 22 by $[X]$ yields equation for specific degradation rate $q_S$ in terms of specific cell growth rate ($\mu$):

$$\frac{1}{[X]}\frac{d[S]}{dt} = q_S = \frac{A}{[X]}\frac{d[X]}{dt} + B = A\mu + B \quad (23)$$

where, $q_S$ is the specific substrate degradation rate. The above general equation can

be adopted for the degradation of PH and PY in a dual substrate system by substituting expressions for specific cell growth rate for every substrate (Eq. 12 for $S_1$ and Eq. 13 for $S_2$) in a dual substrate system:

$$q'_{S1} = \frac{d[S_1]}{[X_T]dt} = A'_1\mu_{x1} + B'_1 \quad (24)$$

$$q'_{S2} = \frac{d[S_2]}{[X_T]dt} = A'_2\mu_{x2} + B'_2 \quad (25)$$

In Eqs. 24 and 25, the specific growth rates for the two substrates, viz. $\mu_{x1}$ and $\mu_{x2}$ can be substituted from Eqs. 12 and 13. It may be noted that the Monod constants ($K_{S1}$, $K_{S2}$) and inhibition constants ($K_{i1}$, $K_{i2}$, $K'_{i2}$) in Eq. 15 need to be determined with single substrate experiments. These experiments and their kinetic analysis are described in the next section.

***Numerical solution scheme:*** Eqs. 15, 24 and 25 constitute the complete kinetic model for biodegradation of PH and PY in a dual substrate system. These three simultaneous ordinary differential equations were solved (as initial value problem) using Runge–Kutta 4$^{th}$ order method in MATLAB R2019A®. The initial values of the three variables [$X_T$], [$S_1$] and [$S_2$] for numerical solution were as follows: $t$ = 0, [$S_1$] and [$S_2$] = initial concentrations in mg L$^{-1}$ (either 50, 100, 150 or 200 mg L$^{-1}$), $X_T$ = 0.03 g L$^{-1}$. These ordinary differential equations contain 8 kinetic parameters, viz. $I_{a1}$, $I_{b1}$, $I_{a2}$, $I_{b2}$, $A_1'$, $B_1'$, $A_2'$, $B_2'$. The values of these parameters were determined by comparing simulated profiles of biomass and substrate with experimental values using Genetic Algorithm. The numerical values of the kinetic constants were optimized within specified bounds by calculating root mean square (RMS) error between experimental data and the simulations. The objective function (Obj) for the optimization was defined on the basis of minimization of sum total error for all variables (substrates

and biomass):

$Obj = \min\left(\sum_{i=1}^{n} error_i\right)$ where $n$ is the number of experimental data points.

The error between experimental and simulation is defined as:

$$error = \left[\left(C_{X_T}^{\exp} - C_{X_T}^{\text{model}}\right)^2 + \left(C_{S_1}^{\exp} - C_{S_1}^{\text{model}}\right)^2 + \left(C_{S_2}^{\exp} - C_{S_2}^{\text{model}}\right)^2\right]^{1/2}$$

where $C$ represents the concertation of the two substrates and the biomass.

The average fitness of kinetic constants was used for each individual population algorithm with a confidence interval of 95%. The experimental and simulation results were also analysed using variance, and the means using student's *t*–test at 5% significance levels. This analysis is given in Appendix II. Statistical analysis results of *t*–test (assuming equal variances) and *F*–test ($p < 0.05$) suggested that the model exhibits optimum stability.

## 5.3 RESULTS AND DISCUSSION

### 5.3.1 Biodegradation on single substrate system

As noted in experimental section, batch experiments of biodegradation were carried out using cells of *C. tropicalis* MTCC 184 with either PH or PY as the sole carbon source. Previous literature has reported inhibition of cell growth and degradation kinetics by the PAHs like PH and PY at relatively high concentrations (Wang et al., 2019; Jiang et al., 2018a; Jiang et al., 2018b).

Representative cell concentrations profiles for initial substrate concentration of 200 mg $L^{-1}$ for both substrates are shown in Fig. 5.1A, while Fig. 5.1B depicts the profiles of substrate concentrations. These time profiles were fitted to first order kinetics to acquire specific biomass growth rate and specific degradation rate.

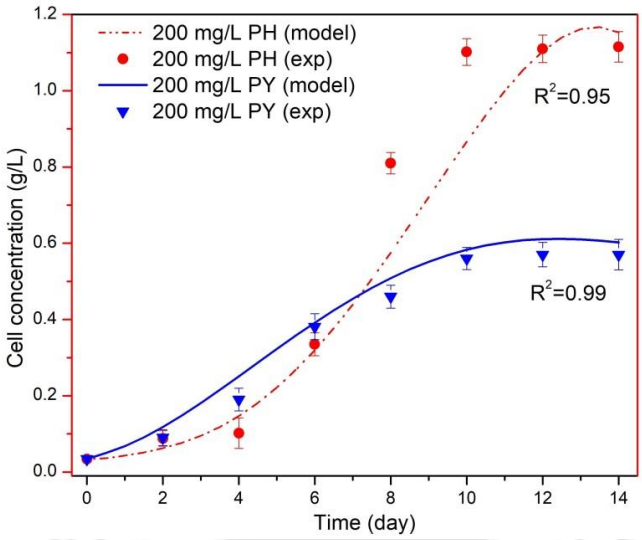


(A)

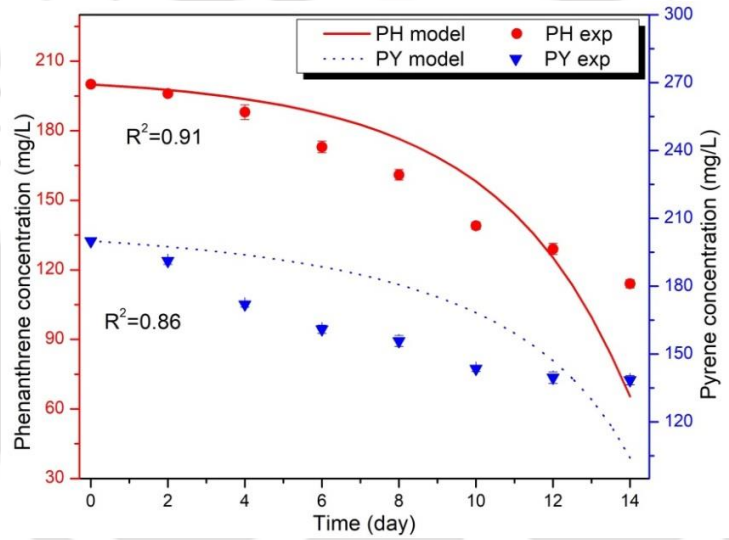


(B)

**Figure 5.1.** Experimental and simulated time profiles of single substrate system. Initial substrate concentration = 200 mg $L^{-1}$ (A) cell or biomass growth with single substrate, (B) substrate degradation with single substrate.

### 5.3.1.1 Kinetic parameters of PH degradation

As noted in previous section, specific growth rate of cells can be acquired by fitting first order kinetics to the time profile of biomass concentration. For the degradation of PH, the specific biomass growth rate can be described using Haldane substrate inhibition model as:

$$\mu_{x,S1} = \left. \frac{\mu_{m,S1}[S_1]}{K_{S1} + [S_1] + [S_1]^2 / K_{i1}} \right|_{[S_1]=[S_{1,0}]} \quad (26)$$

Degradation of first substrate can be assumed to follow 1st order kinetics as:

$d[S_1]/dt = q_{S1}[X]$, where $q_{S1}$ is the specific substrate degradation rate. As the degradation of the substrate is related to biomass growth, a simple relation between $q_{S1}$ and $\mu_{x,S1}$ can be written on basis of Eq. 23 as:

$$q_{S1} = A_1 \mu_{x,S1} + B_1 \quad (27)$$

The values of $q_{S1}$ corresponding to different initial concentrations of $S_1$ can be acquired by slope of the plot of $dS_1/dt$ vs. $X$. The plots of $\mu_{x,S1}$ and $q_{S1}$ versus initial concentrations of $S_1$ (PH) are shown in Figs. 5.2A and 5.2B. Fitting of Eqs. 26 and 27 to these plots using non–linear regression (using MATLAB R2019A®) yields the values of kinetic constants (in Eqs. 26 and 27) as:

$$\mu_{x,S1} = \frac{0.90[S_1]}{62.56 + [S_1] + [S_1]^2 / 149.6} \quad (R^2 = 0.95) \quad (28)$$

$$q_{S1} = 0.1743 \mu_{x,S1} + 0.00166 \quad (R^2 = 0.93) \quad (29)$$

### 5.3.1.2 Kinetic parameters of PY degradation

The kinetic analysis of PY degradation was also done along similar lines as PH. However, due to relatively lesser tolerance of microbial cells towards PY, the Haldane model for specific biomass growth rate was modified by Bai et al. (2007) as:

$$\mu_{x,S2} = \left. \frac{\mu_{m,S2}[S_2]}{K_{S2} + [S_2] + \frac{[S_2]^2}{K_{i2}} + \frac{[S_2]^3}{K'_{i2}}} \right|_{S_2=S_{2,0}} \quad (30)$$

The specific degradation rate is written as:

$$q_{S2} = A_2 \mu_{x,S2} + B_2 \quad (31)$$

The plots of $\mu_{x,S2}$ and $q_{S2}$ versus initial concentrations of $S_2$ (PY) are shown in Figs. 5.2C and 5.2D. Fitting of Eqs. 30 and 31 to these plots using non–linear regression yields the values of kinetic constants (in Eqs. 30 and 31) as:

$$\mu_{x,S2} = \frac{3.4[S_2]}{298.2 + [S_2] + \frac{[S_2]^2}{31.85} + \frac{[S_2]^3}{5124}} \quad (R^2 = 0.90) \quad (32)$$

$$q_{S2} = 0.131\mu_{x2} + 0.002072 \quad (R^2 = 0.94) \quad (33)$$

In order to assess the fitness of expressions of specific growth and degradation rates for each substrate, simulated profiles of biomass concentration and substrate concentrations were generated by substitution of Eqs. 28 and 29 (for PH) and Eqs. 32 and 33 (for PY) in 1st order kinetic expressions for biomass (*dX/dt*) and substrate (*dS/dt*) noted in previous section. Numerical solution of these equations are also plotted in Figs. 5.1A and 5.1B for PH and PY. The regression coefficients of the simulated profiles against the experimental data are ~ 0.9 or higher, which clearly confirms the best–fit between experiments and simulations. In both Eqs. 29 and 33, viz. the specific degradation rates for PH and PY, respectively, the numerical value of $A_1$ is two orders of magnitude higher than $B_1$. This indicates that degradation of both substrates is a growth–associated process.

It could be perceived from Fig. 5.2 that the maximum specific growth and degradation rates for both PH and PY occurred at relatively low initial concentrations, and reduced rapidly with rise in concentrations. The maxima in specific growth rate and specific degradation rate for PH was acquired at initial concentration of 100 mg $L^{-1}$, while that for PY was obtained at 75 mg $L^{-1}$. This essentially indicates stronger

inhibition of cell growth by PY than PH. This behavior is also reflected from the final substrate concentrations in Fig. 5.1B, viz. PH = 120 mg $L^{-1}$ and PY = 140 mg $L^{-1}$. Relatively higher PH consumption by microbial cells under otherwise similar conditions also indicates lesser inhibition and toxicity of PH.

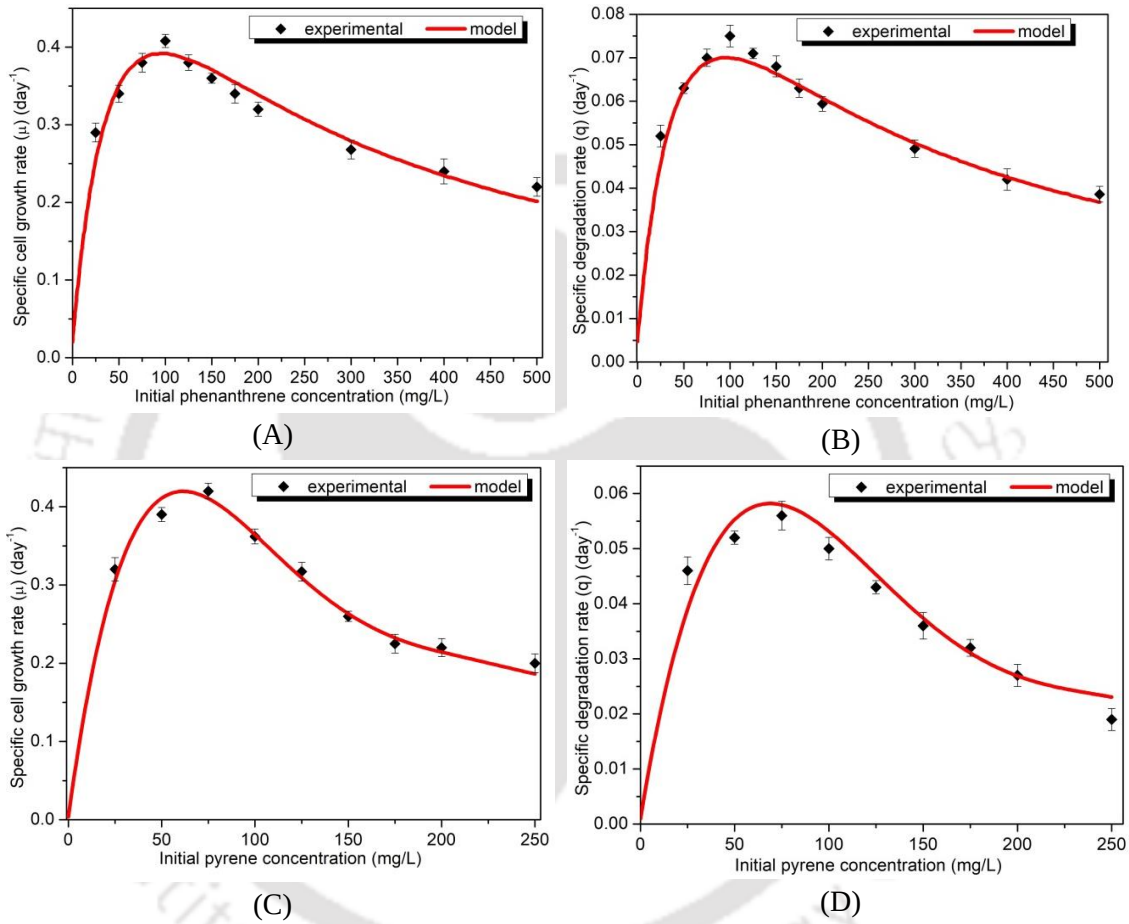


**Figure 5.2.** Profiles of specific growth rate ($\mu$) and specific degradation rate ($q$) with initial substrate concentration in single substrate system. (A and B): phenanthrene as substrate, (C and D): pyrene as substrate. The kinetic parameters related to specific growth and degradation have been determined using these profiles.

### 5.3.2 Biodegradation in dual substrate system

Fig. 5.3 shows the cell or biomass concentration profiles (experimental as well as simulated) in dual substrate system with different combinations of initial concentrations of PH and PY. Figs. 5.4 (A, B and C) depicts the experimental and

simulated profiles of the two substrates for different combinations of initial concentrations.

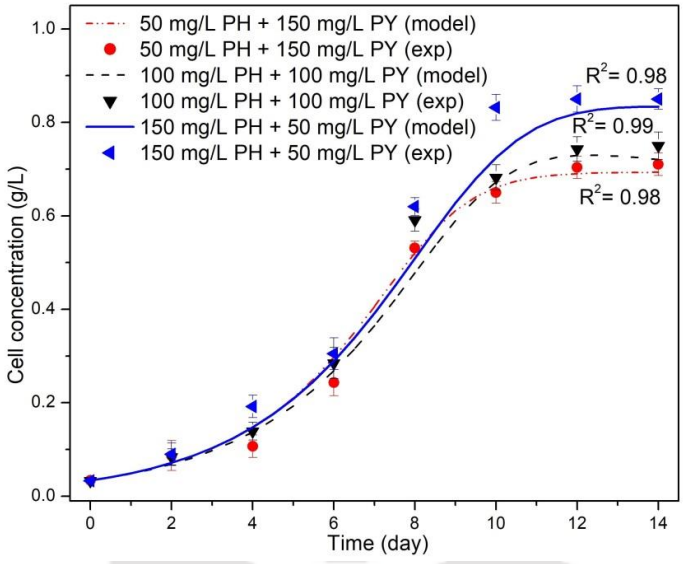


**Figure 5.3.** Experimental and simulated degradation profiles in cell or biomass growth in dual substrate systems.

The numerical values of the kinetic parameters obtained from simulations are given in Table 5.2. It could be seen that the values of constants $A_1'$ and $A_2'$ in specific degradation rate for both substrates at least an order of magnitude higher than constants $B_1'$ and $B_2'$ (Table 5.2B). These results clearly show that (similar to individual substrate system) the degradation of both PH and PY is mostly a growth–associated phenomena – even in dual substrate system. The kinetic parameters in specific growth rate, viz. $I_{a,1}$, $I_{a,2}$, $I_{b,1}$, $I_{b,2}$ represent the nature of substrate inhibition in a dual substrate system. As per the initial analysis reported by Wang et al. (1996) and later extended Kumar et al. (2013), the relative values of the above kinetic parameters indicate different type of inhibition behavior or pattern as described in the footnote of Table 5.2A. By inspecting the relative values of the four constants, we find that values of $I_{a,1}$ and $I_{a,2}$ are at least an order of magnitude higher than $I_{b,1}$ and $I_{b,2}$.

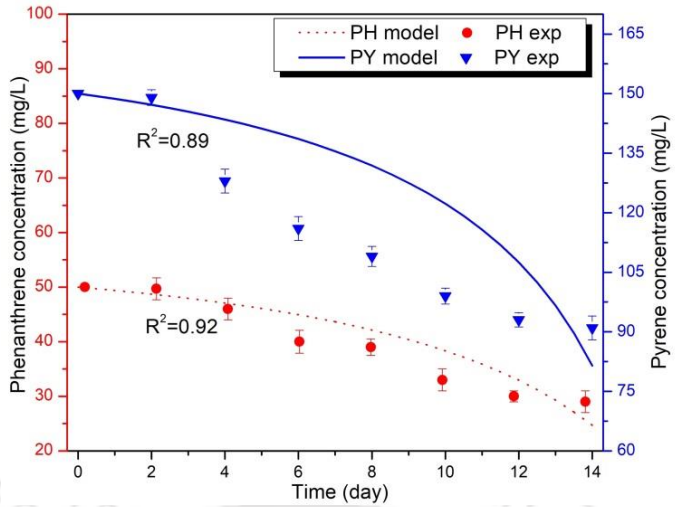


(A)

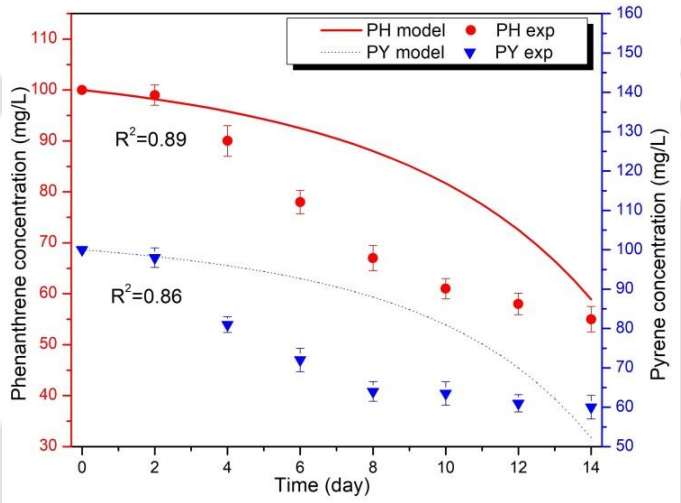


(B)

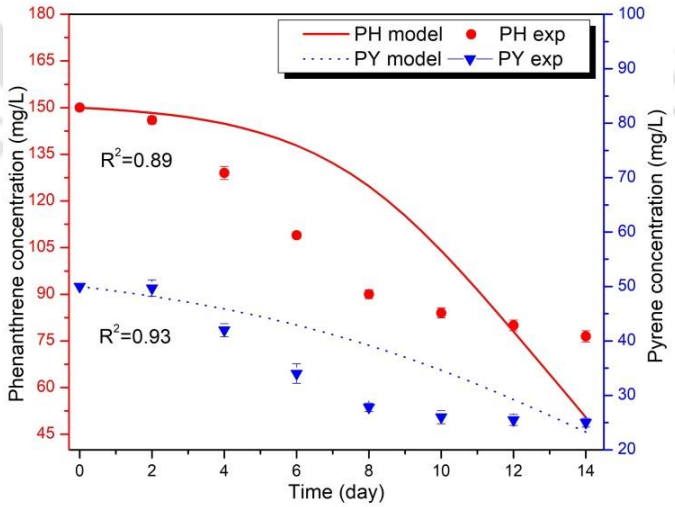


(C)

**Figure 5.4.** Experimental and simulated profiles of substrate degradation in dual substrate system. (A) PH = 50 mg/L + PY = 150 mg/L; (B) PH = 100 mg/L + PY = 100 mg/L; (C) PH = 150 mg/L + PY = 50 mg/L.

Moreover, absolute values of $I_{b,1}$ and $I_{b,2}$ are also quite small (< 0.2). Thus, the nature of inhibition in the present system appears close to competitive cross−inhibition. Table 5.2C presents comparative analysis of actual biomass yield in a dual substrate system, and theoretical or hypothetical biomass yield for no interaction among the metabolic pathways of the two substrates. The hypothetical biomass yield has been obtained by multiplying the biomass yield coefficient ($Y_{X/S}$) for individual substrates (obtained from experiments with single substrate), and actual consumption of the substrates in the dual substrate system.

**Table 5.2.** Kinetic parameters for degradation in dual substrate system

(A) Interaction parameters for inhibition (Eq. 15)

| | | | |
|---|---|---|---|
| $I_{a,1}$ | 1.082 | $I_{a,2}$ | 2.014 |
| $I_{b,1}$ | 0.0102 | $I_{b,2}$ | 0.1773 |

***Note:*** Patterns of inhibition indicated by parameters are as follows (1) Competitive cross−inhibition = $I_{b,1} \approx I_{b,2} \approx 0;\ I_{a,1}, I_{a,2} > 0$ . (2) Uncompetitive cross−inhibition = $I_{a,1} \approx I_{a,2} \approx 0;\ I_{b,1}, I_{b,2} > 0$ . (3) Competitive partial inhibition = $I_{b,1} \approx I_{b,2} \approx 0;$ either $I_{a,1} \approx 0, I_{a,2} > 0$ or $I_{a,2} \approx 0, I_{a,1} > 0$ . (4) Uncompetitive partial inhibition = $I_{a,1} \approx I_{a,2} \approx 0;$ either $I_{b,1} \approx 0, I_{b,2} > 0$ or $I_{b,2} \approx 0, I_{b,1} > 0$ .

(B) Specific degradation (Eqs. 24 and 25)

| | | | |
|---|---|---|---|
| $A_1'$ | 0.2368 | $A_2'$ | 0.102 |
| $B_1'$ | 0.01032 | $B_2'$ | 0.00464 |

(C) Influence of dual substrate on biomass yield

| Initial substrate concentrations (mg $L^{-1}$) | | $(Y_{X/S})_{PH}$ | $(Y_{X/S})_{PY}$ | $(\Delta X)_T$ | $(\Delta X)_E$ |
|---|---|---|---|---|---|
| PH | PY | | | | |
| 50 | 150 | 0.0243 | 0.0115 | 1.186 | 0.676 |
| 100 | 100 | 0.0229 | 0.0191 | 1.795 | 0.717 |
| 150 | 50 | 0.0166 | 0.0347 | 2.085 | 0.817 |

It could be seen from results of Table 5.2C that for all combinations of initial concentrations of PH and PY, the actual biomass yield is significantly smaller than the hypothetical yield. The least actual biomass yield of 0.676 mg $L^{-1}$ is obtained for

the combination PH = 50 mg $L^{-1}$ and PY = 150 mg $L^{-1}$. This is clearly consequence of higher toxicity and inhibition due to PY. The actual biomass yield increases with phenanthrene fraction in substrate and the highest yield of 0.817 mg $L^{-1}$ is obtained for combination PH = 150 mg $L^{-1}$ and PY = 50 mg $L^{-1}$. However, it is rather surprising that the discrepancy between hypothetical and actual yield shows inverse variation. The actual biomass yield for the highest initial PY concentration of 150 mg $L^{-1}$ in mixed substrate is 57% of the hypothetical yield (1.186 mg $L^{-1}$), while for least initial PY concentration of 50 mg $L^{-1}$, the actual biomass yield is just 39% of the theoretical yield (2.085 mg $L^{-1}$).

### 5.3.3 Practical implications and limitations

Effective degradation of organic contaminants including PAHs occurring in terrestrial and aquatic ecosystems poses a daunting challenge. The real–life scenario could be significantly dissimilar than the binary system comprising two PAHs considered in this study. Practical ecosystems may be contaminated with large number of PAHs along with other organic contaminants such as phenols and their derivatives. Depending on their source, the concentrations of these pollutants may also vary over several orders of magnitude. Moreover, the microbial cultures used for onsite bioremediation of such ecosystems are usually mixed consortia comprising of multiple species of bacteria, yeast, fungi etc. The biodegradation pattern in such systems will be far more complicated than the system in this study. Depending on the concentrations of pollutants, the concentration of the intermediate metabolites could also be large, which can induce further interaction and inhibition. The kinetic model used in this study has limitations in terms of simplifying assumptions. Nonetheless, this study has attempted to provide a glimpse of facets and complications of co–bioremediation of PAHs. To map the degradation patterns in practical systems,

rigorous and extensive experimentation is required. Similarly, with mathematical rigor, the kinetic model in this study can be extended to multi–substrate system. Such extended mathematical model along with rigorous experiments can provide at least qualitative insights into the bioremediation of practical eco–systems.

## 5.4 CONCLUSION

The present study has reported the mechanistic features of co–biodegradation of two common PAHs, viz. phenanthrene and pyrene, using the yeast *C. tropicalis*. The experimental results have been analysed using a kinetic model for cell growth that takes into account self– and cross–inhibition of both substrates. In dual substrate system, specific degradation rate of phenanthrene was significantly higher than pyrene, which indicated relatively lower tolerance of *C. tropicalis* cells towards pyrene. The values of interaction parameters of inhibition revealed strong competitive cross–inhibition between two substrates, due to which biomass yield with dual substrates was reduced significantly. Inhibition induced by pyrene on cell growth was higher than phenanthrene. We believe that the mechanistic insights of co–biodegradation of phenanthrene and pyrene reported in this study could form a useful tool for discerning interaction patterns among PAHs in bioremediation of practical (or real life) ecosystems comprising multiple pollutants.

### Nomenclature

***Abbreviations***

| | | |
|---|---|---|
| PH | : | phenanthrene (substrate 1 or $S_1$) |
| PY | : | pyrene (substrate 2 or $S_2$) |
| PAH | : | polycyclic aromatic hydrocarbon |

***Notations***

| | | |
|---|---|---|
| $A_1, A_2$ | : | constants for growth associated substrate consumption for $S_1$ and $S_2$ (single substrate), dimensionless |
| $B_1, B_2$ | : | constants for non-growth associated substrate consumption for $S_1$ and $S_2$ (single substrate), $day^{-1}$ |
| $A_1', A_2'$ | : | constants for growth associated substrate consumption for $S_1$ and $S_2$ (dual substrate), dimensionless |
| $B_1', B_2'$ | : | constants for non-growth associated substrate consumption for $S_1$ and $S_2$ (dual substrate), $day^{-1}$ |
| $I_{a,1}, I_{a,2}$ | : | interactive parameters of inhibition in presence of another substrate, dimensionless |
| $I_{b,1}, I_{b,2}$ | : | interactive parameters of inhibition in presence of both substrates, L $mg^{-1}$ |
| $k_j$ | : | first order reactions rate constants of reactions 1–7 in Table 5.1 ($j$ = +1, –1, +2, +3, –3, +4, –4, +5, –5, +6, –6, +7, –7; units: forward reactions, $(mg\ L^{-1})^{-1}\cdot day^{-1}$; reverse reactions, $day^{-1}$; $k_{+2}$, $day^{-1}$) |
| $k_j'$ | : | first order reactions rate constants of reactions 8–14 in Table 5.1 ($j$ = +1, –1, +2, +3, –3, +4, –4, +5, –5, +6, –6, +7, –7; units: forward reactions, $(mg\ L^{-1})^{-1}\cdot day^{-1}$; reverse reactions, $day^{-1}$; $k_{+2}'$, $day^{-1}$) |
| $K_{S1}, K_{S2}$ | : | saturation constants for cell growth on $S_1$ and $S_2$, g $L^{-1}$ |
| $K_{i1}, K_{i2}$ | : | self-inhibition constants for cell growth on $S_1$ and $S_2$, mg $L^{-1}$ |
| $K_{i2}'$ | : | second order self-inhibition constant for $S_2$, $(mg\ L^{-1})^2$ |
| $m_c$ | : | maintenance energy coefficient, $day^{-1}$ |
| $P$ | : | concentration of product, mg $L^{-1}$ |
| $q_{S1}, q_{S2}$ | : | specific degradation rates for $S_1$ and $S_2$ (single substrate), $day^{-1}$ |
| $q_{S1}', q_{S2}'$ | : | specific degradation rates for $S_1$ and $S_2$ (dual substrate), $day^{-1}$ |
| $[S_1]$ | : | concentration of substrate 1, mg $L^{-1}$ |
| $[S_2]$ | : | concentration of substrate 2, mg $L^{-1}$ |
| $t$ | : | time, day |
| $[X]$ | : | biomass concentration, mg $L^{-1}$ |
| $[X']$ | : | concentration of primary complex of $S_1$, mg $L^{-1}$ |
| $[X'']$ | : | concentration of primary complex of $S_2$, mg $L^{-1}$ |

$[X_T]$ : total biomass concentration, mg $L^{-1}$

$(\Delta X)_E$ : experimental biomass yield (dual substrate), mg

$(\Delta X)_T$ : theoretical biomass yield (dual substrate)

$[X'S_1],[X'S_2]$ : concentrations of secondary complexes of $S_1$, mg $L^{-1}$

$[X''S_1],[X''S_2]$ : concentrations of secondary complexes of $S_2$, mg $L^{-1}$

$[X'S_1^2],[X'S_2^2],[X'S_1S_2]$ : concentrations of ternary complexes of $S_1$, mg $L^{-1}$

$[X''S_1^2],[X''S_2^2],[X''S_1S_2]$ : concentrations of ternary complexes of $S_2$, mg $L^{-1}$

$Y_{X/S}$ : cell (or biomass) yield coefficient on substrate, mg $mg^{-1}$

$Y_{P/S}$ : product yield coefficient on substrate, mg $mg^{-1}$

***Greek symbols***

$\mu_T$ : overall (or total) growth rate (dual substrate), $day^{-1}$

$\mu_{m,S1}, \mu_{m,S2}$ : max. specific growth rate for $S_1$ and $S_2$ (single substrate), $day^{-1}$

$\mu_{x1}, \mu_{x2}$ : specific growth rate for $S_1$ and $S_2$ (dual substrate), $day^{-1}$

$\mu_{x,S1}, \mu_{x,S2}$ : specific growth rate for $S_1$ and $S_2$ (single substrate), $day^{-1}$

## REFERENCES

Ali, O.A. and Tarek, S.J., 2009. Removal of polycyclic aromatic hydrocarbons from Ismailia Canal water by chlorine, chlorine dioxide and ozone. Desalination and Water Treatment, 1 (1–3), 289–298.

Bai, J., Wen, J.P., Li, H.M., Jiang, Y., 2007. Kinetic modeling of growth and biodegradation of phenol and m-cresol using *Alcaligenes faecalis*. Process Biochemistry, 42 (4), 510–517.

Basak, B., Bhunia, B., Dutta, S., Chakraborty, S., Dey, A., 2014. Kinetics of phenol biodegradation at high concentration by a metabolically versatile isolated yeast *Candida tropicalis* PHB5. Environmental Science and Pollution Research, 21 (2), 1444–1454.

Chen, K., Zhu, Q., Qian, Y., Song, Y., Yao, J., Choi, M.M., 2013. Microcalorimetric investigation of the effect of non-ionic surfactant on biodegradation of pyrene by PAH–degrading bacteria *Burkholderia cepacia*. Ecotoxicology and environmental safety, 98, 361–367.

Dutta, K., Shityakov, S., Das, P.P., Ghosh, C., 2017. Enhanced biodegradation of mixed PAHs by mutated naphthalene 1, 2–dioxygenase encoded by *Pseudomonas putida* strain KD6 isolated from petroleum refinery waste. 3 Biotech, 7 (6), 365.

Farag, S. and Soliman, N.A., 2011. Biodegradation of crude petroleum oil and environmental pollutants by *Candida tropicalis* strain. Brazilian Archives of biology and Technology, 54 (4), 821–830.

Hadibarata, T., Khudhair, A.B., Kristanti, R.A., Kamyab, H., 2017. Biodegradation of pyrene by *Candida* sp. S1 under high salinity conditions. Bioprocess and biosystems engineering, 40 (9), 1411–1418.

James, E. B. and David, F. O., 1986. Biochemical Engineering Fundamentals, 2nd Edition, McGraw-Hill Pub, US.

Jiang, Y., Qi, H., Zhang, X.M., 2018a. Co–biodegradation of naphthalene and phenanthrene by *Acinetobacter johnsonii*. Polycyclic Aromatic Compounds. 1–10.

Jiang, Y., Zhang, Z., Zhang, X., 2018b. Co–biodegradation of pyrene and other PAHs by the bacterium *Acinetobacter johnsonii*. Ecotoxicology and environmental safety, 163, 465–470.

Juang, R.S. and Tsai, S.Y., 2006. Growth kinetics of *Pseudomonas putida* in the biodegradation of single and mixed phenol and sodium salicylate. Biochemical Engineering Journal, 31 (2), 133–140.

Kumar, S., Arya, D., Malhotra, A., Kumar, S., Kumar, B., 2013. Biodegradation of dual phenolic substrates in simulated wastewater by *Gliomastix indicus* MTCC 3869. Journal of Environmental Chemical Engineering, 1 (4), 865–874.

Ma, J., Xu, L., Jia, L., 2013. Characterization of pyrene degradation by *Pseudomonas* sp. strain Jpyr–1 isolated from active sewage sludge. Bioresource technology, 140, 15–21.

Mahanty, B., Pakshirajan, K., Dasu, V.V., 2008. Biodegradation of pyrene by *Mycobacterium frederiksbergense* in a two–phase partitioning bioreactor system. Bioresource technology, 99 (7), 2694–2698.

Singh, P. and Tiwary, B.N., 2017. Optimization of conditions for polycyclic aromatic hydrocarbons (PAHs) degradation by *Pseudomonas stutzeri* P2 isolated from Chirimiri coal mines. Biocatalysis and agricultural biotechnology, 10, 20–29.

Umar, Z.D., Zulkifli, S.Z., Muskhazli, M., 2018. Effective phenanthrene and pyrene

biodegradation using *Enterobacter* sp. MM087 (KT933254) isolated from used engine oil contaminated soil. Egyptian journal of petroleum, 27 (3), 349–359.

Wang, Z., Wang, W., Li, Y., Yang, Q., 2019. Co–metabolic degradation of naphthalene and pyrene by acclimated strain and competitive inhibition kinetics. Journal of Environmental Science and Health, Part B, 54 (6), 505–513.

Wang, S.J. and Loh, K.C., 2001. Biotransformation kinetics of *Pseudomonas putida* for cometabolism of phenol and 4–chlorophenol in the presence of sodium glutamate. Biodegradation, 12 (3), 189–199.

Xu, X., Chen, X., Su, P., Fang, F., Hu, B., 2016. Biodegradation potential of polycyclic aromatic hydrocarbons by bacteria strains enriched from Yangtze River sediments. Environmental Technology, 37 (5), 513–520.

Yoon, H., Klinzing, G., Blanch, H.W., 1977. Competition for mixed substrates by microbial populations. Biotechnology and Bioengineering, 19 (8), 1193–1210.

# CHAPTER 6

# Overview and Suggestions for Future Work

# CHAPTER 6

# Overview and Suggestions for Future Work

## 6.1 OVERVIEW

Present thesis has addressed some important fundamental issues related to environmental pollution. Environmentalists all around the globe have been endeavouring to reduce pollution through bioremediation process. An attempt has been made in this thesis to provide a good literature for the upcoming research on PAHs biodegradation by non–ligninolytic fungal species. Researchers have conducted various studies on degradation of PAHs such as phenanthrene, anthracene, pyrene, etc., using bacterial and fungal species. But PAHs biodegradation by yeasts like *Candida* sp. has been less explored. Moreover, fungal or yeast biodegradation studies have always been conducted with the aid of additional carbon or nutritional source.

Therefore, in this study we have investigated the biodegradation potential of *Candida tropicalis* strain on two PAHs (phenanthrene and pyrene) as sole carbon source. The metabolites/intermediates formed during the degradation process were also identified through GC/MS analysis to frame the pathway of degradation. A peculiar feature of this thesis is that the biodegradation capacity of the *Candida tropicalis* cells was also studied by applying ultrasound with an aim to enhance the degradation rate. Researchers have already reported beneficial action of ultrasound for increasing product yield or faster kinetics. Moreover, there has always been a hollow space when it comes to study on the underlying kinetics in biodegradation process. An effort has also been made in this thesis to fulfil the research gap with basic approach of coupling experimental results to simulations. Investigation of mechanistic features in simultaneous degradation of phenanthrene and pyrene was also performed. A summary of various chapters in the thesis is given below:

- Chapter 1 presents general introduction of the theme of the thesis. A brief description is given about the environmental pollution, biodegradation technique followed by mention of PAHs degradation using different community of microbial species. Literature review focussing on biodegradation of multi-PAHs system has also been presented.
- Chapter 2 addresses the primary and essential objective of the biodegradation process, i.e., statistical optimization of the physical operating parameters, followed by the kinetic analysis of growth and degradation of both pollutants (phenanthrene and pyrene). At optimum conditions, for 100 mg $L^{-1}$ initial phenanthrene concentration, a residual concentration of 34 ± 2 mg $L^{-1}$ was obtained after 14 days, which corresponded to ~ 66% degradation.

For 75 mg $L^{-1}$ initial pyrene concentration, a residual concentration of 35 ± 1 mg $L^{-1}$ was obtained, which corresponds to ~ 53% pyrene degradation. Kinetic analysis of biodegradation parameters revealed that Haldane model had the best fit for the profiles of growth and degradation. Reduction in specific growth and degradation rates after a certain initial concentration is an indication of substrate inhibition at relatively higher concentrations of PAHs.

- Chapter 3 presents the attempt of enhancement of biodegradation of phenanthrene and pyrene by the yeast strain, *Candida tropicalis* through the application of ultrasound. Enhancement in the biodegradation was observed when sonication (at 10% duty cycle) was applied at optimized physical operating parameters. Intense microturbulence generated by sonication enhances the cell membrane permeability, which facilitates quicker cellular transport of nutrients, substrate, and other metabolites, deagglomeration of cell clusters, which helps better access to nutrients and substrate in broth, dilution of toxic substances produced during substrate utilization, which helps in reducing cell death and enhancing cell growth. Kinetic parameters of biomass and substrate concentration profiles were positively influenced by the application of ultrasound. Also, investigations on morphological changes and viability of yeast cells (using flow cytometry and FESEM) for ultrasound treated cells revealed that internal complexity and morphology of yeast cells remains unaltered and no cell death occurred during ultrasound exposure.
- Chapter 4 presents the attempt to elucidate the pathway of degradation, enzymes triggering the degradation process and the metabolites/intermediates formed during the degradation process, thereby, aiming to get an in–depth insight into the biomechanism involved in degradation of phenanthrene and pyrene by *C.*

*tropicalis*. The enhancement effect of sonication on phenanthrene and pyrene biodegradation is mainly of physical nature. The metabolic pathway of degradation is not influenced by sonication, as both the PAHs are degraded through *meta*–cleavage pathway in control and ultrasound–treated experiments. GC-MS analysis of intermediate metabolites revealed two parallel pathways, first triggered by intracellular cytochrome P450 monooxygenase enzyme, and second initiated by dioxygenase enzymes. The former pathway yielded sulfate conjugate and dihydrodiols, while the latter resulted in acids and aldehydes that enters the TCA cycle.

- Chapter 5 presents the attempt to investigate mechanistic features of simultaneous degradation of phenanthrene and pyrene by the yeast *Candida tropicalis*. Batch experiments comprising various combinations of initial phenanthrene and pyrene concentrations have been analyzed vis–à–vis kinetic model for cell growth that takes into account self– and cross–inhibition of both substrates. The values of interaction parameters of inhibition revealed strong competitive cross–inhibition between two substrates, due to which biomass yield with dual substrates was reduced significantly. Specific degradation rate of phenanthrene was significantly higher than pyrene, which indicated relatively lower tolerance of the yeast cells towards pyrene. Inhibition induced by pyrene on cell growth was higher than phenanthrene. This study could form a beneficial tool for discerning interaction patterns in PAHs bioremediation of practical ecosystems comprising multiple PAHs.

## 6.2 SUGGESTIONS FOR FUTURE WORK

Present thesis has addressed some important fundamental issues related to

bioremediation of PAHs. The results presented in this thesis can provide basic mechanistic guidelines for degradation studies by yeasts involving PAHs as sole carbon source. Moreover, the methodologies adopted in this thesis can form general framework for further studies in similar systems. The work reported in this thesis can be carried forward and some suggestions in this regard are as follows:

1. Present study has been performed using two PAHs viz., phenanthrene and pyrene. The study may be extended by inclusion of other PAHs such as flourene, anthracene, benzo(a)pyrene, etc. in multi-substrate systems.

2. The complete mineralization assay should be conducted to get clear picture of effect of biodegradation in reducing BOD values.

3. The role of ultrasound can be studied in depth by considering various parameters such as varying the frequency and power input of ultrasound in the system. Multi transducer systems can also be introduced in these processes unlike the single transducer system used in the present study.

4. The present thesis has tried to reveal exact mechanism of ultrasound–induced enhancement of biodegradation of PAHs. Greater effort is needed in this area by mapping of the genes and their overexpression using more rigorous molecular biology techniques.

5. Study of biosurfactant production by *Candida tropicalis* as the yeast strain is known to produce surfactant and identification of its role in biodegradation process. Immobilization study can also be performed on various cost effective environmental waste biomass and its comparison with free yeast strain in terms of degradation potential.

6. As *Candida tropicalis* is an oleaginous yeast, identification of lipids produced during degradation can be performed to check prospects for biodiesel production.

# RESEARCH OUTPUT

## PAPERS IN PEER REVIEWED INTERNATIONAL JOURNALS

1. **Niharika Kashyap,** Kuldeep Roy, Vijayanand S. Moholkar. Mechanistic investigations in ultrasound-assisted biodegradation of phenanthrene. Ultrasonics Sonochemistry 2020, 62, 104890.

2. **Niharika Kashyap,** Kuldeep Roy, Vijayanand S. Moholkar. Mechanistic Investigation in Co-biodegradation of Phenanthrene and Pyrene by *Candida tropicalis* MTCC 184. Chemical Engineering Journal 2020, 125659.

3. **Niharika Kashyap** and Vijayanand S. Moholkar. Intensification of pyrene degradation by native *Candida tropicalis* MTCC 184 with sonication: Kinetic and mechanistic investigation. Chemical Engineering and Processing - Process Intensification 2021, 108415.

## CONFERENCE PRESENTATIONS

1. Poster presentation: Kashyap N, Moholkar VS. Optimization and pathway identification of polycyclic aromatic hydrocarbons (PAHs) degradation by *Candida tropicalis* and its intensification by sonication. International Conference on Biotechnological Research and Innovation for Sustainable development (BioSD-2018) The Biotech Research Society, India (BRSI) and IBA-International Forum for Industrial Bioprocesses (IBA-IFIBiop France), CSIR-IICT, Hyderabad 22$^{nd}$– 25$^{th}$ Nov, 2018.

2. Poster presentation: Kashyap N, Moholkar VS. Optimization of process parameters for intensive biodegradation of polycyclic aromatic hydrocarbons (PAHs) by yeast, *Candida* spp. Recent Trends in Bioprocessing for Healthcare, Energy and Environment. Bioprocessing India. IIT Guwahati, Guwahati 9$^{th}$–11$^{th}$ Dec, 2017.

3. Poster presentation: Kashyap N, Borah AJ, Saynik PB, Moholkar VS. Ultrasound assisted biodegradation of polycyclic aromatic hydrocarbons (PAHs) by yeast, *Candida* spp. International Conference on Emerging Trends in Biotechnology for Waste Conversion (ETBWC). The Biotech Research Society, India (BRSI). NEERI Nagpur 8$^{th}$–10$^{th}$ Oct, 2017.

# APPENDIX I

## APPENDIX FOR CHAPTER 4

**Table A1.** Intermediate metabolites of phenanthrene degradation as detected by GC–MS

| Type of metabolite | Name | Dectected formula | Dectected molecular weight (g $mol^{-1}$) | Retention time (min) |
|---|---|---|---|---|
| Alkali aromatic acid | Benzeneacetic acid | $C_8H_8O_2$ | 136 | 14.78 |
| Fatty acid derivatives | n-Hexadecanoic acid | $C_{16}H_{32}O_2$ | 256 | 23.87 |
| | Eicosanoic acid | $C_{20}H_{40}O_2$ | 312 | 23.72 |
| | Tetradecanoic acid | $C_{14}H_{28}O_2$ | 228 | 20.85 |
| | Heneicosanoic acid, methyl ester | $C_{22}H_{44}O_2$ | 340 | 22.73 |
| | 8-Octadecenoic acid, methyl ester | $C_{19}H_{36}O_2$ | 296 | 25.22 |
| | cis-5-Dodecenoic acid | $C_{12}H_{22}O_2$ | 198 | 26.54 |
| | Oleic acid | $C_{18}H_{34}O_2$ | 282 | 30.51 |
| Aromatic organic compounds | Menthyl salicylate | $C_{17}H_{24}O_3$ | 276 | 23.56 |
| | 1,2-Benzenedicarboxylic acid, decyl octyl ester | $C_{26}H_{42}O_4$ | 418 | 33.62 |
| Alkane derivative | Hexadecane, 1-(ethenyloxy) | $C_{18}H_{36}O$ | 268 | 13.62 |
| | Tetradecane, 1-chloro- | $C_{14}H_{29}Cl$ | 232 | 13.61 |
| Sulfates | 4'-Methylphenyl-1c-sulfonyl-$\beta$-d-galactoside | $C_{13}H_{18}O_7S$ | 318 | 14.82 |
| | Dodecane, 1,1'-thiobis | $C_{24}H_{50}S$ | 370 | 29.84 |
| Aldehyde | Benzaldehyde, 3-benzyloxy-2-fluoro-4-methoxy- | $C_{15}H_{13}O_3F$ | 260 | 13.21 |
| Epoxy derivatives | Oxiraneundecanoic acid, 3-pentyl-, methyl ester, cis | $C_{19}H_{36}O_3$ | 312 | 25.17 |
| TCA cycle intermediate | Oxalic acid, allyl octadecyl ester | $C_{23}H_{42}O_4$ | 382 | 26.49 |
| Aliphatic organic compound | Hexanedioic acid, bis(2-ethylhexyl) ester | $C_{22}H_{42}O_4$ | 370 | 29.17 |
| Diol/Triol derivatives | E,E,Z-1,3,12-Nonadecatriene-5,14-diol | $C_{19}H_{34}O_2$ | 294 | 25.32 |
| Alcohol derivatives | Z,E-3,13-Octadecadien-1-ol | $C_{18}H_{34}O$ | 266 | 25.38 |
| | Oleyl alcohol | $C_{18}H_{36}O$ | 268 | 27.01 |

**Table A2.** Intermediate metabolites of pyrene degradation as detected by GC–MS

| Type of metabolite | Name | Dectected formula | Dectected molecular weight (g $mol^{-1}$) | Retention time (min) |
|---|---|---|---|---|
| Aromatic organic compounds | Phenol, 2,4-bis (1,1 dimethylethyl) | $C_{14}H_{22}O$ | 206 | 17.55 |
| TCA cycle intermediate | Oxalic acid, allyl octadecyl propyl ester | $C_{23}H_{44}O_4$ | 384 | 21.06 |
| Epoxy derivatives | Oxiraneundecanoic acid, 3-pentyl-, methyl ester, cis | $C_{19}H_{36}O_3$ | 312 | 22.77 |
| Alkane derivatives | Decane, 4-cyclohexyl- | $C_{16}H_{32}$ | 224 | 23.86 |
| | Dodecane, 6-cyclohexyl- | $C_{18}H_{36}$ | 252 | 26.19 |
| Fatty acid derivatives | 6-Octadecenoic acid-, methyl ester | $C_{19}H_{36}O_2$ | 296 | 25.17 |
| | Hexanoic acid | $C_6H_{12}O_2$ | 116 | 8.58 |
| | Octadecanoic acid, phenylmethyl ester | $C_{25}H_{42}O_2$ | 374 | 16.38 |
| | Heneicosanoic acid, methyl ester | $C_{22}H_{44}O_2$ | 340 | 22.73 |
| | Butanoic acid, 3-methyl | $C_5H_{10}O_2$ | 102 | 8.63 |
| Sulfates | Thiazole-5-carboxylic acid, 2-tert-butylthio-4-methyl | $C_9H_{13}O_2NS_2$ | 231 | 12.94 |
| Aromatic organic compounds | 1,2-Benzenedicarboxylic acid, butyl cyclohexyl ester | $C_{18}H_{24}O_4$ | 304 | 23.92 |
| Alkali aromatic acid | Benzeneacetic acid, 2-tridecyl ester | $C_{21}H_{34}O_2$ | 318 | 16.18 |
| Diol/Triol derivatives | 1-naphthalenepropanol, $\alpha$-ethyldecahydro-5 | $C_{20}H_{36}O_2$ | 308 | 26.43 |
| Alcohol derivatives | 13-Tetradece-11-yn-1-ol | $C_{14}H_{24}O$ | 208 | 25.35 |
| | Oleyl alcohol | $C_{18}H_{36}O$ | 268 | 25.32 |

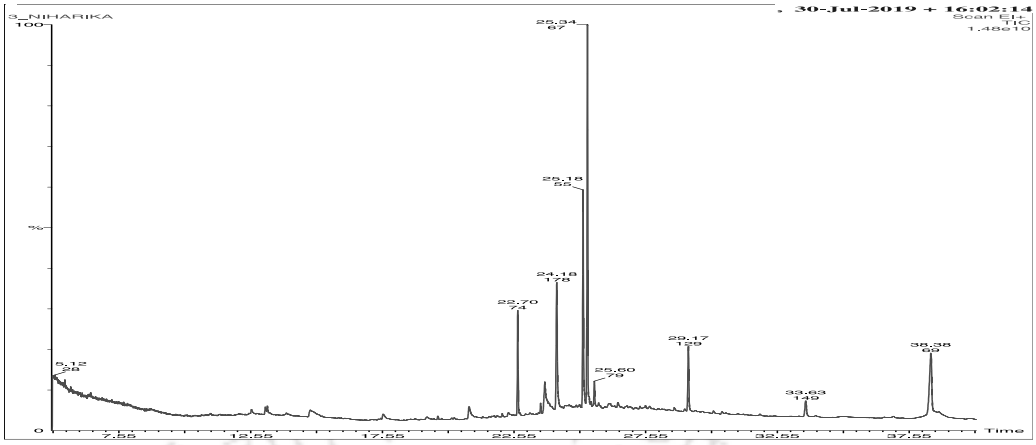


(A)

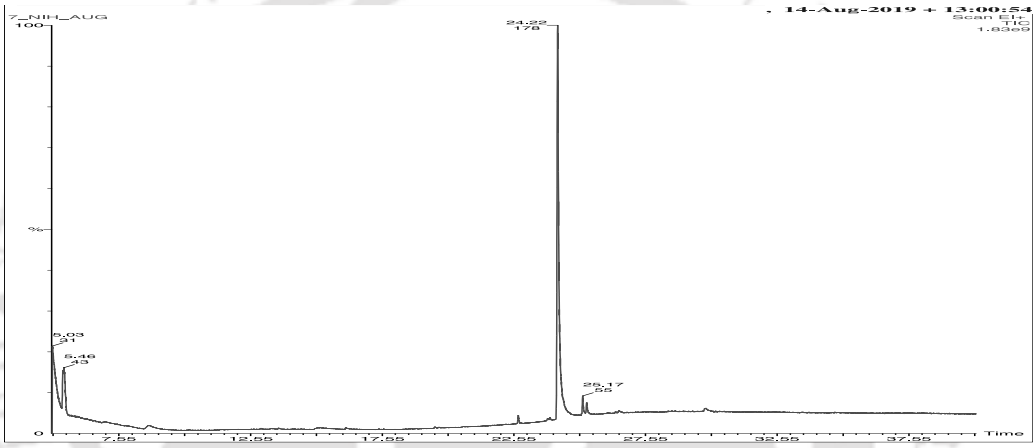


(B)

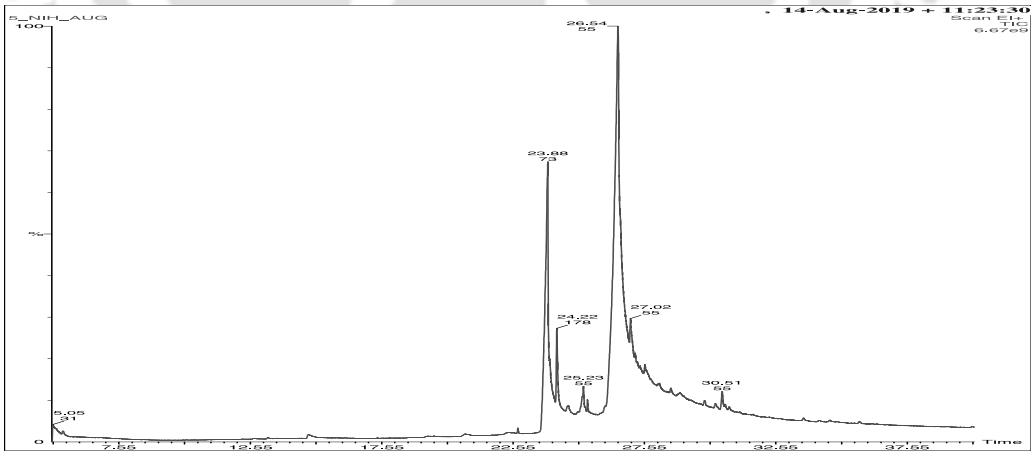


(C)

**Figure A1.** GC–MS spectra of phenanthrene degradation obtained on 6$^{th}$ day (A), 10$^{th}$ day (B) and 12$^{th}$ day (C) of degradation.

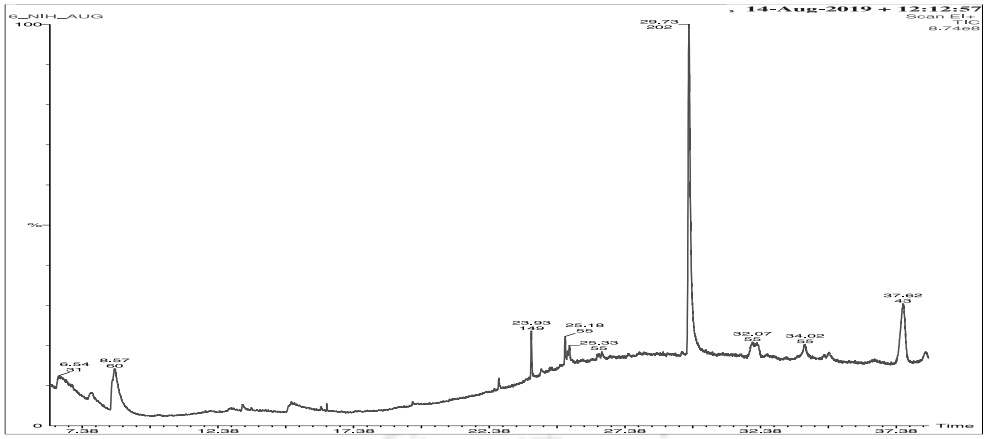


(A)

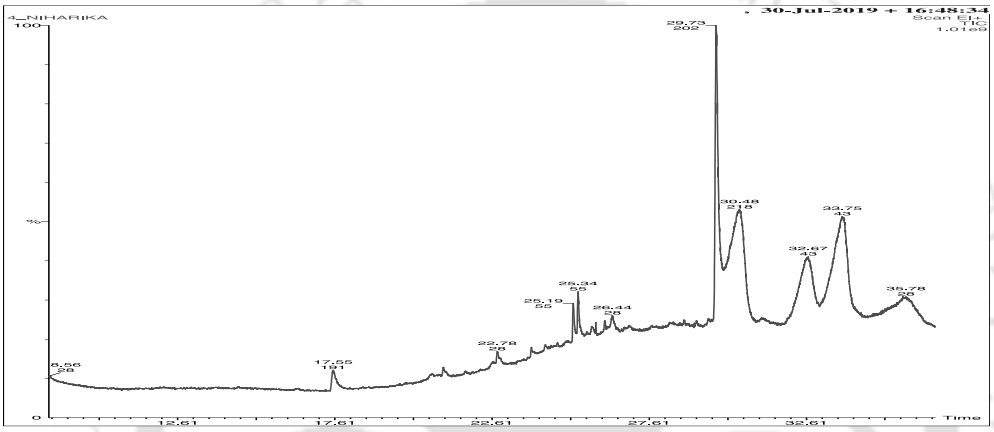


(B)

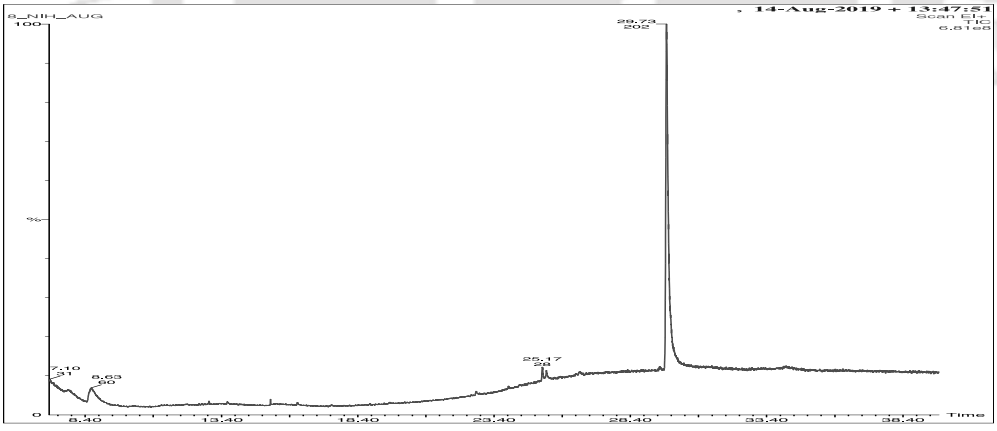


(C)

**Figure A2.** GC–MS spectra of pyrene degradation obtained on 6$^{th}$ day (A), 10$^{th}$ day (B) and 12$^{th}$ day (C) of degradation.

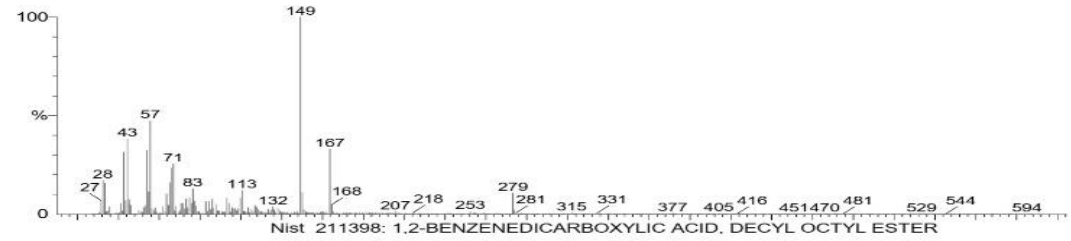


(A)

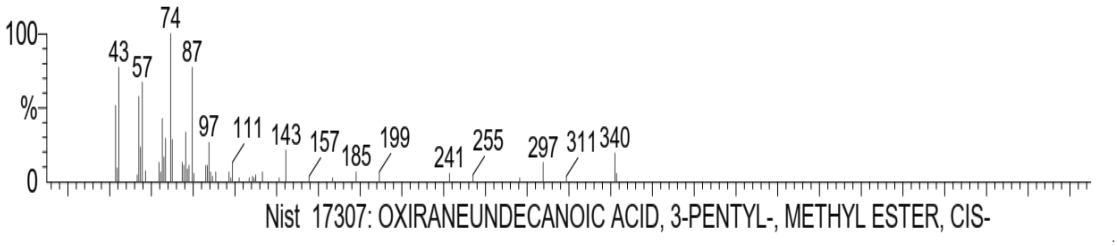


(B)

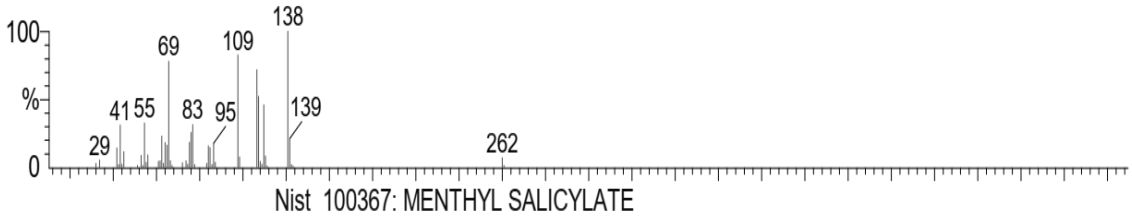


(C)

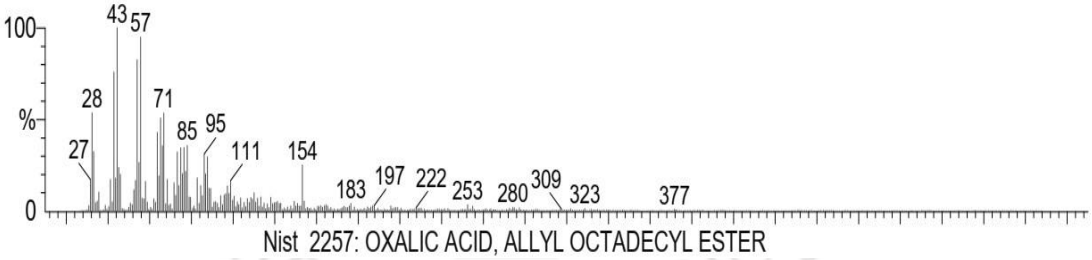


(D)

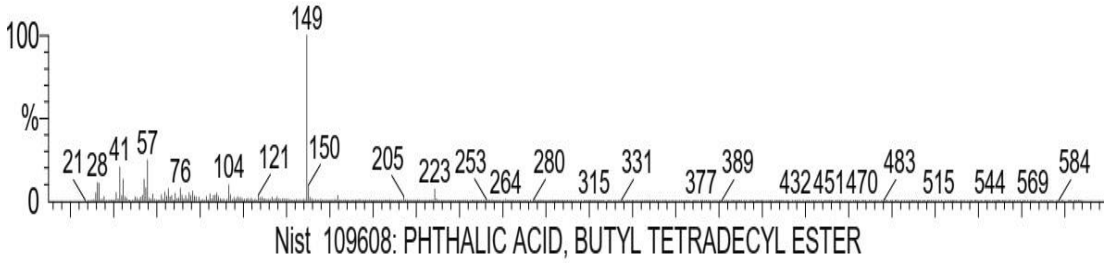


(E)

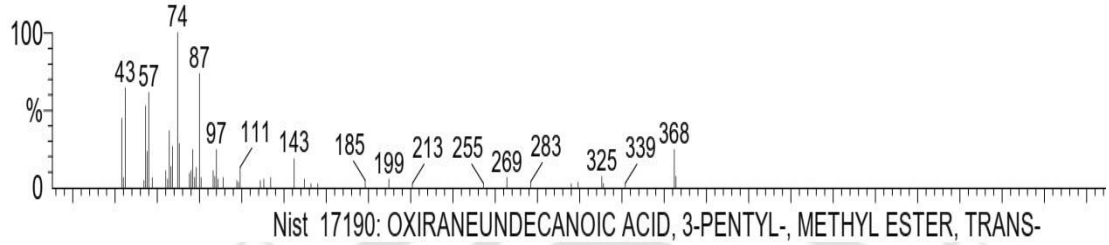


(F)

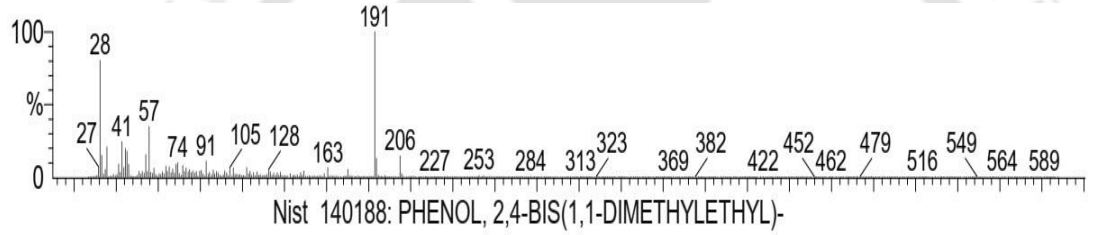


(G)

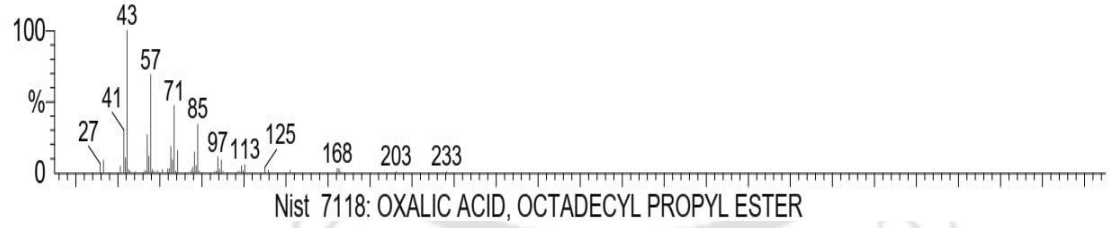


(H)

**Figure A3.** GC–MS analysis of samples. (A), (B), (C) & (D) are metabolites of phenanthrene degradation. (E), (F), (G) and (H) are metabolites of pyrene degradation.

# APPENDIX II

## APPENDIX FOR CHAPTER 5

## Mass balances for the intermediate species in the cell metabolism

On the basis of reaction scheme for first substrate (reactions 1 to 7) reported in Table 5.1 of Chapter 5, the pseudo steady state mass balances for the secondary and ternary complexes are written as:

$$\frac{d[X'S_1]}{dt} = k_{+3}[X'][S_1] - k_{-3}[X'S_1] = 0 \quad \text{(A.1)}$$

$$\frac{d[X'S_2]}{dt} = k_{+4}[X'][S_2] - k_{-4}[X'S_2] = 0 \quad \text{(A.2)}$$

$$\frac{d[X'S_1^2]}{dt} = k_{+5}[X'S_1][S_1] - k_{-5}[X'S_1^2] = 0 \quad \text{(A.3)}$$

$$\frac{d[X'S_2^2]}{dt} = k_{+6}[X'S_2][S_2] - k_{-6}[X'S_2^2] = 0 \quad \text{(A.4)}$$

$$\frac{d[X'S_1S_2]}{dt} = k_{+7}[X'S_1][S_2] - k_{-7}[X'S_1S_2] = 0 \quad \text{(A.5)}$$

Using the pseudo steady state concentration of primary complex for first substrate, $[X'] = k_{+1}[X][S_1]/(k_{-1} + k_{+2})$, the pseudo steady state concentrations of the secondary and ternary complexes are obtained as:

$$[X'S_1] = \frac{k_{+3}}{k_{-3}}[X'][S_1] = \frac{k_{+3}}{k_{-3}}\frac{k_{+1}}{k_{-1}+k_{+2}}[X][S_1]^2 \quad \text{(A.6)}$$

$$[X'S_2] = \frac{k_{+4}}{k_{-4}}[X'][S_2] = \frac{k_{+4}}{k_{-4}}\frac{k_{+1}}{k_{-1}+k_{+2}}[X][S_1][S_2] \quad \text{(A.7)}$$

$$\left[X'S_1^2\right]=\frac{k_{+5}}{k_{-5}}\left[X'S_1\right]\left[S_1\right]=\frac{k_{+5}}{k_{-5}}\frac{k_{+3}}{k_{-3}}\frac{k_{+1}}{k_{-1}+k_{+2}}\left[X\right]\left[S_1\right]^3 \quad \text{(A.8)}$$

$$\left[X'S_2^2\right]=\frac{k_{+6}}{k_{-6}}\left[X'S_2\right]\left[S_2\right]=\frac{k_{+6}}{k_{-6}}\frac{k_{+4}}{k_{-4}}\frac{k_{+1}}{k_{-1}+k_{+2}}\left[X\right]\left[S_1\right]\left[S_2\right]^2 \quad \text{(A.9)}$$

$$\left[X'S_1S_2\right]=\frac{k_{+7}}{k_{-7}}\left[X'S_1\right]\left[S_2\right]=\frac{k_{+7}}{k_{-7}}\frac{k_{+3}}{k_{-3}}\frac{k_{+1}}{k_{-1}+k_{+2}}\left[X\right]\left[S_1\right]^2\left[S_2\right] \quad \text{(A.10)}$$

On the basis of reaction scheme for second substrate (reactions 8 to 14) reported in Table 5.1, the pseudo steady state mass balances for the secondary and ternary complexes are written as:

$$\frac{d\left[X''S_1\right]}{dt}=k'_{+3}\left[X''\right]\left[S_1\right]-k'_{-3}\left[X''S_1\right]=0 \quad \text{(A.11)}$$

$$\frac{d\left[X''S_2\right]}{dt}=k'_{+4}\left[X''\right]\left[S_2\right]-k'_{-4}\left[X''S_2\right]=0 \quad \text{(A.12)}$$

$$\frac{d\left[X''S_1^2\right]}{dt}=k'_{+5}\left[X''S_1\right]\left[S_1\right]-k'_{-5}\left[X''S_1^2\right]=0 \quad \text{(A.13)}$$

$$\frac{d\left[X''S_2^2\right]}{dt}=k'_{+6}\left[X''S_2\right]\left[S_2\right]-k'_{-6}\left[X''S_2^2\right]=0 \quad \text{(A.14)}$$

$$\frac{d\left[X''S_1S_2\right]}{dt}=k'_{+7}\left[X''S_1\right]\left[S_2\right]-k'_{-7}\left[X''S_1S_2\right]=0 \quad \text{(A.15)}$$

Using the pseudo steady state concentration of primary complex for second substrate, $\left[X''\right]=k'_{+1}\left[X\right]\left[S_2\right]/\left(k'_{-1}+k'_{+2}\right)$, the pseudo steady state concentrations of the secondary and ternary complexes are obtained as:

$$\left[X''S_1\right]=\frac{k'_{+3}}{k'_{-3}}\left[X''\right]\left[S_1\right]=\frac{k'_{+3}}{k'_{-3}}\frac{k'_{+1}}{k'_{-1}+k'_{+2}}\left[X\right]\left[S_2\right]\left[S_1\right] \quad \text{(A.16)}$$

$$[X''S_2] = \frac{k'_{+4}}{k'_{-4}}[X''][S_2] = \frac{k'_{+4}}{k'_{-4}}\frac{k'_{+1}}{k'_{-1}+k'_{+2}}[X][S_2]^2 \quad \text{(A.17)}$$

$$\left[X''S_1^2\right] = \frac{k'_{+5}}{k'_{-5}}[X''S_1][S_1] = \frac{k'_{+5}}{k'_{-5}}\frac{k'_{+3}}{k'_{-3}}\frac{k'_{+1}}{k'_{-1}+k'_{+2}}[X][S_2][S_1]^2 \quad \text{(A.18)}$$

$$\left[X''S_2^2\right] = \frac{k'_{+6}}{k'_{-6}}[X''S_2][S_2] = \frac{k'_{+6}}{k'_{-6}}\frac{k'_{+4}}{k'_{-4}}\frac{k'_{+1}}{k'_{-1}+k'_{+2}}[X][S_2]^3 \quad \text{(A.19)}$$

$$[X''S_1S_2] = \frac{k'_{+7}}{k'_{-7}}[X''S_1][S_2] = \frac{k'_{+7}}{k'_{-7}}\frac{k'_{+3}}{k'_{-3}}\frac{k'_{+1}}{k'_{-1}+k'_{+2}}[X][S_2]^2[S_1] \quad \text{(A.20)}$$

**Table A1.** Statistical analysis for dual substrate degradation

| Experimental set | Pollutants concentration | *t*-stat | *p*-value | Confidence level (95%) | |
|---|---|---|---|---|---|
| | | | | Lower 95% | Upper 95% |
| Set 1 (dual substrate) | 50 PH | 6.1531 | 0.000845 | -12.2469 | 18.5421 |
| | 150 PY | 3.9373 | 0.007649 | -33.4263 | 91.4824 |
| Set 2 (dual substrate) | 100 PH | 4.6397 | 0.003542 | -5.87564 | 62.0901 |
| | 100 PY | 2.8813 | 0.002801 | -22.7051 | 77.0954 |
| Set 3 (dual substrate) | 150 PH | 3.8859 | 0.008115 | -67.1783 | 78.2356 |
| | 50 PY | 4.6103 | 0.003652 | -3.06933 | 26.9852 |
| Set 4 (single substrate) | 200 PH | 5.5889 | 0.001395 | -147.3717 | 43.8924 |
| Set 5 (single substrate) | 200 PY | 3.0424 | 0.002273 | -148.8374 | 139.0943 |